

Immunometabolism and lipoprotein metabolism during thermogenesis

Dissertation

Zur Erlangung der Würde des Doktors der Naturwissenschaften des
Fachbereichs Chemie,
der Fakultät für Mathematik, Informatik und Naturwissenschaften
der Universität Hamburg,

vorgelegt von
Nicola Schaltenberg
aus München

Hamburg, 2019

1. Gutachter: Prof. Dr. Markus Fischer

2. Gutachter: Prof. Dr. Jörg Heeren

Die vorliegende Arbeit wurde von August 2015 bis November 2018 extern am Institut für Biochemie und Molekulare Zellbiologie des Universitätsklinikums Hamburg-Eppendorf unter der Leitung von Prof. Dr. Jörg Heeren angefertigt. Die Arbeit wurde von Herrn Prof. Dr. Markus Fischer am Fachbereich Chemie der Universität Hamburg betreut.

Disputation: 26.04.2019

Datum der Druckfreigabe: 26.04.2019

1 Publications, presentations and posters at national and international congresses

1.1 Publications

- 1 F. Siracusa*, N. Schaltenberg*, E. J. Villablanca, S. Huber, N. Gagliani, 'Dietary Habits and Intestinal Immunity: From Food Intake to CD4⁺ T_H Cells', *Front. Immunol.*, 9 (2019), 3177.
- 2 V. Booz, C. B. Christiansen, R. E. Kuhre, M. Y. Saltiel, G. Sociali, N. Schaltenberg, A. W. Fischer, J. Heeren, E. Zocchi, J. J. Holst, S. Bruzzone, 'Abscisic acid stimulates the release of insulin and of GLP-1 in the rat perfused pancreas and intestine', *Diabetes Metab Res Rev*, e3102 (2018).
- 3 Bartelt*, C. John*, N. Schaltenberg*, J. F. Berbée*, A. Worthmann*, M. L. Cherradi, C. Schlein, J. Schmidt, M. R. Boon, F. Rinninger, M. Heine, K. Toedter, A. Niemeier, S. K. Nilsson, M. Fischer, S. L. Wijers, W. van Marken Lichtenbelt, L. Scheja, P. C. Rensen and J. Heeren, 'Thermogenic adipocytes promote HDL turnover and reverse cholesterol transport', *Nat Commun*, 8 (2017), 15010.
- 4 A. Worthmann*, C. John*, M.C. Rühlemann, M. Baguhl, F.-A. Heinsen, N. Schaltenberg, M. Heine, C. Mineo, M. Fischer, M. Dandri, C. Kremoser, L. Scheja, A. Franke, P. W. Shaul, J. Heeren, 'Cold-induced bile acid synthesis shapes the gut microbiome', *Nat Med*, 7 (2017), 839-849.
- 5 K.L. Lokken*, J. P. Mooney*, B. P. Butler, M. N. Xavier, J. Y. Chau, N. Schaltenberg, R. H. Begum, J. W. Müller, S. Luckhart, R. M. Tsois, 'Malaria parasite infection compromises control of concurrent systemic non-typhoidal Salmonella infection via IL-10-mediated alteration of myeloid cell function', *PLoS Pathog*, 10(7) (2014).
- 6 J. P. Mooney, B. P. Butler, K.L. Lokken, M. N. Xavier, J. Y. Chau, N. Schaltenberg, S. Dandekar, M. D. George, R. L. Santos, S. Luckhart, R. M. Tsois, 'The mucosal inflammatory response to non-typhoidal Salmonella in the intestine is blunted by IL-10 during concurrent malaria parasite infection', *Mucosal Immunol*, 7 (2014), 1302-11.
- 7 T. Wuensch, S. Ullrich, S. Schulz, M. Chamailard, N. Schaltenberg, E. Rath, U. Goebel, R. B. Sator, M. Prager, C. Büning, P. Bugert, H. Witt, D. Haller, H. Daniel, 'Colonic expression of the peptide transporter PEPT1 is downregulated during intestinal inflammation and is not required for NOD2-dependent immune activation', *Inflamm Bowel Dis*, 20 (2014), 671-84.

* shared first authorship

1.2 Presentations at national and international congresses

- *Brown and beige adipocyte activity controls metabolic flux through the HDL compartment*
Nicola Schaltenberg, Alexander Bartelt, Clara John, Anna Worthmann, M. Lisa Cherradi, Franz Rinninger, Markus Heine, Stefan K. Nilsson, Ludger Scheja, and Joerg Heeren. **2015**, XIX Lipid Meeting Leipzig, Leipzig, Germany
- *Brown and beige adipocyte activity controls metabolic flux through the HDL compartment*

Nicola Schaltenberg, Alexander Bartelt, Clara John, Anna Worthmann, M. Lisa Cherradi, Franz Rinninger, Markus Heine, Stefan K. Nilsson, Ludger Scheja, and Joerg Heeren. **2016**, 84th European Atherosclerosis Society Congress, Innsbruck, Austria

- *Brown and beige adipocyte activity controls metabolic flux through the HDL compartment*

Nicola Schaltenberg, Alexander Bartelt, Clara John, Anna Worthmann, M. Lisa Cherradi, Franz Rinninger, Markus Heine, Stefan K. Nilsson, Ludger Scheja, and Joerg Heeren. **2016**, 39th European Lipoprotein Club meeting, Tutzing, Germany

1.3 Posters at national and international congresses

- *Brown and beige adipocyte activity controls metabolic flux through the HDL compartment*

Nicola Schaltenberg, Alexander Bartelt, Clara John, Anna Worthmann, M. Lisa Cherradi, Franz Rinninger, Markus Heine, Ludger Scheja, and Joerg Heeren. **2016**, 22nd Annual Scandinavian Atherosclerosis Conference, Humlebæk, Denmark

- *Brown and beige adipocyte activity controls metabolic flux through the HDL compartment*

Nicola Schaltenberg, Christian Schlein, Clara John, Alexander Bartelt, Anna Worthmann, Julia Schmidt, Philipp Werner, Maria Trusch, Klaus Tödter, Markus Fischer, Ludger Scheja and Jörg Heeren. **2016**, ISAS Lipidomics Meeting, Dortmund, Germany

- *Activation of lipoprotein lipase and endothelial lipase in thermogenic adipocytes promotes HDL turnover and reverse cholesterol transport*

Nicola Schaltenberg, Alexander Bartelt, Clara John, Anna Worthmann, M. Lisa Cherradi, Franz Rinninger, Markus Heine, Ludger Scheja, and Joerg Heeren. **2017**, 23rd Annual Scandinavian Atherosclerosis Conference, Humlebæk, Denmark

- *Thermogenic adipocytes promote HDL metabolism in an LPL- and EL-dependent manner*

Nicola Schaltenberg, Alexander Bartelt, Clara John, Anna Worthmann, M. Lisa Cherradi, Franz Rinninger, Markus Heine, Ludger Scheja, and Joerg Heeren. **2017**, Lipid Signaling in Health and Disease, Zürich, Switzerland

Table of contents

1	Publications, presentations and posters at national and international congresses.....	I
1.1	Publications.....	I
1.2	Presentations at national and international congresses.....	I
1.3	Posters at national and international congresses	II
	Part A Summary	1
	Part B Zusammenfassung	3
	Part C Introduction.....	5
1	Lipoprotein metabolism.....	5
1.1	Exogenous lipoprotein metabolism	5
1.2	Endogenous lipoprotein metabolism.....	6
1.3	Reverse cholesterol transport.....	7
2	Regulatory molecules mediating lipoprotein metabolism	8
2.1	Apo-lipoproteins.....	8
2.2	Transfer proteins	9
2.3	Lipases.....	9
2.3.1	Lipoprotein lipase.....	10
2.3.2	Endothelial lipase.....	10
2.3.3	Hepatic lipase.....	11
3	Brown adipose tissue (BAT) metabolism	12
3.1	Activation of brown adipose tissue.....	12
3.2	Immunometabolism in BAT.....	14
4	Impact of thermogenesis on lipoprotein metabolism and its relevance for atherosclerosis development	15
4.1	Atherosclerosis development and treatment options.....	15
4.2	BAT activation modulates lipoprotein metabolism	16
	Part D Aims of the study.....	18
	Part E Materials and methods	19
1	Mice	19
2	Analysis of parenchymal cells, non-parenchymal cells and macrophages from adipose tissues.....	19
2.1	MACS®-based cell separation.....	20
2.2	RNA extraction, cDNA synthesis and relative real-time PCR	20
2.3	UPLC-ESI-QqTOF-method for semi-quantitative lipid analysis	21
3	Plasma analysis	23
3.1	Blood withdrawal	23
3.2	Lipoprotein profiling.....	23
3.3	Measurement of triglycerides and cholesterol in plasma	23
3.4	ApoA1 ELISA.....	23
3.5	UPLC-ESI-QqTOF-method for semi-quantitative lipid analysis in HDL particles from plasma.....	23
4	Gene expression in tissue.....	23
5	HDL turnover.....	24
5.1	Experimental setup.....	24
5.2	Generation of labeled HDL particles.....	24
5.3	Quantification of radioactivity in plasma and tissues	24

6	<i>In vivo</i> reverse cholesterol transport assay (RCT).....	25
6.1	Experimental setup.....	25
6.2	Generation of <i>ex vivo</i> labeled macrophages.....	25
6.3	Quantification of radioactivity in plasma, tissues and feces.....	25
	Part F Results.....	26
1	Characterization of parenchymal cells, non-parenchymal cells and macrophages from thermogenic adipose tissues.....	26
1.1	Separation of parenchymal cells, non-parenchymal cells and macrophages from thermogenic adipose tissues using MACS® technique.....	27
1.2	Lipid composition in extracted adipocytes from BAT and inguinal WAT.....	30
1.3	Lipid composition in isolated endothelial cells from BAT and inguinal WAT.....	31
1.4	Analysis of isolated macrophages from BAT and inguinal WAT.....	33
1.4.1	Lipid remodeling.....	34
1.4.2	Polarization.....	35
2	Intravascular alterations in lipoprotein metabolism during thermogenesis.....	36
2.1	Cold-mediated effects on systemic cholesterol metabolism.....	37
2.1.1	Effects of thermogenesis on plasma lipid parameters and lipoprotein profiles.....	37
2.1.2	Effects of thermogenesis on HDL turnover in pre- and postprandial conditions.....	39
2.1.3	Effects of thermogenesis on reverse cholesterol transport <i>in vivo</i>	42
2.2	Impact of LPL and SR-B1 on HDL metabolism during thermogenesis.....	43
2.3	Role of EL on lipoprotein metabolism during thermogenesis.....	46
2.3.1	Consequences of global genetic EL ablation (eIKO) on gene expression in metabolic organs in thermoneutrality and cold.....	47
2.3.2	Plasma lipid parameters and lipoprotein profile in eIKO mice after BAT activation by cold housing.....	50
2.3.3	Effects of EL loss on HDL lipid remodeling during thermogenesis.....	51
2.3.4	Impact of EL on cold-induced acceleration of HDL turnover.....	53
2.3.5	Distribution of EL to cold-induced enhanced reverse cholesterol transport.....	55
	Part G Discussion.....	58
1	Immunometabolism in thermogenic adipose tissue.....	58
2	Thermogenesis-induced alterations in HDL metabolism.....	62
3	Significance of lipases in BAT-accelerated HDL metabolism.....	63
	Part H References.....	69
	Part I Attachement.....	78
1.	Supplementary figures.....	78
2.	Materials and buffers.....	80
	Part J Register of figures.....	85
	Part K Register of tables.....	86
	Part L Danksagung.....	87
	Part M Eidesstattliche Erklärung.....	88

Abbreviations

³ H-CEt	³ H-cholesterol oleyl ether
ABCA1	<i>ATP-binding cassette transporter A1</i>
ABCG5	<i>ATP-binding cassette transporter G5</i>
ABCG8	<i>ATP-binding cassette transporter G8</i>
ANGPTL	<i>angiopoietin-like proteins</i>
BAT	brown adipose tissue
CD11B	<i>cluster of differentiation 11 B</i>
CD31	<i>cluster of differentiation 31</i>
CD36	<i>cluster of differentiation 36</i>
CE	cholesterol ester
CETP	cholesterol ester transfer protein
CHD	coronary heart disease
CM	chylomicron
CVD	cardiovascular disease
DIO2	<i>type 2 iodothyronine deiodinase</i>
EL	endothelial lipase
ER	<i>endoplasmatic reticulum</i>
FA	fatty acid
FA	fatty acid
FABP	<i>fatty acid binding protein</i>
FATP	<i>fatty acid transport protein</i>
FDG-PET-CT	fluorine-18-deoxyglucose-poitron emission tomography
FFA	free fatty acid
FPLC	<i>fast-performance liquid chromatography</i> <i>glycosylphosphatidylinositol anchored high-density</i> <i>lipoprotein binding protein 1</i>
GPIHBP1	<i>glycosylphosphatidylinositol anchored high-density</i> <i>lipoprotein binding protein 1</i>
HDL	<i>high-density lipoprotein</i>
HL	hepatic lipase
HMGCR	<i>3-hydroxy-3-methylglutaryl-CoA reductase</i>
HSPG	<i>heparan sulfate proteoglycan</i>
IDL	<i>intermediate density lipoprotein</i>
LCAT	lecithin-cholesterol acyltransferase
LDL	<i>low-density lipoprotein</i>
LDLR	<i>low-density lipoprotein receptor</i>
LPL	lipoprotein lipase
LRP1	<i>low-density lipoprotein receptor-related protein 1</i>
LXR	<i>liver X receptor</i>
MTTP	<i>microsomal triglyceride-transfer protein</i>
NPC1L1	<i>Niemann-Pick-C 1-like 1</i>
PC	phosphatidylcholine
PCSK9	<i>proprotein convertase subtilisin/kexin type 9</i>
PE	phosphatidylethanolamine
PI	phosphatidylinositol

Abbreviations

PKA	protein kinase A
PL	phospholipid
PLTP	phospholipid transfer protein
PPAR γ	<i>peroxisome proliferator-activated receptor γ</i>
RCT	reverse cholesterol transport assay
ROS	reactive oxygen species
SM	sphingomyelin
SR-B1	<i>scavenger receptor-B1</i>
SREBP	<i>sterol regulatory element-binding protein</i>
T ₄	thyroxin
TG	triglyceride
TICE	<i>transintestinal cholesterol excretion pathway</i>
TNF	<i>tumor necrosis factor</i>
TRL	triglyceride-rich lipoprotein
UCP1	<i>uncoupling protein 1</i>
VLDL	<i>very low-density lipoprotein</i>
WAT	white adipose tissue

Part A Summary

Brown adipose tissue (BAT) is activated upon a cold stimulus to combust energy rich substrates for heat production in order to maintain the body temperature, a process known as adaptive thermogenesis. Cold exposure promotes lipoprotein processing in BAT and accelerates the clearance of plasma triglycerides (TGs). Accordingly, the activation of BAT could be a promising strategy to treat hyperlipidemia and atherosclerosis. Recent studies detected altered lipid composition in lipoproteins after activating BAT and thus the first aim of this thesis project was to elucidate whether lipoprotein processing in response to cold exposure results in an altered lipid composition and functionality of adipocytes and non-parenchymal immune cells. The second aim was to delineate the molecular basis for BAT-dependent intravascular lipoprotein processing.

To investigate the first aim of my thesis, BAT and inguinal white adipose tissue (WAT) from thermoneutral- (30° C) or cold- (6° C) housed mice were subjected to magnetic cell separation (MACS®) to isolate adipocytes from endothelial cells and macrophages. In each cell fraction gene expression was analyzed by qPCR and lipid composition was determined by using an LC-MS/MS-based approach. One week of cold activation resulted in upregulation of thermogenic genes in adipocytes isolated from BAT and inguinal WAT. Furthermore, adipocytes isolated from BAT of cold-housed mice showed a reduction in triglycerides which was absent in adipocytes from inguinal WAT. Whereas endothelial cells isolated from BAT and inguinal WAT did not present major alterations in lipid composition after cold housing, BAT-isolated macrophages displayed an increase in cholesteryl esters (CEs). Additionally, in macrophages isolated from BAT of cold-housed mice, genes mandatory for lipid processing and uptake, namely *Lpl*, *Lipg* (encoding the endothelial lipase (EL)) and *Cd36*, were upregulated. Furthermore, a polarization towards an M2 phenotype was observed, evident by an increased *Il10* and *Arg1* expression and decreased *Il6* expression. In inguinal WAT, cold housing did not change the lipid composition in macrophages, however, expression of genes in lipid processing and uptake trended towards higher mRNA transcripts and *Arg1* was upregulated whereas *Il6* expression decreased upon cold stimulation.

In summary, the results of the first part of my thesis suggest an M2 polarization of macrophages within thermogenic adipose tissues after one week of cold housing. In future studies, it needs to be investigated whether the upregulation of EL in macrophages isolated from BAT after thermogenic activation explains the increased

uptake of CE and whether this lipid uptake determines the anti-inflammatory phenotype.

In the second part of my thesis, I focused on BAT-induced alterations in the HDL metabolism and investigated the role of LPL, SR-B1 and EL in this process by using corresponding knockout mice. In HDL turnover and *in vivo* reverse cholesterol transport (RCT) assays, I found that one week of BAT activation accelerated HDL turnover and promoted macrophage-to-feces cholesterol flux. Adipocyte-specific loss of LPL and global deletion of SR-B1 or EL resulted in an impaired BAT-induced HDL turnover, and the loss of EL also diminished macrophage-to-feces cholesterol disposal. Besides studying HDL functionalities, lipids from HDL particles were extracted which were isolated from plasma of wildtype and EL-knockout (eLKO) mice. In addition to increased cholesterol levels within the HDL fraction of eLKO mice, LC-MS/MS-based lipid analysis revealed an accumulation of phospholipids (PLs) in HDL lipids derived from eLKO mice when compared to HDL lipids from wildtype mice.

In summary, the results from the second part of my thesis underpin the importance of LPL and EL in BAT-accelerated HDL metabolism. Furthermore, the beneficial impact of EL on reverse cholesterol metabolism during cold exposure might be explained by PL remodeling of HDL particles.

Overall, the results obtained in my thesis demonstrate the relevance of lipoprotein lipolysis for the inflammatory milieu in adipose tissues and efficient intravascular lipid transport towards the liver. These studies highlight the importance of adaptive thermogenesis and BAT physiology, which may help to develop novel therapeutic strategies for the treatment of chronic inflammatory metabolic diseases such as type 2 diabetes, cardiovascular disease or steatohepatitis.

Part B Zusammenfassung

Braunes Fettgewebe wird durch Kälte stimuliert und verbrennt daraufhin Energie, um die Körpertemperatur aufrecht zu erhalten. Dieser Vorgang wird als adaptive Thermogenese bezeichnet. Im braunen Fettgewebe fördert die Kälteexposition die Prozessierung von Lipoproteinen und verstärkt die Klärung von Triglyzeriden aus dem Plasma. Demzufolge bildet die Aktivierung von braunem Fettgewebe einen vielversprechenden Therapieansatz zur Behandlung von Hyperlipidämien und der Arteriosklerose. Studien konnten zeigen, dass sich nach Aktivierung von braunem Fettgewebe die Lipidzusammensetzung in Lipoproteinen verändert. Darauf basierend sollte im ersten Teil meiner Doktorarbeit herausgefunden werden, welchen Einfluss die adaptive Thermogenese auf die Lipidzusammensetzung und die Funktionalität der Adipozyten sowie der Immunzellen im aktivierten Fettgewebe ausübt. Das Ziel im zweiten Teil der Arbeit war das intravaskuläre Prozessieren der Lipoproteine, welches durch Aktivierung des braunen Fettgewebes stattfindet, auf molekularer Ebene zu verstehen.

Um die erste Fragestellung meiner Arbeit zu bearbeiten wurde aus braunem sowie inguinalem weißem Fettgewebe aus thermoneutral (30° C) und kalt (6° C) gehaltenen Mäusen mittels magnetischer Zellseparation (MACS®) die Adipozyten, Endothelzellen und Makrophagen isoliert. Jede erhaltene Zellfraktion wurde durch qPCR analysiert und die Lipidzusammensetzung wurde durch eine LC-MS/MS-basierte Methode bestimmt. Eine Woche Kälteexposition führte zur Induktion von Thermogenese-assoziierten Genen in Adipozyten, die aus braunem oder inguinalem weißem Fettgewebe isoliert wurden. Zudem wiesen die aktivierten Adipozyten aus braunem Fettgewebe im Gegensatz zu Adipozyten aus inguinalem weißem Fettgewebe eine Reduktion in Triglyzeriden auf. Wohingegen Endothelzellen aus braunem Fettgewebe nach Kälteexposition keine prägnanten Veränderungen in der Lipidzusammensetzung zeigten, stieg die Menge an Cholesterinestern in Makrophagen, die aus aktiviertem braunem Fettgewebe isoliert wurden an. Zusätzlich verstärkten diese Makrophagen die Expression von Genen, die für Lipidverarbeitung und -aufnahme unabdinglich sind (z.B. *Lpl*, *Lipg*, welches die endotheliale Lipase codiert (EL) und *Cd36*). Außerdem wurde eine Polarisierung hin zu dem M2 Phänotyp festgestellt, da die Expression von *Il10* und *Arg1* anstieg und *Il6* abfiel. Im inguinalen Fettgewebe hingegen wurde durch die Kälteexposition keine veränderte Lipidzusammensetzung der Makrophagen induziert. Jedoch konnte auch hier auf mRNA Ebene ein Trend hin zu verstärkter Expression von Genen beobachtet werden,

die wichtig für die Lipidverarbeitung und -aufnahme sind und auch *Arg1* war induziert und *Il6* reduziert.

Zusammenfassend weisen die Ergebnisse des ersten Teils meiner Arbeit darauf hin, dass Makrophagen aus metabolisch aktivem Fettgewebe nach Kälteaktivierung ihren Phänotyp hin zu einer M2 Polarisierung ändern. In zukünftigen Studien muss geklärt werden, ob die Induktion der EL in den Makrophagen des braunen Fettgewebes während der adaptiven Thermogenese die erhöhte Aufnahme von Cholesterinestern erklärt und ob diese Lipidaufnahme den anti-inflammatorischen Phänotyp hervorruft.

Der zweite Teil meiner Arbeit bearbeitet die Veränderungen im HDL Stoffwechsel, die durch Aktivierung der adaptiven Thermogenese hervorgerufen werden und untersucht die Rolle der LPL, des SR-B1 und der EL in diesem Prozess, indem entsprechende *knockout* Mäuse verwendet werden. Durch Anwendung von *HDL turnover* Studien und *in vivo reverse cholesterol transport* (RCT) Studien konnte ein beschleunigter HDL Stoffwechsel als auch ein verstärkter Cholesterintransport von Makrophagen hin zu den Fäzes beobachtet werden. Adipozyten-spezifische Deletion der LPL und globale Deletion der EL (eIKO) führten zu einer Beeinträchtigung des HDL Stoffwechsels nach Aktivierung des braunen Fettgewebes und der Verlust der EL resultierte auch in einer Verschlechterung in der Cholesterinausscheidung. Zusätzlich zu den funktionellen Eigenschaften der HDL untersuchte ich auch die Lipidzusammensetzung von HDL Partikeln, die aus dem Plasma von Wildtyp und eIKO Mäusen isoliert wurden. Neben erhöhten Cholesterinkonzentrationen in der HDL Fraktion der eIKO Mäuse, wurde mittels einer LC-MS/MS-basierten Methode ein Anstieg der Phospholipide (PL) beobachtet, wenn HDL aus eIKO Mäusen mit denen aus Wildtyp-Mäusen verglichen wurde.

Zusammenfassend lässt sich aus dem zweiten Teil meiner Arbeit sagen, dass sowohl die LPL als auch die EL wichtige Moleküle im reversen Cholesterinstoffwechsel bilden, der während der Kälteexposition verstärkt ist. Außerdem lassen die Daten vermuten, dass der förderliche Effekt der EL im Kälte-induzierten HDL Stoffwechsel durch eine Veränderung der PL der HDL Partikel hervorgerufen wird.

Insgesamt verdeutlicht meine Arbeit die Bedeutung der Lipolyse von Lipoproteinen für das inflammatorische Milieu im Fettgewebe und für den effizienten intravaskulären Lipidtransport hin zur Leber. Die durchgeführten Studien bestätigen die bedeutsame Rolle der adaptiven Thermogenese und der Physiologie des braunen Fettgewebes und dies mag dazu verhelfen neue Therapieansätze für die Behandlung von chronischen metabolischen Erkrankungen, wie z.B. Typ 2 Diabetes, kardiovaskulären Erkrankungen oder Steatohepatitis zu finden.

Part C Introduction

1 Lipoprotein metabolism

The blood circulation represents a hydrophilic fluid, thus transport mechanisms are mandatory to shuttle hydrophobic lipids throughout the organism. Free fatty acids (FFA) are coupled to albumin, whereas more complex lipids such as triglycerides (TGs) and cholesterol require incorporation into lipoproteins. The class of lipoproteins consists of different subclasses which can be categorized by their density and lipid composition: the chylomicrons (CMs) and the *very low-density lipoproteins* (VLDL) forming the TG-rich species, and *low-density lipoprotein* (LDL) and *high-density lipoprotein* (HDL) being TG-rich. In general, the lipoproteins consist of a phospholipid (PL) monolayer which harbors free cholesterol, whereas cholesteryl esters (CEs) and TGs are located within the lipoprotein core. The particles not only contain lipids but they also contain apolipoproteins. On the one hand, these sustain particle structure and on the other hand exert functional activities. Table 1 lists the different lipoprotein classes with their associated lipoproteins and lipid composition.

Table 1. Lipoprotein classification. Size in nm, density in kg/l, structural and functional apolipoproteins and the lipid composition in percentages are displayed for chylomicrons (CM), very low-density lipoproteins (VLDL), low-density lipoproteins (LDL) and high-density lipoproteins (HDL). TG = triglycerides, CE = cholesteryl ester, FC = free cholesterol, PL = phospholipids.

lipoprotein	diameter (nm)	density (kg/l)	apolipoproteins		components (-%)				
			structural	functional	apo	TG	CE	FC	PL
CM	<10 ⁴	<1,000	B48	A4, A5, C1-3, E	2	90	2	1	5
VLDL	50	<1,005	B100	A5, C1-4, E	10	54	13	7	16
LDL	21	<1,063	B100		23	4	41	11	21
HDL	8	<1,125	A1	A2, A4, A5, C4, E	42	5	13	5	35

1.1 Exogenous lipoprotein metabolism

The exogenous lipoprotein metabolism represents the postprandial route of lipids, namely from food to metabolically active organs for storage or combustion. Digestion of lipids starts in the proximal part of the small intestine, the duodenum. Pancreatic juices and bile enter the intestinal lumen via the hepato-pancreatic ampulla in which bile induces the formation of micelles with ingested lipids. Such micelle assembly allows hydrolysis by pancreatic lipases and consequent release of FFA and monoacylglycerol. Via diffusion, *fatty acid transport proteins* (FATPs) and *cluster of differentiation 36* (CD36), FFAs and monoacylglycerols are shuttled into epithelial cells and transported in the cytosol by ligation to *fatty acid binding proteins* (FABPs). Cholesterol and other dietary sterols are taken up via *Niemann-Pick-C 1-like 1* (NPC1L1) into enterocytes and are esterified to CEs. *ATP-binding cassette*

transporter G5 (ABCG5) and ATP-binding cassette transporter G8 (ABCG8) in the apical enterocyte membrane are able to excrete cholesterol and phytosterols back into intestinal lumen, thereby regulating net cholesterol uptake.

In general, the lipid absorption mainly takes place in the proximal parts of the small bowel. Recently, the small intestinal microbiota was shown to influence the digestive and absorptive capacity of enterocytes by interfering with expression of e.g. CD36 and FATPs.{2} At the *endoplasmic reticulum (ER)*, TGs, CEs and PLs are packaged into CMs, a process catalyzed by *microsomal triglyceride-transfer protein (MTTP)* and loaded with ApoB48. TG-rich chylomicrons are released into the lymph via *Ductus thoracicus* and enter the blood circulation in which they partake in apolipoprotein and lipid exchange across lipoprotein species (described in 1.2). CMs which belong to the TG-rich lipoproteins (TRLs) are targeted by endothelial-bound lipoprotein lipase (LPL) in order to release fatty acids (FAs) for uptake into metabolically active tissues e.g. heart, muscle, brown adipose tissue (BAT) or for storage in white adipose tissue (WAT) (Figure 1). The remaining TG-poor CM remnants are cleared from the circulation by *LDL receptor (LDLR)/LDLR-related protein 1 (LRP1)*-mediated uptake into the liver which requires an enrichment of the remnant lipoproteins with the receptor ligand ApoE.{3, 4}

1.2 Endogenous lipoprotein metabolism

The endogenous lipoprotein metabolism describes the endogenous formation of TRLs by the liver, namely VLDL, which sustain lipid supply in pre-prandial conditions (Figure 1). VLDL synthesis in the liver is similar to the intestine, as MTTP regulates particle assembly at the ER. In contrast to chylomicrons that contain ApoA48, VLDL are characterized by carrying ApoB100. The TG content of VLDL is reduced by LPL-mediated hydrolysis and the remaining intermediate density lipoproteins (IDLs) acquire ApoE which makes them susceptible for clearance by the liver. IDL are also targeted by hepatic lipase (HL) which further decreases the TG content leading to the formation of LDL. LDL can be internalized by the liver via LDLR/LRP1. Then, LDLR-bound LDL is endocytosed and degraded within lysosomes. By uptake and degradation of LDL, cellular cholesterol levels increase which inhibits *sterol regulatory element-binding proteins (SREBPs)* and consequently LDLR and *proprotein convertase subtilisin/kexin type 9 (PCSK9)* synthesis. PCSK9 determines if LDLR is degraded or restored at membrane surface, thus mediating lipid clearance from the blood and recently developed drugs inhibiting PCSK9 paved new ways in treating cardiovascular disease (CVD).{5}

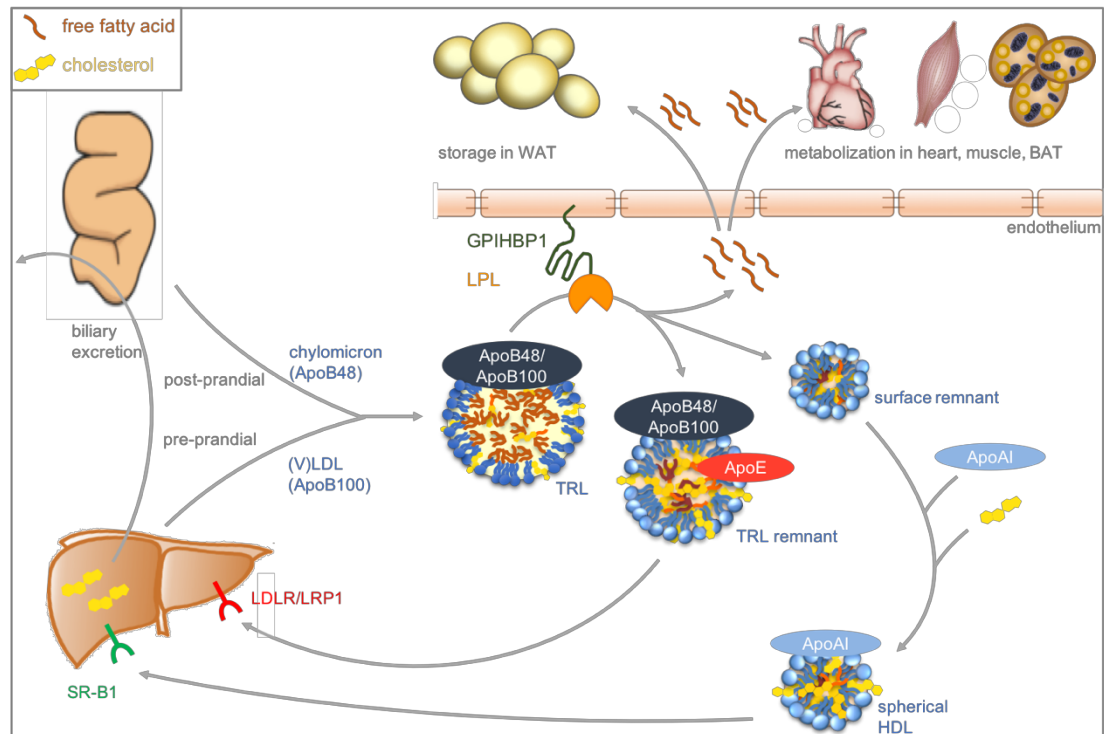


Figure 1. Lipoprotein Metabolism. TG-rich lipoproteins (TRLs) can derive from the intestine, then called chylomicrons, after ingestion of exogenous lipids and are characterized by the presence of ApoB48. In fasted states the liver produces TRLs, namely the VLDL particles, which carry ApoB100. The lipoproteins are targeted by the lipoprotein lipase (LPL) which is anchored to the endothelium via *glycosylphosphatidylinositol anchored high-density lipoprotein binding protein 1* (GPIHBP1). Lipolytic cleavage of TGs from TRL particles results in release of free fatty acids which are taken up by white adipose tissue (WAT) for storage or metabolized in heart, muscle or brown adipose tissue (BAT). The remaining TRL remnants acquire ApoE and are cleared by the liver in an LDLR/LRP1-mediated manner. During TRL hydrolysis, the particle shrinks and a surplus of PLs detaches which forms the so-called surface remnant. According to the *surface remnant theory*, it can fuse with ApoA1 and take up peripheral cholesterol, thereby contributing to reverse cholesterol transport via SR-B1-dependent excretion via the liver.

1.3 Reverse cholesterol transport

HDL particles present unique features among the lipoproteins as they facilitate the reverse cholesterol transport (RCT) and thereby cholesterol excretion in the form of bile acids. HDL particles have the highest density within the different lipoproteins (Table 1) and are characterized by the presence of ApoA1 which is synthesized in the liver and in the intestine. The multi-step formation of mature HDL starts with secretion of discoidal HDL harboring ApoA1, ApoE (and, if generated by liver, ApoA2) which then fuse with CEs and PLs leading to the formation of mature HDL. *ATP-binding cassette transporter A1* (ABCA1) facilitates efflux of cholesterol and PLs from hepatocytes, enterocytes, macrophages and other cells and mutations in ABCA1 result in hypoalphalipoproteinemia and CE depositions (Tangier's disease).

Discoidal HDL can also be generated by the lipolysis of TRLs in which TG hydrolysis leads to a shrinkage in particle size. A surplus of PLs occurs which, according to the *surface remnant theory*, encapsulates from the TRL particle and forms a so-called

PL-rich surface remnant (Figure 1).{6, 7} By fusion with ApoA1, these surface remnants implement HDL functionalities and contribute to RCT.

Furthermore, pre- β HDL are generated by interconversion of mature HDL. Namely, HDL processing by transfer proteins (described in 2.2) and remodeling by HL, endothelial lipase (EL) and *scavenger receptor-B1* (SR-B1) brings about lipid-poor pre- β HDL that can again contribute to reverse cholesterol metabolism. In an SR-B1-mediated mechanism, cholesterol-rich HDL particles dispense cholesterol into the liver where they are converted into bile acids (Figure 1). Via the *bile canaliculus*, bile acids are secreted into the gut lumen to contribute to lipid digestion and 90% of bile is re-internalized into the entero-hepatic cycle. Another newly discovered mechanism for bile-independent cholesterol excretion is mediated via the *transintestinal cholesterol excretion pathway* (TICE).{8-10}

2 Regulatory molecules mediating lipoprotein metabolism

2.1 Apo-lipoproteins

In general, apolipoproteins can be categorized in structural and functional components of lipoproteins. At least in humans, ApoB48 is exclusively secreted by the intestine and thus is the signature apolipoprotein of intestinal-produced CMs. Enterocytes also express ApoA1 and ApoA4, which are loaded onto CMs. Together with ApoC2 and ApoA5, ApoA4 is an important regulator of LPL function and thus the presence of these positive LPL regulators are necessary to prevent hypertriglyceridemia.{11, 12} ApoC3, however, is a negative regulator of LPL activity, especially when LPL is bound to *glycosylphosphatidylinositol anchored high-density lipoprotein binding protein 1* (GPIHBP1), and thus missense variants in the ApoC3 gene are linked to TG-lowering effects.{13, 14} Besides an intracellular contribution to TG metabolism, ApoA5 was described to enhance TRL hydrolysis by generating proximity of TRL and LPL through binding to LPL-anchoring proteins on the surface of endothelial cells, and furthermore, by enhancing receptor-mediated TRL remnant clearance by the liver.{15-18}

As mentioned above, VLDL carry ApoB100. LDL structure is also maintained by the presence of ApoB100, as it is generated by intravascular degradation of VLDL. During intravascular lipolysis, exchange of apolipoproteins and lipids between the different lipoprotein classes occurs. Whereas CMs transfer ApoA1, ApoA4, ApoC and PLs to HDL particles, they receive ApoE from HDL. In addition, VLDL particles fuse with ApoE and ApoC which they acquire from HDL and the presence of ApoE allows clearance by the liver via LDLR/LRP1.{3, 19-21}

2.2 Transfer proteins

In addition to exchange of apolipoproteins, lipid transfer also contributes to dynamic interconversion of lipoproteins and thereby mediates lipid homeostasis in the blood circulation. Transport of cholesterol in the blood is facilitated by esterification and incorporation into the core of lipoproteins. Only 30% free cholesterol is comprised in the circulation which mainly localizes in the PL mono-layer of lipoproteins. Lecithin-cholesterol acyltransferase (LCAT) mediates the conversion of cholesterol to CE by transferring a FA from a PL to free cholesterol. Although dysfunction of LCAT results in substantial HDL-C decrease, no association with coronary heart disease (CHD) are reported in humans with a hetero- or homozygotic loss of function mutation.{22, 23} HDL-CE are targeted by cholesterol ester transfer protein (CETP) which, as the name indicates, transfers CE from HDL particles to ApoB-containing lipoproteins and, in turn, TGs from ApoB-containing lipoproteins to HDL. Inhibition of CETP in clinical trials reduced the CVD risk, mainly by lowering non-HDL-C levels. {24-27} Apart from CE and TG transfer, phospholipid transfer protein (PLTP) facilitates shuttling of PL between different lipoproteins. Briefly, in exchange with free cholesterol, PLTP catalyzes the movement of PL from VLDL to HDL, thus affecting HDL-C levels and atherosclerosis progression in mice.{28-30} Altogether, PLTP, LCAT and CETP are main players in determining HDL-C levels in the circulation and are of therapeutic interest to advance cholesterol homeostasis in the blood.

2.3 Lipases

The LPL family consists of three important members, namely LPL, EL and HL, which all contribute to hydrolysis and remodeling of lipoproteins. The different members vary in their mode of action, preferring hydrolysis of TGs or PLs, respectively, and in their specificity of targeted lipoproteins (Table 2). The distinct substrate specificity is due to differences in the lid lesion area.{31-34} All members contribute to maintaining cholesterol and lipid homeostasis in the circulation; however, compensatory mechanisms are likely to occur in states of dysfunction of one member. For instance, EL and HL both present high PL activity and are able to substitute each other in their function. EL shows high lipolytic activity towards PLs, however, it is also able to hydrolyze TGs that might indicate that EL is also able to compensate a LPL loss.{35-37}

Endogenous inhibitors of the LPL family prevent overactivity of lipases and, thus are considered as potential therapeutic targets to modulate plasma lipid parameters. Current research focusses on blocking the *angiopoietin-like proteins* (ANGPTLs), thereby promoting lipase activity and treating hyperlipidemia. Inactivating mutations

in ANGPTL4 were found to correlate with reduced risk of CVD and clinical trials using monoclonal antibodies directed against ANGPTL3 are ongoing.{38-41}

Table 2. Members of the LPL family. Size (in kDa), expression pattern, targeted lipoproteins and lipase activity of lipoprotein lipase (LPL), endothelial lipase (EL) and hepatic lipase (HL).

lipase	size (kDa)	expressed in	main target	lipase activity	
				TG	PL
LPL	56	adipocytes, skeletal muscle, cardiac muscle	TRL	+++	+
EL	68	endothelium, smooth muscle cells, macrophages	HDL	+	+++
HL	65	hepatocytes, macrophages	LDL, HDL	++	+

2.3.1 Lipoprotein lipase

LPL was first isolated and characterized from rat heart in 1955 by Korn ED.{42} Two LPL molecules form a head-to-tail dimer which ensures proximity of the substrate binding site at the C-terminus with the lipolytic active site at the N-terminus.{43} LPL presents high affinity to hydrolyze TGs, mainly from TRLs and it requires the presence of ApoC2 as co-factor for its action.{44, 45} LPL is expressed mainly by adipocytes, skeletal and cardiac muscle, as they rely on FA oxidation, and is presented on the endothelial surface by linkage to *heparan sulfate proteoglycan* (HSPG) or GPIHBP1, facing the vascular lumen. TRLs carrying ApoC2 are bound to LPL and TGs are hydrolyzed in order to free FAs for uptake into underlying tissues (Figure 1). Due to its high presence and TG specificity, LPL forms the rate-limiting enzyme in coordinating plasma TG levels and LPL activity was negatively correlated with plasma TG levels in mice and human.{46, 47}

Endogenous inhibitors of LPL are formed by the ANGPTL family, as mentioned in 2.3. Nevertheless, ANGPTLs can modulate lipase activity in different ways depending on the organ of action. In post-prandial conditions, ANGPTL3 is secreted by the liver and inhibits LPL in BAT and muscle, whereas LPL in WAT is not affected. As a result, ingested lipids are taken up by WAT in order to store lipids for upcoming fasting periods. Explanation for the tissue-specific mechanisms need to be clarified, however, ANGPTL8 seems to be a possible mediator in pre-/post-prandial regulation of LPL.{48}

2.3.2 Endothelial lipase

As the name indicates, EL is mainly expressed in endothelial cells of various tissues and was firstly characterized by two independent groups in 1999.{49, 50} It presents a size of 68 kDa and is activated by cleavage into its active form by the proprotein convertase.{51, 52} EL gene shares 44% amino acid homology to LPL and 41% to HL, however, it highly differs in its lipolytic action. EL preferentially hydrolyzes PLs

from HDL particles that might be due to a highly different lid lesion sequence compared to LPL and HL which determines the specificity of the lipase. EL is secreted from endothelial cells where it can exert its functionalities.

On the one hand, it displays heparin-binding properties which allows attachment to HSPG on the endothelial surface. On the other hand, it captures lipoproteins via its lipid-binding-properties. Besides its lipolytic function, EL impacts on vascular lipoprotein metabolism by a non-lipolytic, bridging function which promotes lipoprotein incorporation. ANGPTL3 was described as endogenous inhibitor of EL as it competes with binding of EL to HSPG by displaying an HSPG binding site itself.{53} Both functionalities of EL contribute to modulating plasma HDL-C levels in mice and humans, however, its impact on RCT is controversially discussed and no associations of EL activity with CVD could yet be drawn.{54-56}

As well as its dual functional roles, EL shows dual locations of action which both might influence atherosclerosis development. By being expressed in the vasculature and taking part in lipid remodeling, it contributes to lipoprotein metabolism and thus indirectly to atherosclerosis. Additionally, it was also found to be expressed within the vessel wall by smooth muscle cells and macrophages and affecting monocyte adhesion and cholesterol accumulation in atherosclerotic plaques that was shown to directly promote atherosclerosis progression.{57-60} However, the existing studies are controversial, as Ko et. al could not obtain pro-atherogenic effects of EL loss in mouse models of atherosclerosis (ApoE^{-/-} and LDLR^{-/-}) despite increased HDL-C concentrations.{61} Yet, in the current state of research, conflicting results are described when investigating EL impact on atherosclerosis development.

2.3.3 Hepatic lipase

HL is 65 kDa in size and almost exclusively expressed by hepatocytes, with minor expression in macrophages. Similar to EL, HL presents dual functionalities: besides its lipolytic activity, it functions as a ligand for CM remnants which is important for effective clearance by the liver.{62, 63} The lipolytic activity of HL targets TGs and PLs and drives the conversion of IDL to LDL, thus further decreasing TG levels in plasma. Furthermore, HL impacts on HDL metabolism as TG-rich HDL are transformed to TG-poor HDL by HL action. Therefore, on the one hand HL acts to regenerate HDL, however, on the hand side it generates LDL, a profound risk factor for atherosclerosis. In mice, HL deficiency was found to be athero-protective, whereas in humans homozygous loss-of-function mutations were associated with increased risk of CVD.{54} So far, it remains unclear how HL could be targeted for treating dyslipidemias.

3 Brown adipose tissue (BAT) metabolism

Brown adipose tissue (BAT) is an adipose tissue implementing non-shivering (adaptive) thermogenesis in order to maintain the body temperature. It was reported to be active especially in hibernating mammals and in newborns in order to effectively cope with cold stress. By using chemical energy, heat is produced independently of muscle shivering.^{64} In humans, BAT was long thought to be inactive in adulthood, however, in 2009, several studies identified its presence and possible reactivation by fluorine-18-deoxyglucose-positron emission tomography (FDG-PET-CT) and found an inverse correlation of BAT presence with body-mass-index (BMI).^{65-69} Furthermore, repeated cold exposure in humans was shown to positively influence metabolism, thereby raising profound interest in understanding BAT physiology as it is a promising target to therapeutically interfere with high incidence of adiposity and associated diseases.^{70, 71}

Moreover, cold exposure also stimulates the conversion of white into beige adipose tissue (“beigeing”) (Figure 2), especially in subcutaneous fat depots. The beigeing process refers to formation of brown-like adipocytes within WAT which can originate from precursor cells or transdifferentiate from white adipocytes.^{72-74} Activating BAT is a promising target to treat metabolic disease as its activity demands high nutrient turnover and thus positively influences blood lipid parameters. However, inducing the conversion of white into beige adipocytes would furthermore lead to a favorable reduction in white adipocyte mass, which, in excess, induces a state of low-grade, chronic inflammation.^{75}

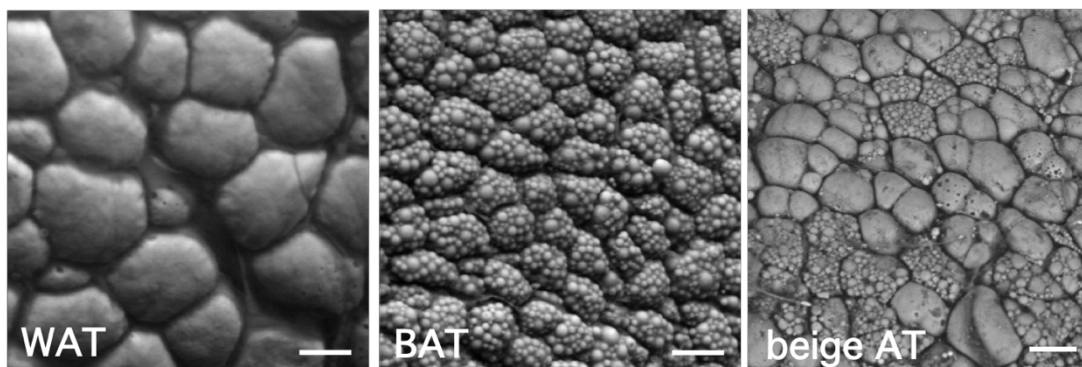


Figure 2. Morphology of white, brown and beige adipose tissues of mice. White adipose tissue (WAT) is characterized by a single lipid droplet within each cell, whereas brown adipose tissue (BAT) harbors multiple smaller lipid droplets within each cell. Beige adipose tissue (AT) presents an intermediate phenotype with uni- and multi-locular cells. Pictures obtained via electron microscopy are derived from publication by Bartelt and Heeren, 2014.^{76}

3.1 Activation of brown adipose tissue

In states of activated thermogenesis, brown and beige adipocytes demand high nutrient supply in order to maintain heat production. Thermogenic adipocytes express β 3-adrenergic receptors that are activated by norepinephrine, which is released in

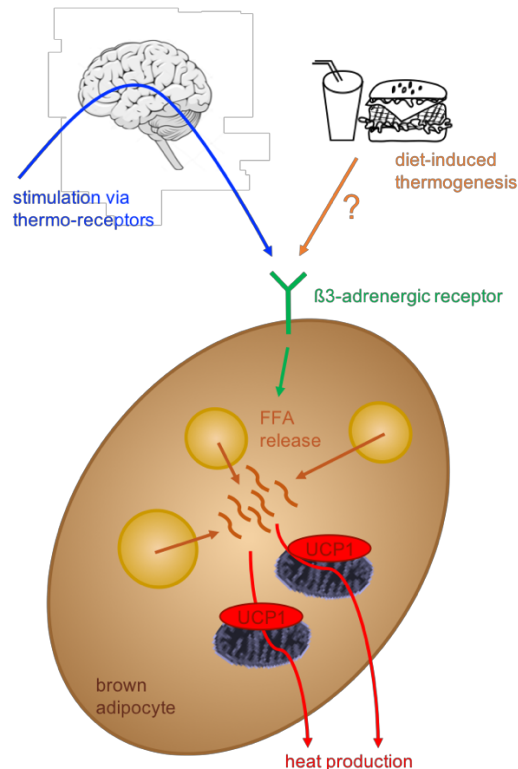
response to different stimuli by nerves from the sympathetic nervous system (Figure 3). Thermoreceptors in the skin sense the environmental temperature and signal via the central nervous system to BAT once temperature deceeds the thermoneutral zone. The thermoneutral zone describes the environmental temperature in which an organism does not need to combust energy in order to maintain body temperature. Furthermore, adaptive thermogenesis is activated in post-prandial conditions, by the meal itself. The mechanisms of diet-induced thermogenesis are not yet completely understood.

Intracellularly, adrenergic stimulation of β_3 - receptors activate a G_s -coupled signaling cascade which results in an elevated cAMP concentration in the cell which in turn leads to activation of protein kinase A (PKA) (Figure 3). PKA activation mobilizes FAs from lipid droplet-stored TGs. FAs are shuttled to mitochondria and metabolized to generate reduction equivalents that are necessary to establish a proton gradient across the mitochondrial membrane via the complexes of the respiratory chain reaction. The presence of the *uncoupling protein 1* (UCP1), allows the uncoupling of proton transfer from adenosine triphosphate production. Besides mobilization of FAs, PKA activates transcription factors resulting in expression of e.g. thermogenesis-related genes like *Ucp1*, *peroxisome proliferator-activated receptor gamma coactivator 1-alpha* (*Pgc1 α*) and *type 2 iodothyronine deiodinase* (*Dio2*).{77} *Pgc1 α* expression further contributes to adaptive thermogenesis by inducing *Ucp1* and a set of key genes important for mitochondrial function.{78} DIO2 converts the inactive form of thyroid hormone, thyroxin (T_4), into the active triiodothyronine which also contributes to enhancement of *Ucp1* expression.{76} It becomes obvious that once BAT is activated, several mechanisms are initiated to instantly actuate effective thermogenesis.

In order to sustain prolonged BAT activation, intracellular lipid stores have to be replenished through uptake of lipids and glucose from the circulation. In an insulin-dependent manner, upregulation of glucose transporter *Glut4* and of genes important for lipid processing and uptake is induced.{79} Mainly due to the lipolytic activity of LPL, circulating TRLs are targeted, thereby releasing FAs that are shuttled to adipocytes via CD36 for replenishing lipid storages. Although BAT induces glucose uptake, generation of energy in thermogenic adipocytes mainly relies on FA oxidation.{80, 81} Interestingly, the glucose uptake does not lead to its oxidation but glucose is used for *de novo* FA synthesis in states of high BAT activation. Measurements of BAT activity in humans depend on FDG-PET-CT scans with glucose as tracer molecule which might therefore, underestimate the presence of thermogenic active tissues in humans as the uptake of lipids is not detected.

Figure 3. Activation of brown adipocytes.

Cold stress is sensed via thermoreceptors and signal via the central nervous system to the brown adipose tissue. Noradrenalin release activates β 3-adrenergic receptors leading to activation of a cAMP- and PKA-dependent intracellular signaling cascade. Also, consumption of food activates adaptive thermogenesis via the β -3 receptors, however, details of the underlying mechanism remains elusive. PKA activation induces release of FAs into the cytoplasm which are then shuttled to mitochondria and metabolized. Due to the presence of *uncoupling protein 1* (UCP1), electron transfer from the respiratory chain is uncoupled and heat is produced to sustain body temperature.



3.2 Immunometabolism in BAT

The term immunometabolism describes on the one hand the impact of immune cells on metabolic homeostasis and on the other hand metabolic pathways of immune cells and consequences for their function. Gokhan Hotamisligil was the first to describe the expression of immune mediators by adipocytes and their impact in metabolic disease.{82} In states of positive energy balance, excess nutrients are stored within adipocytes leading to hypertrophy. Adipocyte hypertrophy triggers expression of pro-inflammatory cytokines, which in turn recruits and activates immune cells. Moreover, hypertrophy, adipocyte necrosis, tissue hypoxia and ER stress possibly contribute to the onset of inflammation.{68}

Macrophages make up the largest proportion of immune cells within adipose tissue and upon obesity in mice and humans, macrophages increase dramatically.{83-86} In lean conditions, anti-inflammatory or alternatively activated M2 macrophages that contribute to tissue homeostasis are abundant.{87} However, in obesity, the pro-inflammatory environment induces a polarization towards the pro-inflammatory or classically activated M1 macrophages which release pro-inflammatory cytokines such as IL-6.

Overall, the shift towards an inflammatory environment during obesity contributes to insulin resistance, increasing the risk for type 2 diabetes.{88} In the last decade, interest has emerged in studying the macrophages in BAT and beige adipose tissue and their potential contribution to adaptive thermogenesis. A very recent publication

was able to show that cold housing induced secretion of CXCL14 by brown or beige adipocytes, thereby finding a mechanism for the recruitment of M2 macrophages to the adipose depots.{89}

One possible hypothesis as to how macrophages contribute to thermogenesis was raised by the group of Ajay Chawla: that M2 macrophages within BAT and beige adipose tissue contribute to energy expenditure by producing catecholamines.{90, 91} However, their theory was proven to be wrong by independent groups in the field of BAT research.{92} Another possible mechanisms explaining how BAT-resident macrophages contribute to thermogenesis might be how they modulate tissue innervation and thereby energy expenditure.{93} Overall, recent interest has been focused on elucidating the role of macrophages for adaptive thermogenesis. M2 presence in activated BAT or beige adipose tissue, as described before, was shown by several independent groups, however, if and how M2 macrophages contribute to energy expenditure is still unclear.

4 Impact of thermogenesis on lipoprotein metabolism and its relevance for atherosclerosis development

4.1 Atherosclerosis development and treatment options

Atherosclerosis describes a disease of lipid accumulation and inflammation within the vessel wall and ranks among the diseases affecting the majority of the world's population. In brief, hypercholesterolemia drives accumulation of cholesterol within intima infiltrating macrophages, leading to the formation of foam cells. Together with induction of inflammatory processes, the smooth muscle cells start to proliferate and start to form plaques. In later stages of disease progression, plaques convert to fibrotic plaques due to apoptotic foam cells and smooth muscle cells. Depending on the size of the plaque, blood flow can be disturbed or rupture of the plaque can lead to the formation of a thrombus which by circulating via the vessels can lead to closure in other organs such as brain or heart.{94-96}

The initiation of atherosclerosis development starts already in youth and precariousness about its progression relies on multiple influence factors. The pitfall about atherosclerosis is its quiescent progression enduring over decades which might at one stage result in deadly cardiovascular events. Each year, 17.9 million people die from CVD which accounts for one third of deaths worldwide (http://www.who.int/cardiovascular_diseases/en/), therefore, substantial need for therapeutic interventions are required.{97} The multiple factors influencing atherosclerosis development were taken together to calculate the Framingham risk score which estimates the 10-year risk to suffer a cardiovascular event.{98} In addition

to age, smoking and blood pressure, total plasma cholesterol and HDL-C are consulted to predict the CVD risk.

Statins are a broadly used therapy to lower LDL-C levels by inhibiting the *3-hydroxy-3-methylglutaryl-CoA reductase* (HMGCR), the rate-limiting step in the endogenous cholesterol synthesis. However, statin tolerance and the emerging need to drastically reduce LDL-C pushes research towards new therapeutic approaches. By using combination therapies of statins with other drugs, the LDL-C lowering effect often can be promoted. Other cholesterol lowering drugs comprise blockage of the NPC1L1 transporter, bile acid aggregators and PCSK9 inhibitors.{99, 100} Another possible target to improve plasma lipid status is to raise the HDL-C. Clinical studies tested niacin and CETP inhibitors which effectively raised HDL-C, however, did not show significant effects on reducing CVD.{101, 102}

4.2 BAT activation modulates lipoprotein metabolism

As described earlier, BAT activation mainly requires combustion of lipids that are taken up from the blood circulation, thus correcting hyperlipidemia and obesity in mice and men.{46, 66, 67, 103, 104} The high intravascular lipolysis rate during non-shivering thermogenesis interferes with the lipoprotein metabolism and, therefore, activating BAT in patients with lipoprotein disorders such as atherosclerosis became of interest as a treatment option.

Interestingly, studies investigating the role of BAT activation for the development of atherosclerosis yielded conflicting results. On the one hand, in mice with a humanized lipoprotein profile (*E3L.CETP*), prolonged BAT activation was shown to reduce cholesterol levels and attenuate the progression of atherosclerosis.{105} Here, Berbée et. al could explain these findings by a reduction in LDL-C levels and an improved clearance of CM remnants by the liver. On the other hand, cold activation in two other mouse models, that are used to study atherosclerosis in mice (*ApoE*^{-/-} and *LDLR*^{-/-}), resulted in an accumulation of lipoprotein remnants in the plasma and consequently, accelerated atherosclerotic plaque progression.{106} Of note, mice lacking ApoE or the LDLR have an impairment of CM remnant clearance by the liver and in turn CM remnants accumulate within the plasma. This could explain the different study outcomes as high CM remnant concentration within the blood in turn, potentially accelerates plaque progression. Thus, due to high CM turnover during cold, cold housing of *ApoE*^{-/-} and *LDLR*^{-/-} mice led to increased atherosclerosis progression.{106} Nevertheless, in response to cold, Dong et al. observed an overall improvement of plasma lipid levels in wildtype mice, e.g. lower LDL-C and TG concentrations. Additionally, hepatic expression of *Ldlr* and *ApoE* were upregulated

during cold housing of wildtype mice, underpinning their importance in cold-induced improvement of plasma lipid parameters.

Intriguingly, in the previously mentioned *E3L.CETP*-humanized mouse model, besides an inverse association with LDL-C, BAT activation also positively correlated with HDL-C levels. Already after 4 weeks of β 3-receptor agonist treatment (CL), a significant increase in HDL-C was observed which was prolonged over the study duration of 10 weeks (Figure 4. a) In addition, the HDL-C was inversely correlated with the atherosclerosis burden (Figure 4. b). So far, the mechanistic relation of this BAT-HDL-C-atherosclerosis axis was not investigated and was addressed in my PhD project.

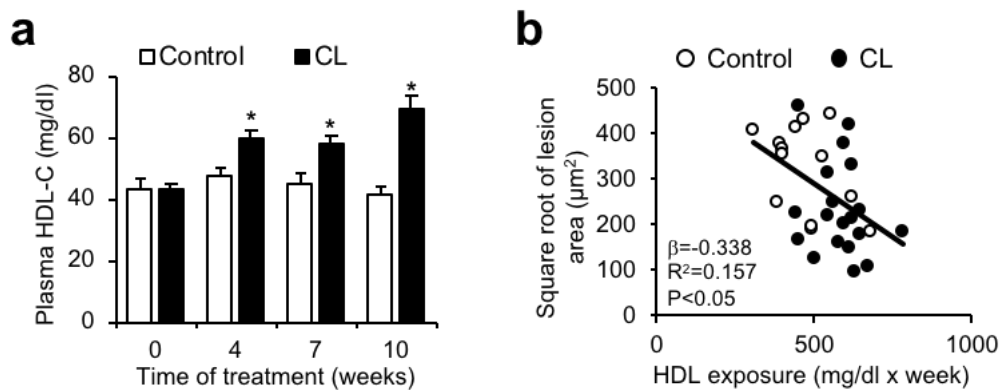


Figure 4. BAT activation elevates HDL-C and thereby attenuates atherosclerosis progression. Mice with humanized plasma lipid profile (*E3L.CETP*) were treated with a β 3-receptor agonist (CL316,243) or vehicle control for 10 weeks. **a** Fasting plasma HDL-C levels after 4,7,10 weeks of CL316,243 treatment. **b** Correlation of HDL-C with size of atherosclerotic plaques after vehicle or CL316,243 treatment. Graphs obtained from Bartelt et. al, 2017.^{107}

Part D Aims of the study

Since the discovery of active BAT in adult humans, research has focused on unraveling BAT and beige adipocyte physiology in order to find new therapeutic options for treating dyslipidemias and consequently atherosclerosis development. In addition to the sympathetic tone, tissue-resident macrophages present in adipose tissues have been discussed to modulate energy expenditure by thermogenic adipocytes. In my thesis project, I wanted to study the role of intravascular lipid processing for macrophage function in thermogenic adipose tissues in response to cold exposure. Therefore, macrophages from BAT and inguinal WAT should be separated from endothelial cells and adipocytes and the lipid composition in each cell population should be determined by an LC-MS/MS-based approach. Furthermore, polarization of the macrophages should be investigated by gene expression analysis of macrophage markers using qPCR approaches.

In addition, in the group of Prof. Heeren it has been shown that BAT-induced LPL activity mediates lipoprotein remodeling, especially altering TG composition in TRL and HDL particles (PhD thesis of Dr. rer. nat. Clara John). The second aim of my project was to investigate the role of BAT activation for HDL metabolism and the impact of LPL and EL during cold intervention. In functional studies, HDL metabolism and RCT should be studied in mice acclimated to the cold. In addition to the impact of LPL and SR-B1 for HDL metabolism during cold, the role of EL in adaptive thermogenesis should be elucidated. EL is known to specifically hydrolyze PLs of HDL particles, which led to the hypothesis that EL might impact on BAT-induced lipoprotein remodeling. In order to study the function of EL during adaptive thermogenesis, *in vivo* HDL turnover experiments and a RCT assay in cold-housed mice lacking the EL should be performed. To study potential alterations in lipid remodeling of EL knockout mice during cold interventions, the lipid composition of HDL particles from transgenic mice should be determined using mass spectrometry.

Altogether, this study should characterize immunometabolic consequences in thermogenic adipose tissues, and, it should address how BAT activity modulates intravascular HDL-dependent cholesterol transport.

Part E Materials and methods

All reagents, solutions, buffers, kits and devices are listed in Part I.

1 Mice

All animal experiments were approved by the Animal Welfare Officers of the University Medical Center Hamburg-Eppendorf (UKE) and Behörde für Gesundheit und Verbraucherschutz Hamburg. Mice were received from Charles River or bred in-house at the UKE animal facility of the UKE. Mice were bred and raised on 22° C room temperature, had unlimited access to standard chow diet (Altromin) and water and were exposed to a light/dark cycle of 12 hours. For all experiments, male mice between the age of 10-14 weeks were used. For experiments in which mice were housed at thermoneutrality (30° C), mice were allowed an adaptation time of 4-5 days to deactivate thermogenic activity. Then, if not stated otherwise, 30° C or 6° C housing temperature, respectively, was conducted 7 days prior to organ harvest. Mice were fasted 4 hours prior to organ harvest if not stated otherwise and anaesthetized with a lethal dose (15 µl/g body weight) of ketamine (10 mg/ml)/xylazine (2%) in 0.9% NaCl. Cardiac blood was withdrawn using EDTA-filled syringes (5 µl of 0.5 M EDTA), organisms were perfused with ice-cold heparin-enriched PBS (10 U/ml heparin) and organs were excised and stored accordingly.

The following mouse lines were used for the following experiments:

- C57BL/6J wildtype mice (ordered from Charles River)
- adipocyte-specific knockout of LPL (aIKO) (fabp4-Cre+lpl-floxed animal generated of crossing B6.129S4-Lpltm1l1g/J with B6.Cg-Tg(Fabp4-cre)1Rev/J (Jackson Laboratory) {108}
- *Scarb1*^{-/-} mice carrying a global deletion of SR-B1 (ordered from Jackson Laboratory; Ben Harbor; ME; #03379)
- Endothelial lipase knockout mice (eIKO) carrying a global deletion of *Lipg* (ordered from Jackson Laboratory; Ben Harbor; ME; # 005681)

Ordered knockout mice were used for establishing a colony within the UKE animal facility. Wildtype littermate animals were used as controls.

2 Analysis of parenchymal cells, non-parenchymal cells and macrophages from adipose tissues

12-14 week old male C57BL/6 mice were fasted for 4 hours prior to organ harvest. The mice were perfused as described above before intrascapular BAT and inguinal

WAT was excised and stored in PBS on ice. Organs of 5 mice were pooled for MACS®-based cell separation.

2.1 MACS®-based cell separation

5 organs per group were thoroughly chopped up with operation scissors and digested at 37° C for 40 min in PBS with 1.8 U/mg dispase II, 0.19 U/mg collagenase D and 1 mM CaCl₂. Received cell suspension was filtered through a 100 µm cell strainer and centrifuged (600 x g, 5 min, 4° C). The bigger, floating adipocytes were collected and later on combined with the last remaining flow through, thereby allowing analysis of smaller preadipocytes (last flow through) and mature adipocytes (floating fraction). Rest of supernatant was discarded, cell pellet resuspended in ice-cold MACS® buffer (PBS with 2 mM EDTA, 0.5% BSA, 2 mM glucose), passed through a 40 µm cell strainer and centrifuged (600 x g, 5 min, 4° C). Pellet was resuspended in MACS® buffer and by using antigen-specific magnetic beads specific cell populations could be extracted due to their expression of marker surface molecules: *cluster of differentiation B1* (CD11B⁺) on the surface of macrophages and *cluster of differentiation 31* (CD31⁺) on endothelial surface. Briefly, cells which were then coupled to magnetic beads via an antigen-antibody complex were retrieved in LS columns, attached to a magnetic rack, and then after detachment from magnetic rack flushed out. First, CD11B⁺ cells were extracted, second, CD31⁺ cells and remaining flow through was considered to mainly contain preadipocytes which were then pooled with mature adipocytes collected previously. Cell fractions were then applied to mRNA isolation (Part E-2.2), DNA quantification (using Quant-iT™ dsDNA Broad-Range Assay; according to manufacturer's protocol) and lipidomic analysis (Part E-2.3).

2.2 RNA extraction, cDNA synthesis and relative real-time PCR

Cell pellets from MACS®-isolated cell fractions were resuspended in peqGOLD TriFast™, RNA was precipitated by using chloroform {109} and extracted using NucleoSpin RNA II Kit. RNA concentration was determined with NanoDrop and 400 ng of RNA was used to reverse transcribe it into cDNA by using High Capacity cDNA Reverse Transcription Kit, according to manufacturer's protocol. Received cDNA was applied to quantitative real-time PCR with an ABI Prism 7900HT Sequence Detection System. The TaqMan Assay-on-Demand™-Primer sets displayed in Table 1 were used to analyze the different cell populations. Measured values were normalized to large ribosomal protein P0 (*36b4*) housekeeper gene and relative gene expression was calculated via the 2- $\Delta\Delta$ Ct-method.{110}

Table 3. TaqMan™ probes used for analysis in MACS®-isolated cell fractions.

Genname	Assay-on-Demand™	Genname	Assay-on-Demand™
<i>mAdipoq</i>	Mm00456425_m1	<i>mIi10</i>	Mm00439616_m1
<i>mArg1</i>	Mm00475988_m1	<i>mLipg</i>	Mm00495368_m1
<i>mCd36</i>	Mm00432403_m1	<i>mLpl</i>	Mm00434764_m1
<i>mEmr1</i>	Mm00802530_m1	<i>mPgc1a</i>	Mm00447183_m1
<i>mGpihbp1</i>	Mm01205849_g1	<i>mUcp1</i>	Mm00494069_m1
<i>mIi6</i>	Mm00446190_m1		

2.3 UPLC-ESI-QqTOF-method for semi-quantitative lipid analysis

The extraction of cell fractions was performed according to the method developed by Bligh and Dyer. {111} 100 µl of adipocyte fractions (total volume of 5 ml) or CD11B⁺ and CD31⁺ cell pellet which was resuspended in 100 µl MACS buffer was brought together with 500 µl BHT-containing methanol, 60 µl of 1/10 diluted internal standard (

Table 8) and 350 µl chloroform. Then the samples were sonicated (20% for 30 seconds) before 550 µl chloroform and 450 µl water was added and vortexed for 30 seconds. Then, samples were centrifuged at 3,000g, 6° C for 15 minutes. The lower phase was transferred to a new tube and vaporized in order to be dry. The remaining pellet was resuspended in eluent B (Table 4) and transferred to a glass vial with teflon-coated crimping cap and stored at -80° C until measurement.

The lipid extracts from the different cell populations were applied to Dionex3000 UPLC (ultra high-performance liquid chromatography), coupled to an ESI-UHR-QqTOF (electro spray-ultra high resolution-quadrupole-quadrupole-time-of-flight) maXis3G mass spectrometer. Table 4 depicts measurement parameters of the apparatus and the solvent gradient used in the measurements.

Raw data was analyzed with the softwares DataAnalysis 4.0 and TargetAnalysis 1.3 provided by Bruker. First, each measurement was calibrated to lock mass (hexakis(1H, 1H, 2H-perfluoroethoxy)phosphazene), and second, to external standard which was applied via syringe pump in calibration segment (ESI-L-tuning-mix). For each individual lipid class, an internal standard was added during lipid extraction. Such reference substances, MS/MS spectra and the data bank of LIPID MAPS® (www.lipidmaps.org) was used to identify lipid species.

Table 4. Parameters of mass spectrometer.

Pump parameter			
duration	29 min		
mobile phase	eluent A: water, 5 mM ammonium acetate eluent B: methanol/isopropanol, 4/6, v/v, 5 mM ammonium acetate		
flow rate	0.3 ml/min		
solvent gradient	time [min]	eluent A [%]	eluent B [%]
	0	20	80
	2	13	87
	8	13	87
	10	5	95
	20	1	99
	21	1	99
	22	20	80
	29	20	80
Column oven parameter			
column	Kintex C18, Phenomenex (150 x 2.1 mm; 1.7 µm)		
temperature	55 ° C		
Parameter of mass spectrometer			
mode	full scan		
mass spectra	50 - 1250 m/z		
rolling average	off		
spectra Rate	3.00 Hz		
segments	2 Segment 1: 28 min, divert valve to source, not marked as calibration segment Segment 2: 1 min, divert valve to wast, marked as calibration segment (for external calibration with ESI-L tuning mix running viasyringepump at 20 µL/h)		
Segment 1		Segment 2	
Mode		Mode	
save line spectra only		save line spectra only	
use maximum intensity		use maximum intensity	
absolute threshold (per 1000 sum.)	10 cts.	absolute threshold (per 1000 sum.)	10 cts.
absolute threshold	27 cts.	absolute threshold	27 cts.
peak summation width	5 pts.	peak summation width	5 pts.
Source		Source	
end plate offset	500 V	end plate offset	500 V
capillary	4500 V	capillary	4500 V
nebulizer off		nebulizer off	
dry gas	9 l/min	dry gas	9 l/min
dry temp	200 °C	dry temp	200 °C
source 1-2		source 1-2	
Tune		Tune	
Transfer		Transfer	
funnel 1 RF	200.0 Vpp	funnel 1 RF	400.00 Vpp
isCID energy	0.0 eV	isCID energy	0.0 eV
multipole RF	200.0 Vpp	multipole RF	400.00 Vpp
Quadrupole		Quadrupole	
ion energy	4.0 eV	ion energy	4.0 eV
low mass	200.00 m/z	low mass	200.00 m/z
Collision Cell		Collision Cell	
collision energy	8.0 eV	collision energy	8.0 eV
collision RF	400.0 Vpp	collision RF	1200.0 Vpp
transfer time	75.0 µs	transfer time	80.0 µs
pre pulse storage	10.0 µs	pre pulse storage	10.0 µs
MS/MS		MS/MS	
auto MS/MS on		auto MS/MS on	
no. of precursors	3	no. of precursors	3
width	+/- 5	width	+/- 5
absolute (per 1000 sum.)	3000 cts.	absolute (per 1000 sum.)	3000 cts.
absolute (per 1000 sum.)	8259 cts.	absolute (per 1000 sum.)	8259 cts.
relative	80 %	relative	80 %
active exclusion on		active exclusion on	
exclude after	3 Spectra	exclude after	3 Spectra
release after	0.20 min	release after	0.20 min
reconsider precursor if current int./previous int.	5.0	reconsider precursor if current int./previous int.	5.0
smart exclusion on	5 x	smart exclusion on	5 x
Calibration		Calibration	
tuning mix MMI-TOF (ESI) (pos)		tuning mix MMI-TOF (ESI) (pos)	
zooming	+/- 0.1 %	zooming	+/- 0.1 %
calibration mode	enhanced quadratic	calibration mode	enhanced quadratic
Software			
Chromeleon®, 6.80 Hystar 3.2 MicroTOF Control SR2 DataAnalysis 4.0 TargetAnalysis 1.3			

3 Plasma analysis

3.1 Blood withdrawal

For performing plasma and lipoprotein analysis, retro-orbital blood puncture was used to collect blood. Samples were stored on ice and serum collected via centrifugation (10,000 g, 4° C, 10 min).

3.2 Lipoprotein profiling

The different lipoprotein fractions were separated via *fast-performance liquid chromatography* (FPLC). Superose 6 Increase 10/300 GL was used as a separation column with a flow rate of 0.4 ml/min. Received 40 fractions were collected in a MegaBlock® plate in a volume of 500 µl and applied for triglyceride and cholesterol measurement (described in 3.3).

3.3 Measurement of triglycerides and cholesterol in plasma

The Cholesterol CHOD-PAP and Triglyceride GPO-PAP kits were used to determine the cholesterol and TG concentration, respectively. Briefly 20 µl of each FPLC fraction was diluted with 80 µl PBS and mixed with 200 µl reagent. After 10 min incubation at 37° C, extinction was measured at 540 nm. Different Precipath® standards were run accordingly and used to calculate a linear regression.

3.4 ApoA1 ELISA

Mouse plasma was applied to ELISA technique in order to quantify the amount of ApoA1 protein. Therefore, the ELISA Kit for ApoA1 was used and measurement was performed according to manufacturer's protocol.

3.5 UPLC-ESI-QqTOF-method for semi-quantitative lipid analysis in HDL particles from plasma

The extraction of plasma samples was performed according to the method developed by Bligh and Dyer.^{111} 160 µl of FPLC fractions (described in 3.2) was brought together with 500 µl BHT-containing methanol, 25 µl of 1/10 diluted internal standard (Table 8) and 350 µl chloroform and vortexed for 30 seconds. Then 550 µl chloroform and 450 µl water was added and vortexed again. Then samples were centrifuged at 3,000g, 6° C for 15 minutes. The lower phase was transferred to a new tube and vaporized in order to be dry. The remaining pellet was resuspended in eluent B (Table 4) and transferred to a glass vial with teflon-coated crimping cap and stored at -80° C until measurement. Measurement was performed as described in 2.3.

4 Gene expression in tissue

10-30 mg tissue was shock frozen in liquid nitrogen and stored at -80° C until RNA extraction. 500 µl peqGOLD TriFast™ and metal beads were added and homogenized

by using Tissue Lyzer 2 time for 2 min, 20 s⁻¹. Tissue homogenate was applied to RNA extraction as described in Part E, 2.2. As *house keeper* gene for tissue samples *TATA-box binding protein (Tbp)* was used.

Table 5. TaqMan™ probes used for analysis in BAT, inguinal WAT and liver.

Gencode	Assay-on-Demand™	Gencode	Assay-on-Demand™
<i>mAbca1</i>	Mm00442646_m1	<i>mCyp7b1</i>	Mm00484157_m1
<i>mAbca1</i>	Mm00442646_m1	<i>mDio2</i>	Mm00515664_m1
<i>mAbcg1</i>	Mm00437390_m1	<i>mGlut4</i>	Mm01245502_m1
<i>mAbcg1</i>	Mm00437390_m1	<i>mHmgcr</i>	Mm01282499_m1
<i>mAbcg5</i>	Mm00446249_m1	<i>mLdlr</i>	Mm00440169_m1
<i>mAbcg8</i>	Mm00445970_m1	<i>mLpl</i>	Mm00434764_m1
<i>mAngptl3</i>	Mm00803820_m1	<i>mLrp1</i>	Mm00464608_m1
<i>mAngptl4</i>	Mm00480431_m1	<i>mPgc1a</i>	Mm00447183_m1
<i>mApoa1</i>	Mm00437568_g1	<i>mSrebf2</i>	Mm00550338_m1
<i>mApoe</i>	Mm01307193_g1	<i>mTbp</i>	Mm00446973_m1
<i>mCd36</i>	Mm00432403_m1	<i>mUcp1</i>	Mm00494069_m1
<i>mCyp7a1</i>	Mm00484150_m1		

5 HDL turnover

5.1 Experimental setup

Wildtype mice and indicated knockout mice (alKO, *Scarb1*^{-/-}, elKO) were housed at 6° C for 7 days before they received an injection of double-labeled HDL particles into the tail vein. The particles circulated for a total duration of 5 hours during which animals were all housed at 30 °C. Blood from the tail vein was collected 10, 30, 60 and 120 and 300 min after injection. After 300 min cardiac blood was collected, organism perfused with ice-cold heparin-enriched PBS (10 U/ml heparin) and organs excised.

5.2 Generation of labeled HDL particles

To generate double-labeled HDL particles C57Bl/6 mice were fasted for 4 hours and then plasma was extracted. HDL particles were isolated by applying ultracentrifugation as described by Havel et. al. [112] Extracted HDL particles were labeled *ex vivo* with ¹²⁵I-tyramine cellobiose in the apolipoprotein compartment and ³H-cholesterol oleyl ether (³H-CEt) in the lipophilic compartment. [113, 114] Briefly, ³H labeling of HDL particles was realized by exchange from donor liposomal particles in the presence of human plasma CETP. [115] Then, the donor particle were separated from the ³H-HDL by flotation. Next, ApoA1 on the labeled HDL was exchanged with ¹²⁵I-NMTC-apo A-1. [114] After incubation at 37° C for 1 hour, the doubly labeled HDL were extracted from the unbound ApoA1 by flotation and exhaustively dialyzed against PBS containing 1 mM EDTA.

5.3 Quantification of radioactivity in plasma and tissues

To determine ¹²⁵I, plasma samples from different timepoints (10, 30, 60, 120, 300 min after injection) and tissue samples were directly measured by using γ -scintillation detector. Plasma samples obtained from different timepoints and tissue samples were

applied to lipid extraction described by Dole.^{116} 50 μ l or up to 267 mg tissue was filled up with PBS to 667 μ l, 3333 μ l mixture of 78% isopropyl alcohol, 20% heptane and 2% sulfuric acid (0.5 M) was added and homogenized with an ultra-turrax. After allowing a 10 min incubation period, samples were centrifuged (1,000 rpm, 10 min). 1 ml of upper phase was mixed with 10 ml scintillation solution, vortexed, rested for 1h and measured with β -scintillation detector.

6 *In vivo* reverse cholesterol transport assay (RCT)

6.1 Experimental setup

Wildtype mice and eIKO mice were housed at 6° C or 30° C for 5 days. 3 days prior to the start of the experiment, mice were switched to a cholesterol-enriched western-type diet (ssniff EF R/M acc. TD88137 mod.). Then, they received an intraperitoneal injection of *ex vivo* labeled peritoneal macrophages. The groups were then housed for another 2 days at 6° C or 30° C, respectively, and feces was collected over the duration after the injection.

6.2 Generation of *ex vivo* labeled macrophages

C57Bl/6 mice were intraperitoneally injected with 1 ml thioglycolate in order to recruit macrophages to the peritoneum. 4 days after the injection, macrophages were isolated by washing the peritoneum with 5 ml 37° C warm DMEM.^{117} Obtained cells were pelleted (700 g, 10 min), erythrocytes lysed (3 min at room temperature) and remaining cells pelleted again (700 g, 10 min). Then, macrophages were cultured in T75 flasks (7.5×10^6 cells per flask). After a resting period, macrophages were *ex vivo* labeled with ³H-cholesterol (100 kBq per mouse) and acetylated LDL (200 μ g/ml) in DMEM (1% FCS). After 24 hours, cells were washed and 1×10^6 labeled cells were injected per mouse using 0.55 x 25 mm 24G x 1" Gr. 17 needles to avoid sheer stress.

6.3 Quantification of radioactivity in plasma, tissues and feces

Feces was collected after 24 hours (collected at day 1 after injection) and 48 hours (between day 1 and 2 after injection) and dried overnight. A homogenate in PBS was generated and 667 μ l were applied to lipid extraction via Dole.^{116} Also plasma and tissue samples were extracted via Dole as described in Part E, 5.3.

Part F Results

1 Characterization of parenchymal cells, non-parenchymal cells and macrophages from thermogenic adipose tissues

The activity of thermogenic adipose tissues, mainly BAT and inguinal WAT is influenced by several mechanisms, as introduced in paragraph 1.3. Physiologically, the most well-known and studied factor regulating the activity of non-shivering thermogenesis is the ambient temperature. The thermoneutral zone, in which non-shivering thermogenesis is completely dormant, varies between humans and mice. While the thermoneutral zone for humans is reached around 22° C, mice need to be housed at 30° C to inactivate non-shivering thermogenesis. When the ambient temperature falls under thermoneutrality, brown adipocytes activate non-shivering thermogenesis by uncoupling electron transfer from the respiratory chain, thereby maintaining core body temperature.

The activation of brown adipocytes via thermoreceptors and consequently neuronal impulses to β 3-adrenergic receptors occurs instantly and alterations of gene expression in browning-related genes can be detected already 24 hours after cold housing of mice. {46, 79} Maintenance of non-shivering thermogenesis demands nutrient uptake from the circulation. In the PhD thesis of Kristina Gottschling, the internalization of TRL particles into inactive and activated BAT was studied. She established MACS® separation technique in the Heeren lab which allowed isolation of brown adipocytes, CD31⁺ endothelial cells and CD11B⁺ macrophages from brown adipose tissue. The method was applied to study the cell type-specific uptake of TRL into BAT from warm and 24 hours cold-housed mice. After a 24 hours cold stimulus, increases in TRL uptake were measured in adipocytes, endothelial cells and interestingly, also in macrophages from BAT. In line with higher lipid uptake, macrophages also expressed higher levels of genes important for lipid processing (*Lpl*, *Cd36* and *Fabp4*). In summary, Kristina Gottschling's work indicated that macrophages within the BAT changed their lipid demands upon activation of thermogenesis. To unravel whether the observed changes in lipid uptake dynamics had further consequences, my PhD work focused on further elucidating the lipid remodeling of adipose tissue macrophages taking place during states of thermogenic activity. Furthermore, it was also investigated whether adipose tissue macrophages change their functionality upon lipid remodeling and might thereby influence the activity of thermogenesis.

For this purpose, we designed an experimental setup in which mice were housed under thermoneutral conditions (30° C) or in a cold environment (6° C) for 7 days.

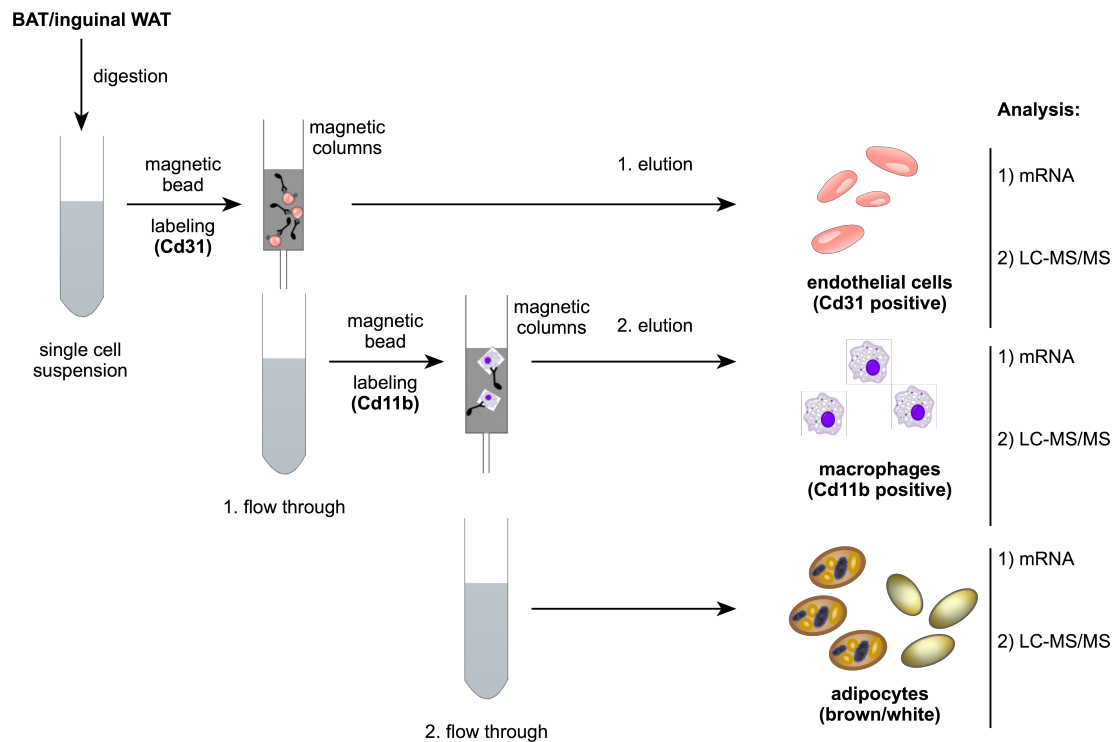


Figure 5. MACS® separation of parenchymal cells, non-parenchymal cells and macrophages from adipose tissues. BAT and inguinal WAT were digested to receive a single cell suspension. Via magnetic bead labeling positive selection of CD31⁺ cells was performed which represents the endothelial cells. Flow through was applied to a second positive magnetic bead selection of CD11b⁺ cells, namely the macrophages. The remaining flow through was considered to mainly contain adipocytes. All cell fractions were applied to mRNA analysis and lipid composition was determined using an LC-MS/MS-based approach.

Sustained cold exposure does not only activate brown adipocytes but also leads to generation of beige adipocytes in WAT, especially within inguinal WAT. In order to evaluate the differences or similarities in brown and beige adipose tissue functionality, BAT and inguinal WAT were harvested from thermoneutral housed mice or mice housed at 6° C for 7 days. Then, cells were applied to MACS® separation technique to isolate different cell population within the adipose tissue (Figure 5). In the following section, cold-induced lipid remodeling within adipocytes, endothelial cells and macrophages from BAT and inguinal WAT was investigated. Furthermore, characteristics of adipose tissue macrophages were analyzed by determining their gene profile, thereby proposing their polarization.

1.1 Separation of parenchymal cells, non-parenchymal cells and macrophages from thermogenic adipose tissues using MACS® technique

In order to characterize macrophages from thermogenic inactive and active adipose tissues, MACS® separation technique was used to extract macrophages, endothelial cells and adipocytes from BAT and inguinal WAT of mice housed under thermoneutrality or cold. Figure 5 depicts the different steps of the isolation process that allowed positive selection of certain cell populations based on their expression of

specific surface molecules: CD31 on endothelial cells, CD11B on macrophages. Briefly, antigen-specific magnetic beads (CD31) were incubated with the single cell

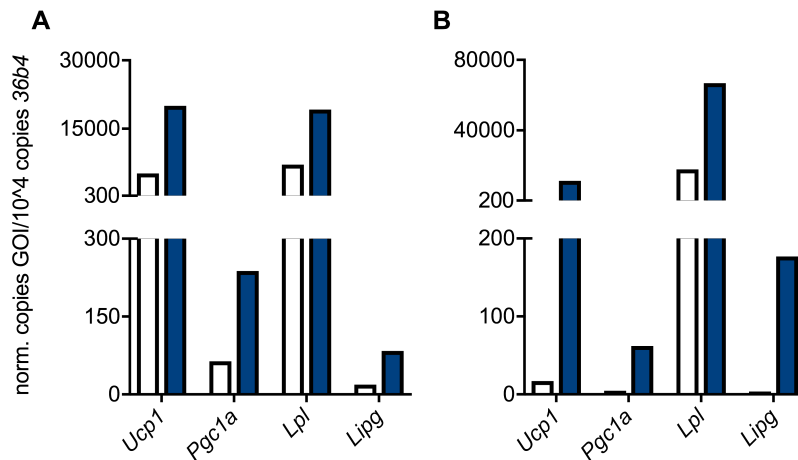


Figure 6. Gene expression of browning-related genes in MACS-isolated adipocytes. Mice were housed at thermoneutrality (30°C) or exposed to the cold (6°C) for 7 days. Organs of 5 mice per group were harvested after a 4-hour fasting period. MACS®-based cell separation was performed to isolate endothelial cells (CD31⁺) and macrophages (CD11B⁺). The flow through depleted of endothelial cells and macrophages was considered to contain mainly adipocytes. After mRNA and cDNA preparation, gene expression analysis was conducted using TaqMan® technique. **A.** Gene expression in BAT. **B.** Gene expression in inguinal WAT. Bars represent mean of one experiment with 4 technical replicates. Expression is normalized to house keeper gene *ribosomal protein, large, P0 (36b4)*.

suspension, received after tissue digestion. Then, antigen-antibody captured cells were restrained in magnetic columns. The flow through was applied to a second magnetic bead isolation, specific for CD11B. The second remaining flow through was considered to mainly harbor adipocytes. After the isolation, endothelial cells, macrophages and adipocytes were applied to mRNA analysis.

In order to validate the cold intervention, cold-induced genes were analyzed in the adipocyte fraction isolated from BAT and inguinal WAT. Marker genes for activated adaptive thermogenesis, namely *Ucp1* and *Pgc1a*, were profoundly induced after 7 days of cold exposure in adipocytes from BAT (Figure 6. A) and inguinal WAT (Figure 6. B). Furthermore, LPL (*Lpl*) and EL (*Lipg*), lipolytic genes important for cleaving FAs from circulating lipoprotein particles, were highly upregulated (Figure 6. A). Expression levels of genes were approximately doubled after 7 days of cold housing in BAT, except *Lipg* which was induced 4-fold (Figure 6. A). In inguinal WAT, mRNA transcripts of *Lpl* were 6-7 times higher in cold-housed mice compared to thermoneutral housing (Figure 6. B). During thermogenesis, *Ucp1* induction was more pronounced in inguinal WAT (approximately 500 times higher to thermoneutral control) compared to the induction seen in BAT during thermogenesis (Figure 6. B). Expression levels of *Pgc1a* and *Lipg* in adipocytes isolated from inguinal WAT were almost undetectable in thermoneutral conditions, however, cold-housing upregulated expression more than 10 times (Figure 6. B).

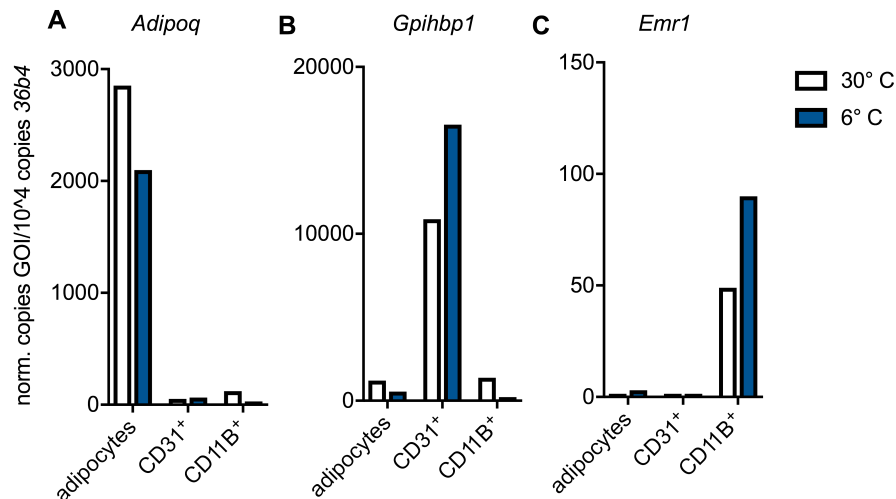


Figure 7. Gene expression in MACS®-isolated adipocytes, endothelial cells and macrophages from BAT. Mice were housed at thermoneutrality (30°C) or exposed to the cold (6°C) for 7 days. Organs of 5 mice per group were harvested after a 4-hour fasting period. MACS®-based cell separation was performed to isolate endothelial cells (CD31⁺) and macrophages (CD11B⁺). The flow through depleted of endothelial cells and macrophages was considered to contain mainly adipocytes. After mRNA and cDNA preparation, gene expression analysis was conducted using TaqMan® technique. **A.** Adiponectin (*Adipoq*) expression in adipocytes, endothelial cells (CD31⁺) and macrophages (CD11B⁺). **B.** *Gpihbp1* expression in adipocytes, endothelial cells (CD31⁺) and macrophages (CD11B⁺). **C.** F4/80 (*Emr1*) expression in adipocytes, endothelial cells (CD31⁺) and macrophages (CD11B⁺). Bars represent mean of one experiment with 4 technical replicates. Expression is normalized to house keeper gene ribosomal protein, large, P0 (36b4).

Furthermore, signature genes for different cell types were determined to control for the purity of isolated cell populations. In thermoneutral- and cold-housed mice, the expression of adiponectin, which expression is characteristic for brown, beige and white adipocytes, was almost exclusively found in the BAT-extracted adipocyte fraction, whereas the endothelial and macrophage fraction presented very low abundance of *Adipoq* transcripts (Figure 7. A). Endothelial cells express *Gpihbp1*, encoding for a protein anchoring LPL to the surface of the endothelial layer in the vasculature, thereby facilitating the uptake of cleaved fatty acids to adipose tissue. The MACS®-isolated endothelial fraction (CD31⁺) showed a high expression of *Gpihbp1* compared to adipocyte and macrophage fraction in BAT from mice in either housing condition (Figure 7. B). Nonetheless, we observed an induction of *Gpihbp1* in cold-housed mice compared to thermoneutral-housed mice.

Emr1 encodes the signature surface marker F4/80 in macrophages in which expression was found to be abundant in the MACS®-isolated macrophage fraction (CD11B⁺) (Figure 7. C). In cold-acclimated mice, higher expression levels of *Emr1* within the CD11B⁺ cells were detected. The expression of *Emr1* in adipocytes and endothelial cells was minor, arguing for a high purity of isolated cell populations. In accordance with the results in BAT, also inguinal WAT represented a successful separation of adipocytes, endothelial cells and macrophages via MACS® technique. Adipocytes showed high expression of *Adipoq*, CD31⁺ fraction was enriched in

expression of *Gpihbp1* and isolated CD11B⁺ cells highly expressed *Emr1* (Figure 8). Adipocyte fraction from inguinal WAT represented highly increased expression of *Adipoq* compared to adipocytes isolated from BAT (Figure 8. A and Figure 8. A). Furthermore, cold stimulus increased expression of *Adipoq* in inguinal WAT (Figure 8. A). In summary, mRNA analysis within isolated cell populations from thermogenic adipose tissues revealed high purity of MACS® sorted cell types.

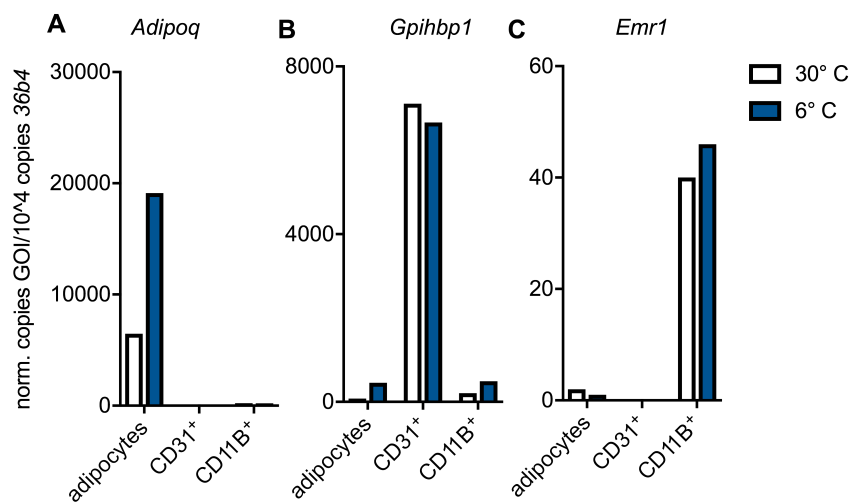


Figure 8. Gene expression in MACS-isolated adipocytes, endothelial cells and macrophages from inguinal WAT. Mice were housed at thermoneutrality (30°C) or exposed to the cold (6°C) for 7 days. Organs of 5 mice per group were harvested after a 4- hour fasting period. MACS®-based cell separation was performed to isolate endothelial cells (CD31⁺) and macrophages (CD11B⁺). The flow through, depleted of endothelial cells and macrophages, was considered to contain mainly adipocytes. After mRNA and cDNA preparation, gene expression analysis was conducted using TaqMan® technique. **A.** Adiponectin (*Adipoq*) expression in adipocytes, endothelial cells (CD31⁺) and macrophages (CD11B⁺). **B.** *Gpihbp1* (*Gpihbp1*) expression in adipocytes, endothelial cells (CD31⁺) and macrophages (CD11B⁺). **C.** F4/80 (*Emr1*) expression in adipocytes, endothelial cells (CD31⁺) and macrophages (CD11B⁺). Bars represent mean of one experiment with 4 technical replicates. Expression is normalized to house keeper gene ribosomal protein, large, P0 (*36b4*).

1.2 Lipid composition in extracted adipocytes from BAT and inguinal WAT

During cold stimulus, activated adipocytes require a high demand of glucose and FAs in order to maintain thermogenesis. Besides mobilization of FAs from lipid droplets within the cell, uptake of lipids from the blood circulation is necessary. FAs cleaved from TRLs or whole lipoprotein particles are taken up by the endothelial cells and shuttled into adipocytes. We analyzed the lipid composition within the separated adipocyte fraction in BAT and inguinal WAT from mice housed at thermoneutrality (30° C) or cold (6° C). Adipose tissues from 5 mice were pooled for isolation process via MACS® technique before lipids were extracted and analyzed via an LC-MS/MS approach (UPLC-ESI-QqTOF-method).

After thermoneutral housing of mice, adipocytes from BAT mainly consisted of TGs (98.4%), whereas phospholipids (phosphatidylcholines (PCs): 1.0%; phosphatidylethanolamines (PEs): 0.2%), CEs (0.1%) and sphingomyelins (SMs) (0.2%) had minor impact (Figure 9. A). Adipocytes isolated from mice housed at 6° C

showed a shift towards lower TG percentage (94.3%) and especially PC (2.7%) and PE (2.1%) percentages increased (Figure 9. B). A similar observation was made when analyzing the lipid composition of adipocytes isolated from inguinal WAT. Housing mice at thermoneutrality resulted in almost exclusive detection of TGs (98.5%) (Figure 9. C). However, cold housing induced a shift towards lower abundance of TGs (90.2%), whereas PCs (3.1%) and other unspecified lipids (others 4.2%) increased in their percentage (Figure 9. D). Taken together, these data indicated a high share of TGs within adipocytes from BAT and inguinal WAT which partly decreased in states of high nutrient demand during thermogenesis.

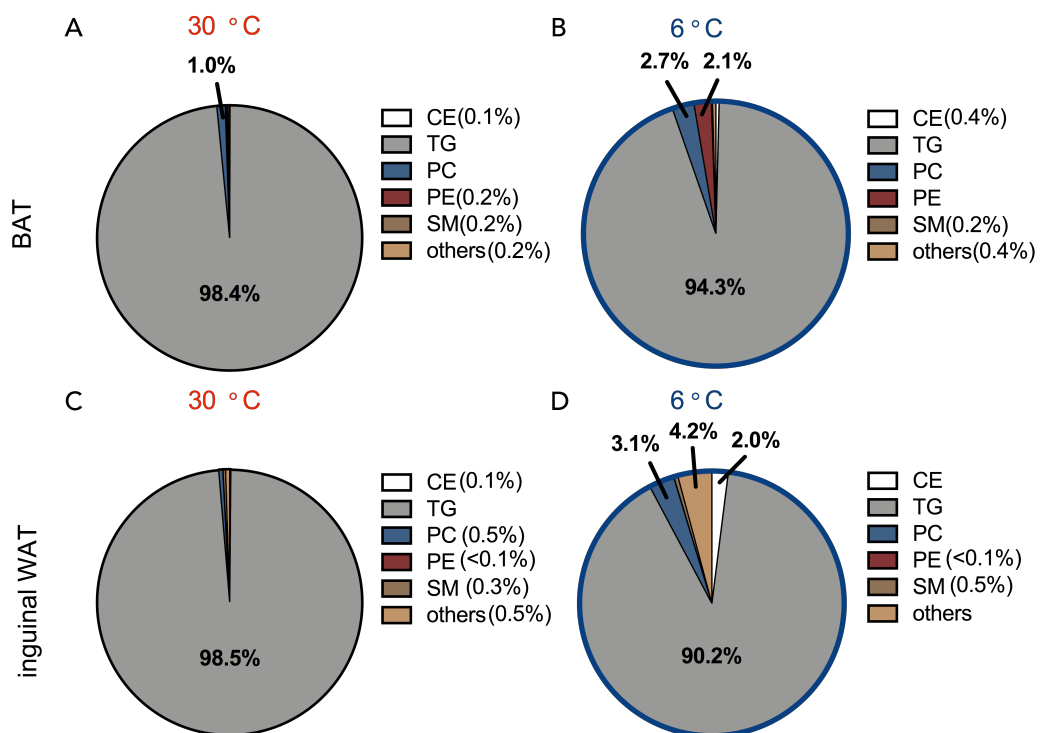


Figure 9. Lipid composition in adipocytes isolated from adipose tissues. Mice were housed at thermoneutrality (30°C) or exposed to the cold (6°C) for 7 days. Organs of 5 mice per group were harvested after a 4-hour fasting period. MACS®-based cell separation was performed to isolate endothelial cells (CD31⁺) and macrophages (CD11b⁺). The flow through, depleted of endothelial cells and macrophages, was considered to contain mainly adipocytes. After lipid extraction via Folch method, extracts were analyzed with and UPLC-ESI-QqTOF-method for semi-quantitative lipid analysis. **A.** Lipid composition in adipocytes isolated from BAT of thermoneutral (30°C) housed mice. **B.** Lipid composition in adipocytes isolated from BAT of mice housed in the cold (6°C) for 7 days. **C.** Lipid composition in adipocytes isolated from inguinal WAT of thermoneutral (30°C) housed mice. **D.** Lipid composition in adipocytes isolated from inguinal WAT of mice housed in the cold (6°C) for 7 days. Indicated value represents percentage of total lipid amount measured per group.

1.3 Lipid composition in isolated endothelial cells from BAT and inguinal WAT

As mentioned above, thermogenic adipose tissues require high nutrient uptake in order to maintain non-shivering thermogenesis. I investigated whether the lipid composition in the endothelium of thermogenic adipose tissue changed in states of highly active lipid trafficking via the endothelial cells. Hence, endothelial cells were

MACS®-sorted from BAT and inguinal WAT from mice housed at thermoneutrality (30° C) and cold (6° C).

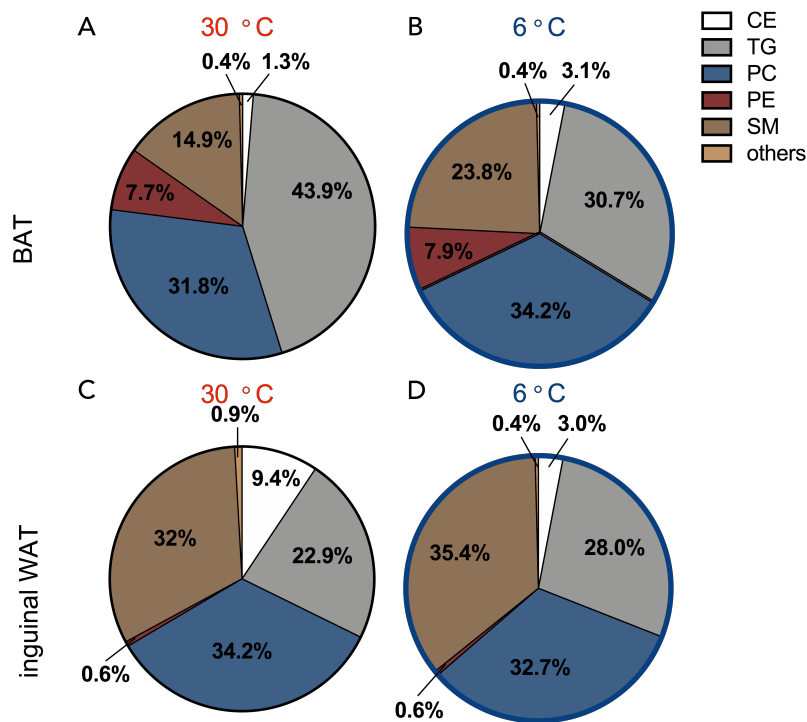


Figure 10. Lipid composition in endothelial cells isolated from adipose tissues. Mice were housed at thermoneutrality (30°C) or exposed to the cold (6°C) for 7 days. Organs of 5 mice per group were harvested after a 4-hour fasting period. MACS®-based cell separation was performed to isolate endothelial cells (CD31⁺) and macrophages (CD11B⁺). The flow through, depleted of endothelial cells and macrophages, was considered to contain mainly adipocytes. After lipid extraction via Folch method, extracts were analyzed with and UPLC-ESI-QqTOF-method for semi-quantitative lipid analysis. **A.** Lipid composition in endothelial cells (CD31⁺) isolated from BAT of thermoneutral (30°C) housed mice. **B.** Lipid composition in endothelial cells (CD31⁺) isolated from BAT of mice housed in the cold (6°C) for 7 days. **C.** Lipid composition in endothelial cells (CD31⁺) isolated from inguinal WAT of thermoneutral (30°C) housed mice. **D.** Lipid composition in endothelial cells (CD31⁺) isolated from inguinal WAT of mice housed in the cold (6°C) for 7 days. Indicated value represents percentage of total lipid amount measured per group.

In BAT of mice housed at thermoneutrality, the majority of lipids within the endothelial cells consisted of TGs (43.9%) (Figure 10. A). The second largest lipid class was represented by PCs (31.8%), followed by SMs (14.9%) and PEs (7.7%). CEs (1.3%) and other detected lipids were negligible. After 7 days of cold exposition, lipid composition within the endothelial cells of BAT changed. PCs (34.2%) assembled the most abundant lipid class (Figure 10. B). The share of TGs decreased to 30.7%, whereas SMs increased to 23.8%. Furthermore, the share of PEs (7.9%) did not change during cold activation, however, CEs formed a part of 3.1%. By analyzing the lipid composition of the endothelium in inguinal WAT, several alterations became obvious when compared to endothelium of BAT. In mice housed at 30° C and 6° C, the TG amount was lower compared to BAT and mildly different between the housing conditions (TG content in 30° C/6° C: 22.9%/28.0%) (Figure 10. C and D). PCs represented approximately one third of total lipids within the endothelium,

independent of the ambient temperature and the adipose tissue depot analyzed (Figure 10). SMs were more abundant in endothelial cells from inguinal WAT compared to BAT, with no profound differences between 30° C- and 6° C-housed mice (Figure 10). In inguinal WAT, only slight amounts of PEs were detected (PEs content in 30° C/6° C: 0.6%/0.6%) and CEs were presented by a share of 9.4% or 3.0% in 30°C or 6° C housing temperatures, respectively (Figure 10. C and D). To summarize, after cold housing, lipid analysis within endothelial cells of adipose tissue showed alterations occurring in BAT, especially in the TG compartment, whereas less pronounced lipid remodeling was detected in endothelial cells from inguinal WAT.

1.4 Analysis of isolated macrophages from BAT and inguinal WAT

Immune cells, especially macrophages, are discussed to contribute to the activation status of brown adipocytes.{90, 92} However, it is still unclear how they sense the activation of thermogenesis and further influence brown adipocyte activity. We addressed the question whether in states of high lipid uptake by thermogenic adipose tissues, macrophages also change their lipid uptake and composition and if that, in turn, alters their polarization.

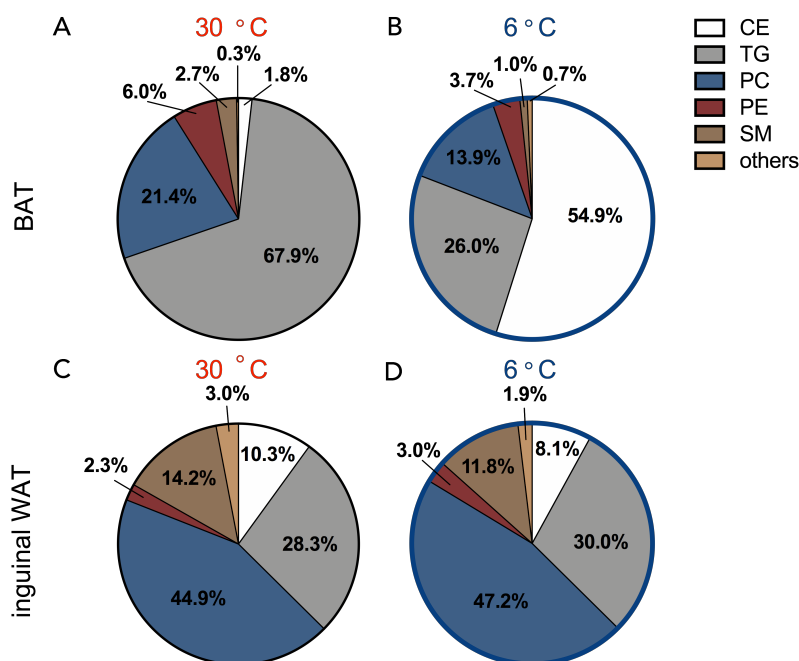


Figure 11. Lipid composition in macrophages (CD11B⁺) isolated from adipose tissues. Mice were housed at thermoneutrality (30°C) or exposed to the cold (6°C) for 7 days. Organs of 5 mice per group were harvested after a 4-hour fasting period. MACS®-based cell separation was performed to isolate endothelial cells (CD31⁺) and macrophages (CD11B⁺). The flow through, depleted of endothelial cells and macrophages, was considered to contain mainly adipocytes. After lipid extraction via Folch method, extracts were analyzed with and UPLC-ESI-QqTOF-method for semi-quantitative lipid analysis. **A.** Lipid composition in macrophages (CD11B⁺) isolated from BAT of thermoneutral (30°C) housed mice. **B.** Lipid composition in macrophages (CD11B⁺) isolated from BAT of mice housed in the cold (6°C) for 7 days. **C.** Lipid composition in macrophages (CD11B⁺) isolated from inguinal WAT of thermoneutral (30°C) housed mice. **D.** Lipid composition in macrophages (CD11B⁺) isolated from inguinal WAT of mice housed in the cold (6°C) for 7 days. Indicated value represents percentage of total lipid amount measured per group.

1.4.1 Lipid remodeling

MACS®-isolated macrophages from BAT and inguinal WAT were applied for lipid analysis via an LC-MS/MS-based approach. In thermoneutral housing conditions, macrophages from murine BAT mainly consisted of TGs (67.9%) (Figure 11. A). The second most abundant lipid class within BAT-isolated macrophages was formed by PCs (21.4%), followed by PEs (6.0%), SMs (2.7%) and CEs (1.8%) (Figure 11. A). After cold-housing of mice, a profound shift in the lipid composition of BAT macrophages occurred. CEs (54.9%) assembled the main lipid share, whereas TGs only accounted for 26.0% of total lipids (Figure 11. B). PCs constituted the third most abundant lipid class (13.9%), followed by PEs (3.7%) and SMs (1.0%) (Figure 11. B).

When analyzing the lipid composition in macrophages isolated from inguinal WAT of thermoneutral- or cold-housed mice, a different fingerprint was observed. Most prominent was the observation that only minor changes occurred in the lipid composition of macrophages from thermoneutral- compared to cold-housed mice (Figure 11. C and D.). During thermoneutrality, macrophages were mainly composed by PCs (44.9%), followed by TGs (28.3%) and SMs (14.2%) (Figure 11. C). Furthermore, CEs accounted for 10.3% of total lipids and PEs for 2.3% (Figure 11. C). A similar composition was determined when measuring macrophages from inguinal WAT of cold exposed mice: PCs (47.2%), TGs (30.0%), SMs (11.8%), CEs (8.1%), PEs (3.0%) (Figure 11. D). In brief, the lipid composition in macrophages from different adipose tissues, namely BAT and inguinal WAT, exhibited profound tissue-specific alterations. In addition, cold-induced changes which occurred in macrophages from BAT, were absent in macrophages from inguinal WAT. Most strikingly was a high increase of CEs within BAT-isolated macrophages from cold-housed mice.

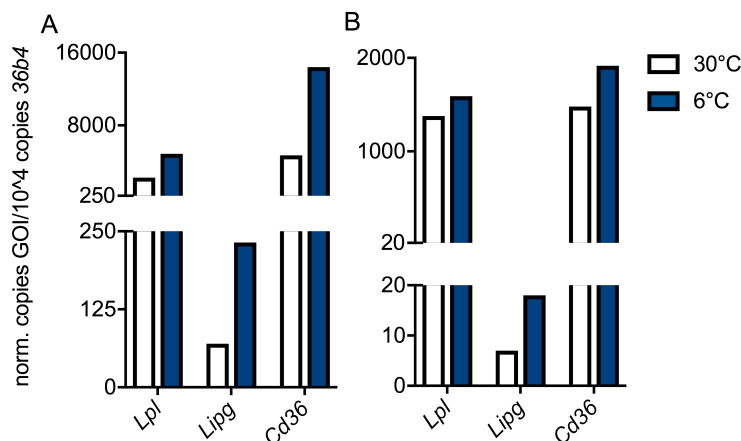


Figure 12. Expression of genes involved in lipid processing in macrophages (CD11B⁺) isolated via MACS® technique. Mice were housed at thermoneutrality (30°C) or exposed to the cold (6°C) for 7 days. Organs of 5 mice per group were harvested after a 4-hour fasting period. MACS®-based cell

separation was performed to isolate endothelial cells (CD31⁺) and macrophages (CD11B⁺). The flow through, depleted of endothelial cells and macrophages, was considered to contain mainly adipocytes. After mRNA and cDNA preparation, gene expression analysis was conducted using TaqMan® technique. **A.** Expression of LPL (*Lpl*), EL (*Lipg*) and CD36 (*Cd36*) in macrophages isolated from BAT of thermoneutral- or cold-housed mice. **B.** Expression of LPL (*Lpl*), EL (*Lipg*) and CD36 (*Cd36*) in macrophages isolated from inguinal WAT of thermoneutral- or cold-housed mice. Bars represent mean of one experiment with 4 technical replicates. Expression is normalized to house keeper gene *ribosomal protein, large, P0 (36b4)*.

In order to elucidate the mechanisms causing different lipid compositions in adipose tissue macrophages, I investigated if genes known to be involved in lipid processing were affected by the different housing conditions. Genes encoding lipases, especially LPL (*Lpl*) are important players in targeting TRLs to maintain nutrient supply. We found that besides expression in adipocytes, MACS®-isolated macrophages from BAT and inguinal WAT expressed high levels of LPL (*Lpl*) and in addition, transcripts of *Lipg* encoding for EL were detected (Figure 12. A). Both lipases showed increased expression upon cold exposure in macrophages isolated from BAT (Figure 12. A). A less pronounced induction of *Lpl* and *Lipg* was observed in macrophages from inguinal WAT (Figure 12. B).

In addition to detection of lipases, also CD36, a FA transporter, was highly expressed by macrophages. In general, one could observe that mRNA transcripts of above-mentioned genes (*Lpl*, *Lipg*, *Cd36*) were profoundly elevated in BAT-isolated macrophages upon cold stimulus (Figure 12. A) which was concomitantly observed in macrophages isolated from inguinal WAT but to a lesser magnitude (Figure 12. B). Taken together, lipid remodeling in adipose tissue macrophages was observed, especially in macrophages from cold-activated BAT which went along with altered expression of genes involved in lipid processing.

1.4.2 Polarization

Taking a conventional look on macrophages, a discrimination between M1 and M2 macrophages can be made with either presenting a pro-inflammatory phenotype or an anti-inflammatory phenotype, respectively. During obesity, adipocyte hypertrophy triggers the release of pro-inflammatory cytokines (e.g. IL-6) which in turn attracts pro-inflammatory macrophages to the adipose tissue resulting in an overall state of low-grade chronic inflammation. Thus, the balance between M1 and M2 macrophages within the adipose depots might contribute to the overall health. To investigate the polarization of MACS®-isolated macrophages from non-activated and activated BAT and inguinal WAT the gene expression of M2 marker genes and the pro-inflammatory cytokine IL-6 was investigated.

In the CD11B⁺ cell fraction isolated from BAT of thermoneutral-housed mice, *Arg1* expression, a marker gene for M2 macrophages, was barely detected, whereas it was tremendously increased during cold stimulus (Figure F9. A). In accordance with the

higher *Arg1* expression, also expression levels of *Il10* increased, an anti-inflammatory cytokine produced by M2 macrophages (Figure F9. A). *Il6* transcripts were detectable in mice housed in thermoneutrality and declined after 7 days cold housing. In inguinal WAT, expression of *Arg1* and *Il6* were much lower compared to the expression in BAT. Their expression levels behaved similar to BAT upon cold stimulation, although induction observed in *Arg1* was much less pronounced (Figure F-9. B). Levels of *Il10* transcript did not differ in macrophages from inguinal WAT between 30° C and 6° C (Figure F-9. B).

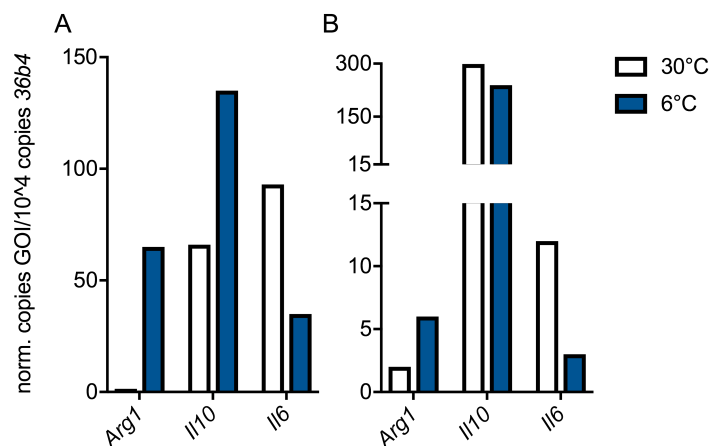


Figure 13. Expression of genes regulating inflammation in macrophages (CD11B⁺) isolated via MACS® technique. Mice were housed at thermoneutrality (30°C) or exposed to the cold (6°C) for 7 days. Organs of 5 mice per group were harvested after a 4-hour fasting period. MACS®-based cell separation was performed to isolate endothelial cells (CD31⁺) and macrophages (CD11B⁺). The flow through, depleted of endothelial cells and macrophages, was considered to contain mainly adipocytes. After mRNA and cDNA preparation, gene expression analysis was conducted using TaqMan® technique. **A.** Expression of arginase 1 (*Arg1*), IL-10 (*Il10*) and IL-6 (*Il6*) in macrophages isolated from BAT of thermoneutral- or cold-housed mice. **B.** Expression of arginase 1 (*Arg1*), IL-10 (*Il10*) and IL-6 (*Il6*) in macrophages isolated from inguinal WAT of thermoneutral- or cold-housed mice. Bars represent mean of one experiment with 4 technical replicates. Expression is normalized to house keeper gene *ribosomal protein, large, P0* (*36b4*).

In summary, these data propose that, especially in macrophages from BAT, M2 marker genes are induced by induction of adaptive thermogenesis, whereas pro-inflammatory cytokine expression is dampened. In future, it will be important to unravel how changes in the lipid composition in response to cold exposure determines the polarization of adipose tissue macrophages.

2 Intravascular alterations in lipoprotein metabolism during thermogenesis

In addition to age, smoking and systolic blood pressure, total cholesterol and HDL-C levels in plasma are consulted to calculate the Framingham risk score that predicts the 10-year risk to suffer a cardiovascular event. BAT activation was effectively shown to reduce cholesterol levels in mice when treated with an agonist specific for β 3-adrenergic receptor.^{105} Berbée et. al could also show a positive correlation of

atherosclerotic lesion area with total cholesterol and (V)LDL-C levels and by activating brown adipocytes (V)LDL-C levels were reduced which was accompanied with smaller lesion areas.

The reduction in (V)LDL-C accounted for approximately 70% of athero-protective functions during BAT activation, 30% of athero-protection during BAT activity could be attributed to an inverse correlation of HDL-C levels with atherosclerotic lesion area.^{107} Although uncertainties about the impact of HDL-C levels for athero-protective functions of HDL remain, clinical trials are ongoing to raise HDL-C levels and to enhance RCT.^{118} Recently, Dr. rer. nat. Clara John demonstrated in her thesis work that pharmacological BAT activation induced by β 3-receptor agonist stimulated RCT in mice, a process that was dependent on LPL. Furthermore, her work highlighted the process of TRL and HDL remodeling which occurred during BAT activation by injecting a β 3-receptor agonist. My work focused on investigating the consequences of cold-activated BAT on HDL metabolism, especially exploring the intravascular turnover of HDL particles and its dependence on BAT-activated lipases.

2.1 Cold-mediated effects on systemic cholesterol metabolism

Under conditions of activated thermogenesis, TGs are hydrolyzed from intracellular lipid droplets of brown adipocytes. In parallel, the activation of extracellular lipases that are located in the intravascular lumen leads to the uptake of FAs and whole TRL particles.^{46} Furthermore, lipolytic cleavage of TRLs generates so-called surface remnants that serve as precursors for HDL maturation. Here, I addressed the question whether high lipolytic activity in BAT leads to alterations in HDL metabolism, thereby effecting lipoprotein remodeling and systemic cholesterol flux.

2.1.1 Effects of thermogenesis on plasma lipid parameters and lipoprotein profiles

In order to assess the impact of a lipolytic environment on systemic cholesterol metabolism, I housed mice either in thermoneutrality (30° C) or in the cold (6° C) for 7 days. After a 4-hour fasting period, blood was withdrawn and plasma lipid parameters and cholesterol levels in the different lipoprotein compartments were determined. Cold stimulation resulted by trend in reduced TG and significant lower cholesterol levels (Figure 14. A and B.). In contrast, similar concentrations for ApoA1 were observed in the plasma of thermoneutral and cold housed mice (Figure 14. C).

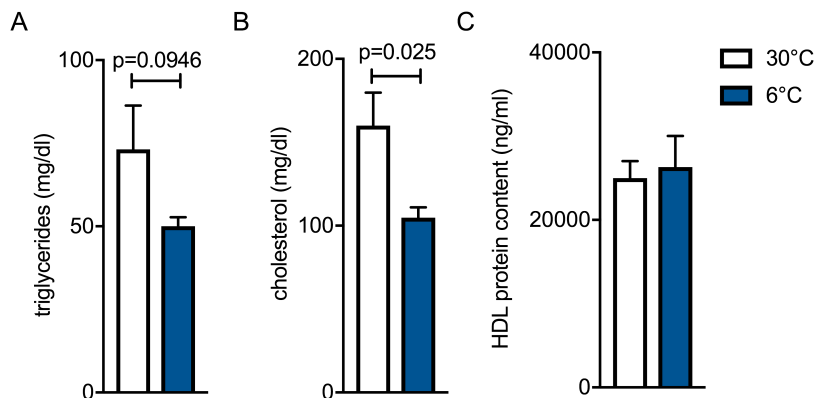


Figure 14. Plasma lipid parameters and ApoA1 concentration in thermoneutral- or cold-housed wildtype mice. Mice were housed at thermoneutrality (30°C) or exposed to the cold (6°C) for 7 days. Plasma lipids were determined after a 4-hour fasting period. **A.** Plasma triglyceride levels in mg/dl. n=4-5 mice. **B.** Plasma cholesterol levels in mg/dl. n=4-5 mice. **C.** ApoA1 concentration in ng/ml in HDL fractionated by using FPLC. n=8 mice. Bars represent mean of indicated number of mice per group with error bars representing \pm SEM. Statistics were performed with Student's t-Test.

To further characterize the cholesterol concentrations in different lipoprotein compartments, plasma was applied to FPLC to fractionate the lipoproteins and measure the cholesterol concentration in each fraction. In the pre-prandial state, reduction in cholesterol could be mainly attributed to a reduction in the HDL fraction (Figure 15. A). Postprandially, after mice received an oil gavage, cold housing showed a similar reduction in HDL-C, however, the decline seemed to be slightly more pronounced in the postprandial compared to the pre-prandial state (Figure 15. B). What this all amounts to is that the cholesterol decrease observed after 7 days of cold-housing was mainly attributed to a reduction in HDL-C independent on pre-or postprandial conditions.

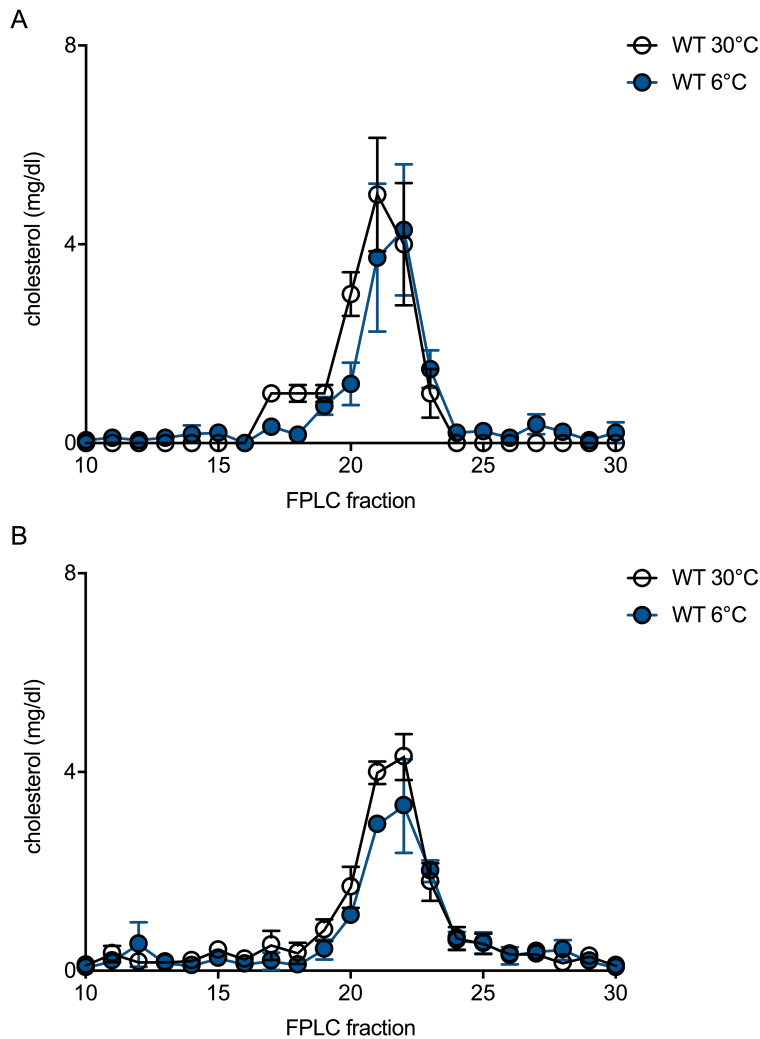


Figure 15. Pre- and post-prandial cholesterol concentrations in FPLC fractions from wildtype mice after cold intervention. Mice were housed at thermoneutrality (30°C) or exposed to the cold (6°C) for 7 days. Pre-prandial plasma lipids were determined after a 4-hour fasting period which was followed by a 200 μ l per mouse corn oil gavage. Postprandial plasma was collected 2 hours after gavage. Plasma was extracted from blood withdrawn by retro-orbital puncture. **A.** Pre-prandial cholesterol concentration in mg/dl in different lipoprotein fractions separated by FPLC. **B.** Post-prandial cholesterol concentration in mg/dl in different lipoprotein fractions separated by FPLC. Dots represent means of 4 mice per group and error bars indicate \pm SEM.

2.1.2 Effects of thermogenesis on HDL turnover in pre- and postprandial conditions

To maintain nutrient supply during adaptive thermogenesis, lipolytic processes are increased which was seen in profound mRNA upregulation of LPL in adipocytes (Figure 12) and EL in endothelial cells (Supplementary Figure 1) after 7 days of cold housing. The findings, that an LPL-dependent remodeling of TRL and HDL particles occurs during adaptive thermogenesis, which were generated in the PhD thesis of Clara John, raised the question, whether BAT activity impacts on systemic HDL metabolism. Therefore, I housed mice at thermoneutrality or cold for 7 days and performed an HDL turnover experiment in mice fasted for 6 hours, which then, were injected intravenously with double-labeled *ex vivo* generated HDL particles. The

Part F Results

particles carried ^{125}I -tyramine cellobiose, thereby labeling the protein core of the HDL particle, and ^3H -cholesterol oleyl ether (^3H -CEt). Particles circulated for total duration of 5 hours prior to organ harvest and blood was withdrawn 10 min, 30 min, 1 hour, 2 hours and 5 hours after injection.

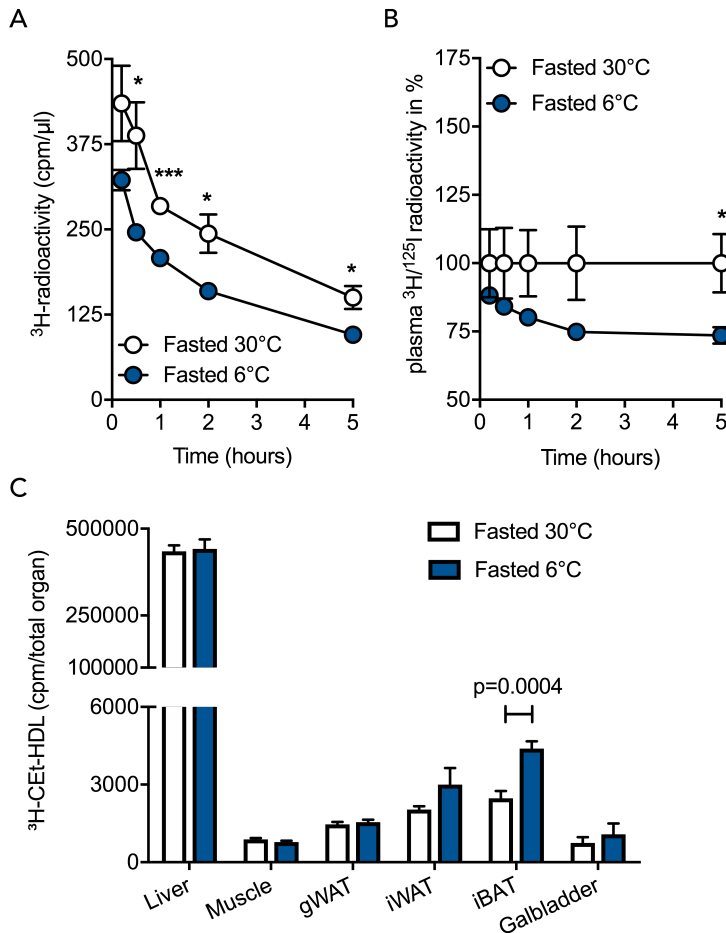


Figure 16. HDL turnover in fasted mice housed at thermoneutrality or cold. Mice were housed at thermoneutrality (30°C) or exposed to the cold (6°C) for 7 days. Mice were fasted 6 hours prior to intravenous injection with double-labeled HDL particles (^{125}I in the protein compartment and ^3H in cholesteryl oleyl ether). 10, 30, 60, 120 and 300 min after injection, blood was withdrawn via the tail and radioactivity determined in extracted plasma. 300 min after injection organs were harvested and radioactivity determined. **A.** Time course of ^3H -radioactivity (cholesteryl oleyl ether) in plasma withdrawn 10, 30, 60, 120 and 300 min after double-labeled HDL particle injection. **B.** Time course of ratio of ^3H -radioactivity (cholesteryl oleyl ether) to ^{125}I -radioactivity (tyramine cellobiose) in plasma withdrawn 10, 30, 60, 120 and 300 min after double-labeled HDL injection. WT control was set to 100% for each time point of blood withdrawal. 6°C values are normalized to mean of 30°C (which was set to 100%) for each time point. **C.** ^3H -radioactivity (cholesteryl oleyl ether) depicted in cpm per total organ 300 min after double-labeled HDL particle injection. Dots/Bars in each graph represents mean of 7 mice. Error bars represent \pm SEM. Statistics are performed with Student's t-Test.

^3H -CEt levels were cleared from plasma over time in thermoneutral- and cold-housed mice, however, plasma clearance in mice acquiring adaptive thermogenesis was significantly accelerated compared to thermoneutral controls (Figure 16. A). The ratio of ^3H -label to ^{125}I -label, mimicking the selective plasma clearance of cholesterol independent of whole HDL particle clearance, also showed increased selective cholesterol clearance in plasma of cold-housed mice over time compared to control mice housed at thermoneutrality (Figure 16. B). ^3H -CEt distribution within different

tissues showed higher uptake into intrascapular BAT, whereas uptake into other metabolically active organs, such as liver or inguinal WAT, was not altered (Figure 16. C).

Next, the interplay of post-prandial conditions together with cold-stimulated BAT activation on HDL functionality was evaluated. Thus, the same experimental setup was performed in thermoneutral- and cold-housed mice being refed for 4 hours after a 6-hour fasting period. The clearance of ^3H -CEt from plasma was profoundly induced in refed cold housed mice (Figure 17. A) and also, particle-independent ^3H -CEt clearance from plasma was significantly intensified during BAT activity in refed mice (Figure 17. B). The magnitude of plasma cholesterol levels and selective clearance was comparable between mice in a fasted or a refed state (Figure 16. A and B, Figure 17. A and B). However, cold-housed refed mice showed elevated ^3H -CEt uptake into metabolic active organs compared to fasted mice (Figure 16. C, Figure 17. C). The uptake into BAT, which was also observed in fasted mice, was expanded in the refed setting and a significant increase in ^3H -CEt levels in the liver and the gallbladder were observed (Figure 17. C). In sum, these data showed BAT-induced acceleration of HDL-C clearance from plasma and higher uptake into BAT in fasted and refed conditions and an elevated HDL-derived cholesterol uptake into the liver and gallbladder in refed conditions.

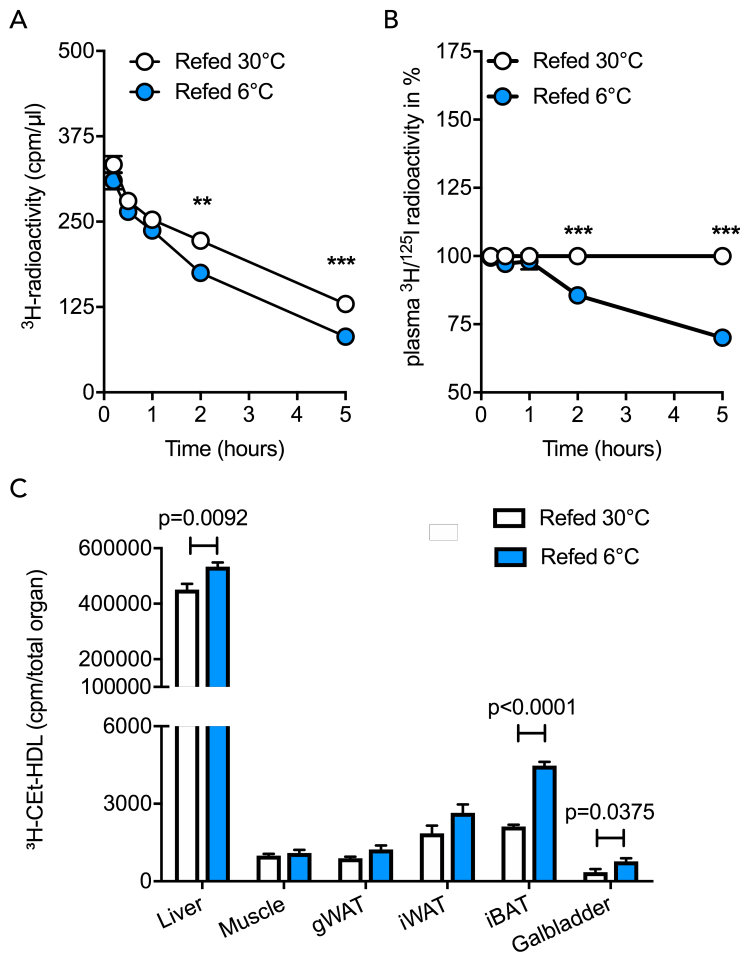


Figure 17. HDL turnover in refeed mice housed at thermoneutrality or cold. Mice were housed at thermoneutrality (30°C) or exposed to the cold (6°C) for 7 days. Mice were fasted 6 hours before being refeed for another 4 hours. Then, they were intravenously injected with double-labeled HDL particles (^{125}I in the protein compartment and ^3H in cholesteryl oleyl ether). 10, 30, 60, 120 and 300 min after injection, blood was withdrawn via the tail and radioactivity determined in extracted plasma. 300 min after injection organs were harvested and radioactivity determined. **A.** Time course of ^3H -radioactivity (cholesteryl oleyl ether) in plasma withdrawn 10, 30, 60, 120 and 300 min after double-labeled HDL particle injection. **B.** Time course of ratio of ^3H -radioactivity (cholesteryl oleyl ether) to ^{125}I -radioactivity (tyramine cellobiose) in plasma withdrawn 10, 30, 60, 120 and 300 min after double-labeled HDL injection. 6°C values are normalized to mean of 30°C (which was set to 100%) for each time point. **C.** ^3H -radioactivity (cholesteryl oleyl ether) depicted in cpm per total organ 300 min after double-labeled HDL particle injection. Dots/Bars in each graph represents mean of 6 mice. Error bars represent \pm SEM. Statistics are performed with Student's t-Test.

2.1.3 Effects of thermogenesis on reverse cholesterol transport *in vivo*

One hallmark of atherosclerosis development is the expansion of foam cells in atherosclerotic plaques which is due to high cholesterol uptake into macrophages. HDL facilitates excretion of cholesterol from lipid-loaded macrophages and transports cholesterol to the liver where it is excreted via the bile into the feces. Results from 2.1.2 showed increased HDL turnover in states of BAT activity and the question was addressed whether in addition to increased HDL turnover, adaptive thermogenesis also affects macrophage-to-feces cholesterol transport.

Therefore, mice were housed in thermoneutrality (30°C) or cold (6°C) 5 days prior to intraperitoneally injection with *ex vivo* ^3H -cholesterol labeled macrophages. After

48 hours of circulation, significantly lower macrophage-derived cholesterol (^3H -cholesterol) was detected in the plasma of cold-housed mice compared to control plasma obtained from mice housed at thermoneutrality (Figure 18. A). The recovery of ^3H -cholesterol in the liver was also decreased ($p=0.0673$) after cold intervention (Figure 18. B). However, analysis of ^3H -cholesterol levels in the feces, which was collected over the experimental duration of 48 hours, showed elevated excretion by trend already after 24 hours and significant differences after 48 hours in cold-compared to thermoneutral-housed mice. Thereby, an accelerated *in vivo* RCT in mice after BAT activation by cold housing could be shown.

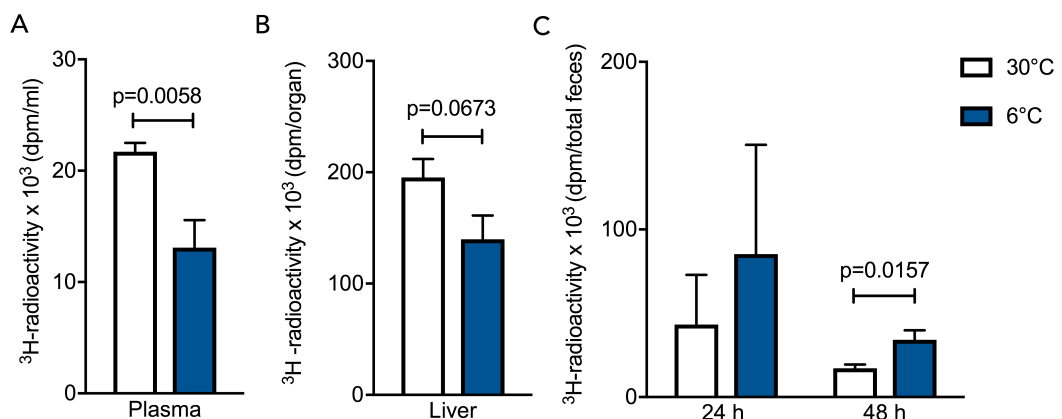


Figure 18. *In vivo* RCT in wildtype mice housed at thermoneutrality or cold. Mice were housed at thermoneutrality (30° C) or cold (6° C) for 5 days before they were intraperitoneally injected with *ex vivo* ^3H -cholesterol-labeled peritoneal macrophages. Circulation of injected macrophages was allowed for 48 hours at indicated housing temperatures prior to organ harvest after a 4-hour fasting period. **A.** ^3H -radioactivity (cholesterol) in plasma extracted from cardiac blood was determined 48 hours after labeled macrophage injection. **B.** ^3H -radioactivity (cholesterol) in the liver was determined 48 hours after labeled macrophage injection. **C.** ^3H -radioactivity (cholesterol) in feces collected 24 hours and 48 hours after macrophage injection. Bars represent mean of 5-6 mice; error bars represent \pm SEM. Statistics are performed with Student's t-Test.

2.2 Impact of LPL and SR-B1 on HDL metabolism during thermogenesis

During BAT activation, expression of LPL, the main driver of FA release from TRLs, was highly upregulated in adipocytes to maintain nutrient supply for adaptive thermogenesis (Figure 6). In the dissertation implemented by Dr. rer. nat. Clara John, the importance of LPL during thermogenesis was investigated. By using a mouse model carrying an adipocyte-specific deletion of LPL (aLKO mouse), LPL importance for BAT-induced TRL and HDL lipid remodeling was revealed. However, how impaired HDL remodeling affects HDL functionalities remained to be elucidated.

Based on her findings, I performed an HDL turnover experiment in cold-acclimated wildtype and aLKO mice, in order to evaluate if LPL impacts on cold-induced acceleration of HDL turnover. After 7 days of cold housing, wildtype and aLKO mice received an intravenous injection of *ex vivo* generated HDL particles carrying ^{125}I -iodine-tyramine cellobiose, thereby labeling the protein core of the HDL particle, and ^3H -cholesterol oleyl ether (^3H -CEt). ^3H -radioactivity (^3H -cholesterol oleyl ether) in

Part F Results

plasma was cleared in wildtype and alKO mice over the 5-hour experimental duration, however, a significant impairment in HDL-derived cholesterol clearance was observed in alKO mice 5 hours after injection (Figure 19. A). When calculating the selective cholesterol clearance ($^3\text{H}/^{125}\text{I}$) from plasma over time, an accumulation of cholesterol became obvious in the cold-housed mice lacking LPL in adipocytes compared to their cold-housed wildtype control (Figure 19. B).

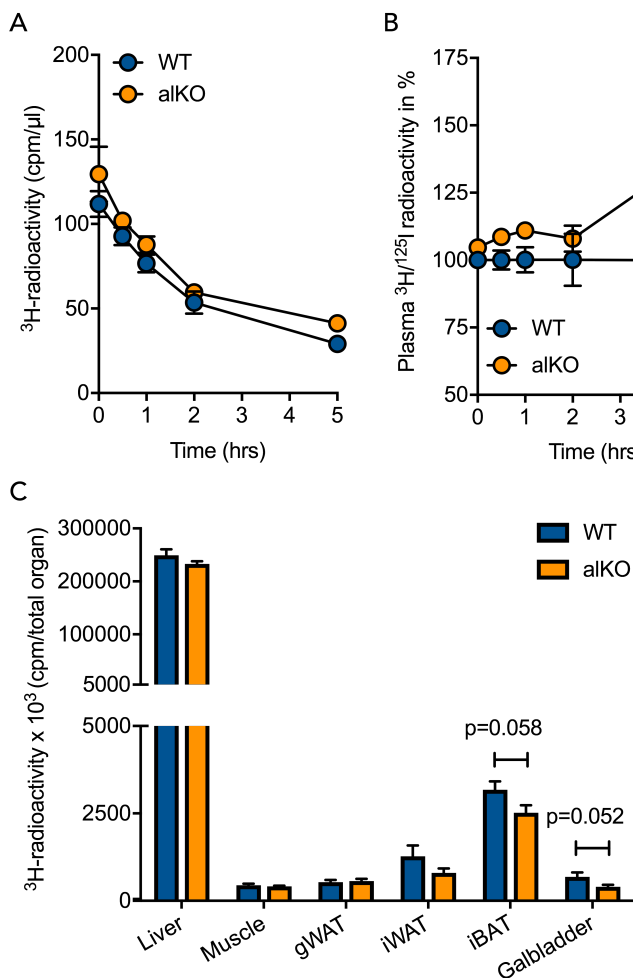


Figure 19. HDL turnover in cold-housed alKO mice. Wildtype mice (WT) or mice with genetic deletion of LPL specific in adipocytes (alKO) were housed at thermoneutrality (30°C) or exposed to the cold (6°C) for 7 days. Mice were fasted 4 hours prior to intravenous injection with double-labeled HDL particles (^{125}I in the protein compartment and ^3H in cholesteryl oleyl ether). 10, 30, 60, 120 and 300 min after injection, blood was withdrawn via the tail and radioactivity determined in extracted plasma. 300 min after injection organs were harvested and radioactivity determined. **A.** Time course of ^3H -radioactivity (cholesteryl oleyl ether) in plasma withdrawn 10, 30, 60, 120 and 300 min after double-labeled HDL particle injection. **B.** Time course of ratio of ^3H -radioactivity (cholesteryl oleyl ether) to ^{125}I -radioactivity (tyramine cellobiose) in plasma withdrawn 10, 30, 60, 120 and 300 min after double-labeled HDL injection. alKO values are normalized to mean of WT (which was set to 100%) for each time point. **C.** ^3H -radioactivity (cholesteryl oleyl ether) depicted in cpm per total organ 300 min after double-labeled HDL particle injection. Dots/Bars in each graph represents mean of 6 mice. Error bars represent \pm SEM. Statistics are performed with Student's t-Test.

Furthermore, alKO mice presented significantly reduced ^3H -CEt uptake into BAT and the gallbladder, whereas liver and inguinal WAT showed a trend towards lower ^3H -CEt amounts (Figure 19. C). These data indicated that during BAT activation via cold stimulus, LPL loss leads to an impairment in HDL turnover.

Another important player for implementing reverse cholesterol metabolism involves SR-B1. First, SR-B1 being expressed on macrophages contributes to cholesterol efflux from lipid-loaded macrophages to HDL particles and second, SR-B1 being expressed by hepatocytes positively mediates the uptake of HDL-C into the liver. I studied the involvement of SR-B1 for reverse cholesterol metabolism during cold intervention. Therefore, cold-housed wildtype mice and cold-housed SR-B1 knockout mice (*Scarb1*^{-/-}) were tested in an HDL turnover experiment.

In plasma, ³H-radioactivity which labeled CEt declined over the experimental duration of 5 hours but was attenuated in *Scarb1*^{-/-} mice 2 and 5 hours after labeled HDL particle injection (Figure 20. A). By calculating the relative selective plasma clearance of HDL-derived cholesterol, already 30 min after particle injection an accumulation of ³H-radioactivity was measured in mice lacking SR-B1 and even further diverged from ³H-levels in wildtype mice over time (Figure 20. B). Cold-housed *Scarb1*^{-/-} mice presented significantly lower levels of ³H-radioactivity in the liver and gallbladder (Figure 20. C). In gonadal WAT, an increased uptake of ³H -CEt was found, whereas inguinal WAT and BAT did not demonstrate differences between wildtype and *Scarb1*^{-/-} mice (Figure 20. C). With these data, it could be shown that during adaptive thermogenesis, LPL and SR-B1 are important players in guiding reverse HDL-derived cholesterol flux.

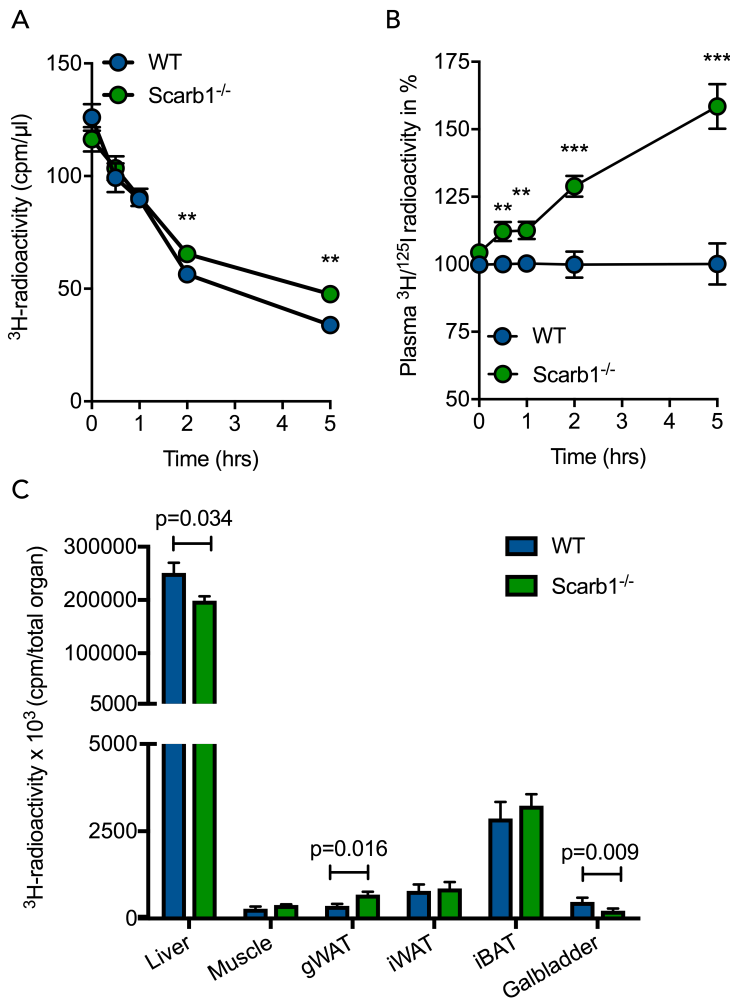


Figure 20. HDL turnover in cold-housed *Scarb1*^{-/-} mice. Wildtype mice (WT) or mice with genetic deletion of SR-B1 (*Scarb1*^{-/-}) were housed at thermoneutrality (30°C) or exposed to the cold (6°C) for 7 days. Mice were fasted 4 hours prior to intravenous injection with double-labeled HDL particles (¹²⁵I in the protein compartment and ³H in cholesteryl oleyl ether). 10, 30, 60, 120 and 300 min after injection, blood was withdrawn via the tail and radioactivity determined in extracted plasma. 300 min after injection organs were harvested and radioactivity determined. **A.** Plasma levels of ³H-radioactivity (cholesteryl oleyl ether) over time; tail blood after 10, 30, 60, 120 and 300 min after labeled HDL particle injection. **B.** Ratio of ³H-radioactivity (cholesteryl oleyl ether) to ¹²⁵I-radioactivity (tyramine cellobiose) in plasma over time; tail blood after 10, 30, 60, 120 and 300 min after labeled-HDL injection. alKO values are normalized to mean of WT (which was set to 100%) for each time point. **C.** ³H-radioactivity in total organs 300 min after circulation of labeled HDL particle injection. In all graphs each group represents mean of 7-8 mice. Error bars represent \pm SEM. Statistics are performed with Student's t-Test.

2.3 Role of EL on lipoprotein metabolism during thermogenesis

As well as LPL, which mainly targets TGs from TRL particles, EL has been shown to be an important player in lipoprotein remodeling. EL is mainly expressed by endothelial cells and macrophages and especially conducts an A1 phospholipase activity, thereby facilitating FA cleavage from the sn-1 position of PLs. [37] We hypothesized that EL might be involved in the highly lipolytic processes occurring during BAT activation because I observed profoundly induced *Lipg* expression in BAT analyzed from wildtype mice housed under 6°C compared to their 30°C-housed control group (Figure 21. A). By using a mouse model lacking EL globally (elKO), I

investigated whether loss of EL alters systemic cholesterol metabolism either in states of thermoneutrality or activated adaptive thermogenesis.

2.3.1 Consequences of global genetic EL ablation (eIKO) on gene expression in metabolic organs in thermoneutrality and cold

Activation of BAT by cold stimulation results in upregulation of a distinct gene profile that involves mediators important to maintain adaptive thermogenesis. Here, it was investigated, if genetic ablation of EL in mice led to altered expression of browning-related genes during adaptive thermogenesis. Therefore, wildtype and eIKO mice were housed at thermoneutrality (30° C) or cold (6° C) for 7 days and harvested metabolically important organs, namely BAT, inguinal WAT and liver after a 4-hour fasting period which was followed by an oil gavage. Expression of genes involved in adaptive thermogenesis and lipoprotein and cholesterol metabolism were analyzed.

2.3.1.3 Gene expression profile in the BAT of eIKO mice

Figure 21. B depicts gene expression profile in BAT from thermoneutral- and cold-housed wildtype and eIKO mice. During BAT activation, *Ucp1*, which uncouples the electron transfer from the respiratory chain in order to produce heat, was induced in wildtype mice and the upregulation during cold-housing was also observed in mice lacking EL (eIKO). No changes in *Ucp1* expression were observed in thermoneutral conditions between the genotypes. *Pgc1a* acts as a thermogenic coactivator and, as expected, cold housing of wildtype mice led to significant increases in its expression level compared to thermoneutral control, yet, eIKO mice did not present cold-induced induction of *Pgc1a* expression. Nonetheless, BAT activation amplified transcripts of genes involved in lipid and glucose uptake from the circulation (*Lip*, *Cd36*, *Glut4*), regardless of EL presence. *Abca1* expression, which exports cholesterol to HDL, was not significantly altered neither by activated adaptive thermogenesis nor by loss of EL, whereas *Abcg1* expression, having a similar function, was significantly induced during cold in wildtype and eIKO mice. Transcripts of *Dio2*, another cold-activated driver of adaptive thermogenesis, was upregulated in wildtype and eIKO mice only by trend in mice housed at 6° C. *Angplt4*, known to inhibit LPL, was unchanged in BAT tissue on mRNA level, regardless of ambient temperature or genotype. Overall, the absence of EL expression did not show changes in the expression of thermogenesis-related molecules in BAT.

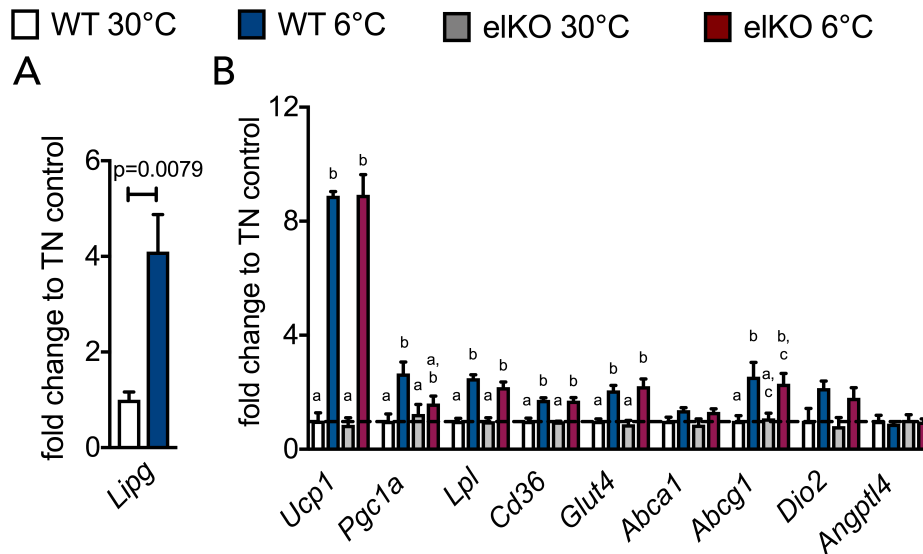


Figure 21. Expression of browning-related genes after cold-housing in wildtype and eIKO mice. Mice were housed at thermoneutrality (TN) (30°C) or exposed to the cold (6°C) for 7 days. Organs were harvested after a 4-hour fasting period and applied to RNA extraction with subsequent cDNA preparation and gene expression analysis conducted using TaqMan® technique. **A.** Gene expression of EL (*Lipg*) after cold-stimulus in BAT of thermoneutral- or cold-housed wildtype mice. Bars represent mean of 4 mice per group and error bars indicate \pm SEM. Statistics were performed with Student's t-Test. **B.** Expression of browning-related genes in wildtype and eIKO mice housed under thermoneutrality or cold. Bars represent mean of 4-6 mice per group and error bars indicate \pm SEM. Statistics were performed using two-way ANOVA comparing all groups among each other.

2.3.1.3 Gene expression profile in the inguinal WAT of eIKO mice

One week of cold housing already results in enhanced transformation of inguinal WAT to a beige phenotype.^{121} To test if EL loss has an impact on expression of browning-related genes in inguinal WAT from thermoneutral- or cold-housed wildtype and eIKO mice, TaqMan™ analysis was performed in samples of inguinal WAT. Figure 22 shows that a 7-day cold-exposure upregulated the marker gene for adaptive thermogenesis, namely *Ucp1*, however, its expression was upregulated independently of the mouse genotype. *Pgc1a* expression in inguinal WAT presented similarly to the expression observed in BAT: wildtype mice induced expression levels upon cold stimulation, which was less pronounced in eIKO mice. Genes important for nutrient uptake (*Lpl*, *Cd36*, *Glut4*) and cholesterol efflux (*Abca1*, *Abcg1*) were unchanged by cold stimulation and loss of EL. Yet, *Dio2* expression was highly induced upon cold housing in mice regardless of the genotype, whereas *Angptl4* was only increased during cold in wildtype mice and not in eIKO mice. In summary, inguinal WAT of wildtype and eIKO mice showed no major differences when comparing the two genotypes.

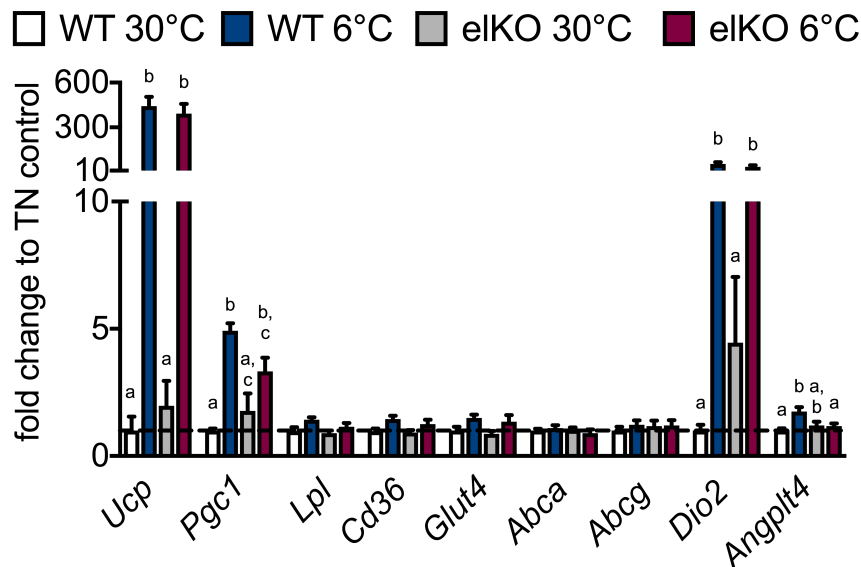


Figure 22. Expression of browning-related genes in inguinal WAT after cold-housing in wildtype and eIKO mice. Mice were housed at thermoneutrality (TN) (30°C) or exposed to the cold (6°C) for 7 days. Organs were harvested after a 4-hour fasting period and applied to RNA extraction with subsequent cDNA preparation and final gene expression analysis conducted using TaqMan™ technique. Bars represent mean of 4-6 mice per group and error bars indicate \pm SEM. Statistics were performed with two-way ANOVA comparing all groups among each other.

2.3.1.3 Gene expression profile in the liver of eIKO mice

Cold housing of mice, on the one hand, leads to activation of thermogenic adipocytes, namely brown adipocytes in BAT and beige adipocytes in WAT, however, by induced lipoprotein and cholesterol flux also the liver is affected by adaptive thermogenesis. To test possible alterations in liver homeostasis after BAT activation and EL loss, we analyzed the expression of genes involved in lipoprotein and cholesterol metabolism in the liver of thermoneutral- and cold-housed wildtype and eIKO mice (Figure 23). Expression of *Ldlr* and *Lrp1*, which encode receptors essential for TRL remnant uptake into the liver, did neither change upon cold stimulus nor due to loss of EL. SR-B1, which presented as a main player in HDL-C clearance (Figure 20), was induced on mRNA level after cold housing in wildtype and eIKO mice, however induction in eIKO mice was not significant. Expression of *Apoa1*, *Apoe* and *Hmgcr* were unchanged independent of ambient temperature or genotype.

Cyp7a1, encoding an enzyme driving the classical pathway of bile acid synthesis in the liver, was unaltered by cold in wildtype and eIKO mice, however, alterations in the alternative pathway of bile acid synthesis were observed since *Cyp7b1* expression was upregulated in cold-housed wildtype and eIKO mice. Excretion of cholesterol into bile is mediated by ABCG5 and ABCG8 and increases in *Abcg5* transcripts in cold-housed wildtype mice were detected, whereas *Abcg5* expression levels in eIKO mice were less affected after cold housing. Furthermore, *Abcg8* expression was unaffected by housing temperature intervention or loss of EL, so were *Angptl3* and *Angptl4* which regulate LPL activity. By analyzing the expression profile of genes involved in

lipoprotein and cholesterol metabolism in the liver, no prominent differences were manifested in mice lacking EL.

□ WT 30°C ■ WT 6°C ▒ eIKO 30°C ■ eIKO 6°C

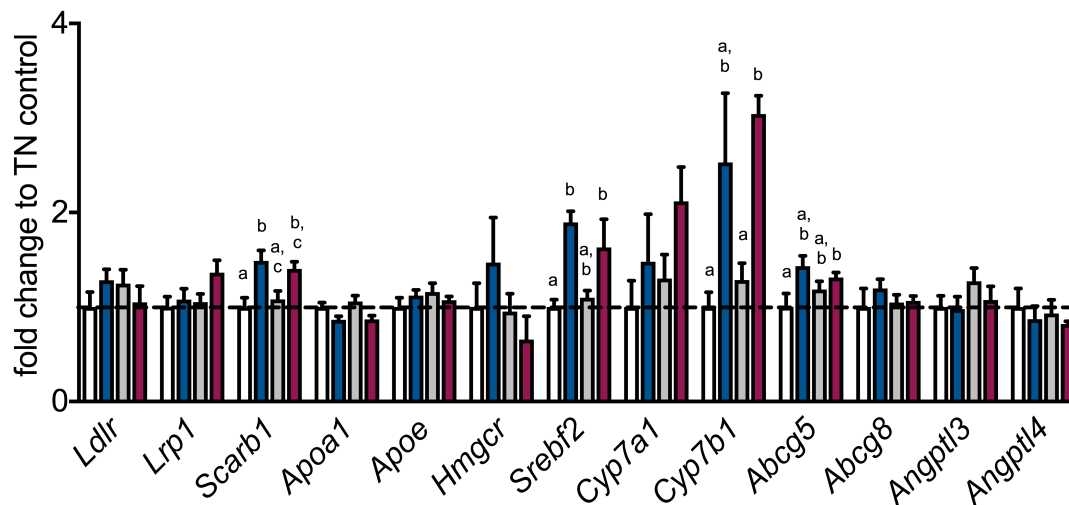


Figure 23. Hepatic expression of genes involved in lipoprotein and cholesterol metabolism after cold-housing in wildtype and eIKO mice. Mice were housed at thermoneutrality (TN) (30°C) or exposed to the cold (6°C) for 7 days. Livers were harvested after a 4-hour fasting period and applied to RNA extraction with subsequent cDNA preparation and final gene expression analysis conducted using TaqMan® technique. Bars represent mean of 4-6 mice per group and error bars indicate +/-SEM. Statistics were performed with two-way ANOVA comparing all groups among each other.

2.3.2 Plasma lipid parameters and lipoprotein profile in eIKO mice after BAT activation by cold housing

In paragraph 2.3.1., gene expression analysis of metabolically active organs, namely BAT, inguinal WAT and liver, revealed no profound alterations in eIKO mice upon cold exposure. By determining plasma lipid concentrations, a cold-induced reduction in cholesterol levels was observed in wildtype mice and eIKO mice (Figure 24. A). In addition, higher cholesterol levels were found in plasma from thermoneutral-housed eIKO mice compared to their thermoneutral-housed wildtype control (Figure 24. A). Analysis of TG amounts showed a tendency to reduced TG concentrations after cold-housing in wildtype mice and such trend was also obvious in thermoneutral- and cold-housed eIKO mice (Figure 24. B). Separation of the different lipoprotein classes by FPLC visualized that the reduction in plasma cholesterol upon cold stimulation could mainly be attributed to a reduction in HDL-C (Figure 24. C) while reduction in TGs was most prominent in the TRL fraction (Supplementary Figure 2). Furthermore, increased plasma cholesterol concentrations in eIKO mice were due to higher cholesterol concentrations within the HDL fraction in thermoneutral and cold housing conditions (Figure 24. C). Taken together, changes in plasma cholesterol concentrations in eIKO mice could primarily be explained to changes in HDL-C.

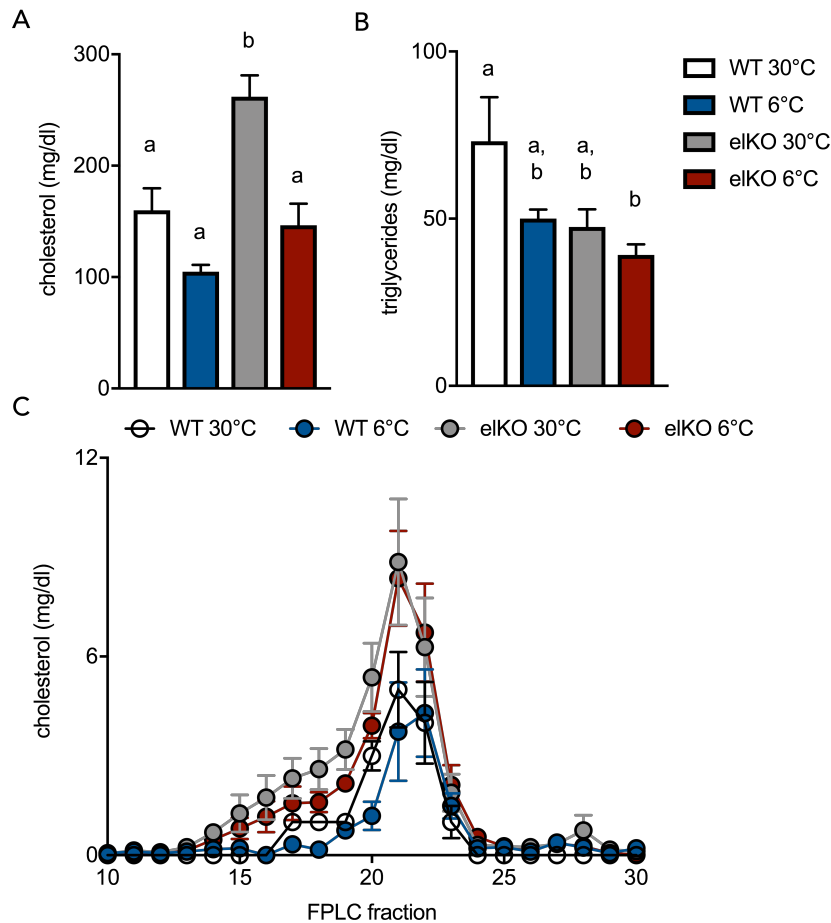


Figure 24. Plasma lipid parameters and lipoprotein profile in thermoneutral- or cold-housed wildtype and eIKO mice. Mice were housed at thermoneutrality (30°C) or exposed to the cold (6°C) for 7 days. Plasma lipids were determined in plasma extracted from blood withdrawn retro-orbitally after a 4-hour fasting period. **A.** Plasma triglyceride levels in mg/dl. **B.** Plasma cholesterol levels in mg/dl. A-B. Bars represent mean of 4-6 mice per group and error bars indicate \pm SEM. Statistics were performed with two-way ANOVA comparing all groups among each other. **C.** Lipoprotein profile was obtained by applying plasma to FPLC separation and cholesterol concentrations were measured. Dots represent means of 4 mice per group and error bars show \pm SEM.

2.3.3 Effects of EL loss on HDL lipid remodeling during thermogenesis

To analyze the lipid composition of HDL particles after cold stimulation, FPLC-separated HDL particles from thermoneutral- and cold-housed mice were applied to LC-MS/MS (UPLC-ESI-QqTOF-method). Pie charts depict no major differences in the overall composition of HDL lipids from wildtype mice housed at 30°C compared to housing at 6°C (Figure 25. A-B). Likewise, in mice lacking the EL (eIKO), cold-intervention (6°C) did not induce major changes in HDL lipid composition compared to eIKO control mice housed at thermoneutrality (Figure 25. C-D). However, comparing the HDL composition from wildtype and eIKO mice, significant differences became obvious when looking at each lipid class individually (Figure 25. E-K). CEs in eIKO mice, housed at thermoneutrality but not in cold, were reduced compared to wildtype mice independent of their ambient housing temperature (Figure 25. E), whereas TG percentages were reduced only in cold-housed eIKO mice compared to

cold-housed wildtype mice (Figure 25. F). Overall, the share of all detected PLs of isolated HDL particles, namely PC (Figure 25. G), lyso-PC (Figure 25. H), PE (Figure 25. I) and phosphatidylinositol (PI) (Figure 25. K), was elevated in eIKO mice, albeit the effect was more distinct in thermoneutral-housed eIKO mice compared to their cold counterpart. SM percentages did not change between the housing conditions or the genotype (Figure 25. J).

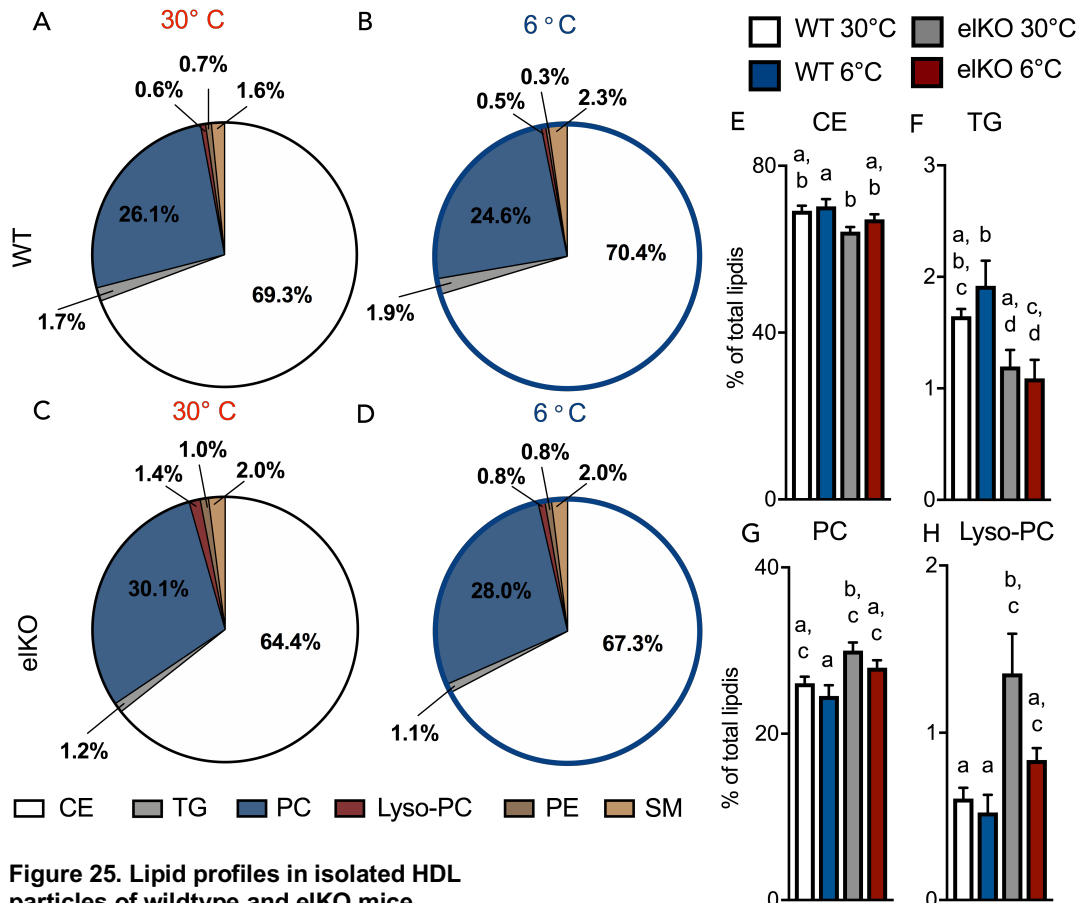


Figure 25. Lipid profiles in isolated HDL particles of wildtype and eIKO mice after activation BAT by cold housing.

Wildtype (WT) and eIKO mice were housed at thermoneutrality (30°C) or exposed to the cold (6°C) for 7 days. Retro-orbital blood was withdrawn after a 4-hour fasting period and plasma was applied to lipoprotein fractionation to isolate HDL particles. Lipidomic analysis in isolated HDL particles was performed by using UPLC-ESI-QqTOF-method for semi-quantitative lipid analysis. Relative amounts were calculated as ratio of all detected lipids. **A-D** shows relative distribution (mean of 4 mice per group) of lipids in HDL isolated from plasma of WT housed at 30° C (A) or 6° C (B) and from plasma of eIKO mice housed at 30° C (C) or 6° C (D). **E-K** represents relative amounts of individual lipid classes as percentage of total lipids. Bars represent means of 4 mice per group. Error bars indicate +/-SEM. Statistics are calculated with two-way ANOVA comparing all groups among each other. Legends: CE=cholesterester; TG=triglyceride; PC=phosphatidylcholine; Lyso-PC=lyso-phosphatidylcholine; PE=phosphatidylethanolamine; SM=sphingomyeline; PI=phosphatidylinositol.

A similar observation was made, when absolute values of the different lipid classes were displayed (Figure 26). Amounts of CEs (Figure 26. A) and TGs (Figure 26. B) were not altered by cold-housing of wildtype mice neither did the loss of EL affect their concentration compared to thermoneutral wildtype mice. On the contrary, the quantity of PLs increased in HDL particles of eIKO mice in comparison to wildtype mice. PCs were significantly increased in thermoneutral- and cold-housed eIKO mice when comparing them to each of their wildtype control (Figure 26. C). Also, lyso-PCs were increased in HDL particles from eIKO mice, however, only elevation in thermoneutral-housed eIKO mice was significantly increased compared to their wildtype control (Figure 26. D). The amount of PEs and SMs were quantitatively unchanged by cold intervention or loss of EL (Figure 26. E-F), whereas PIs presented a profound increase upon genetic ablation of EL regardless of housing conditions (Figure 26. G). Collectively these data suggest, that by comparing the lipid composition of HDL particles isolated from wildtype and eIKO mice, the most prominent alterations occurred in the PL compartment seen on a relative and absolute PL increase in HDL particles isolated from eIKO mice.

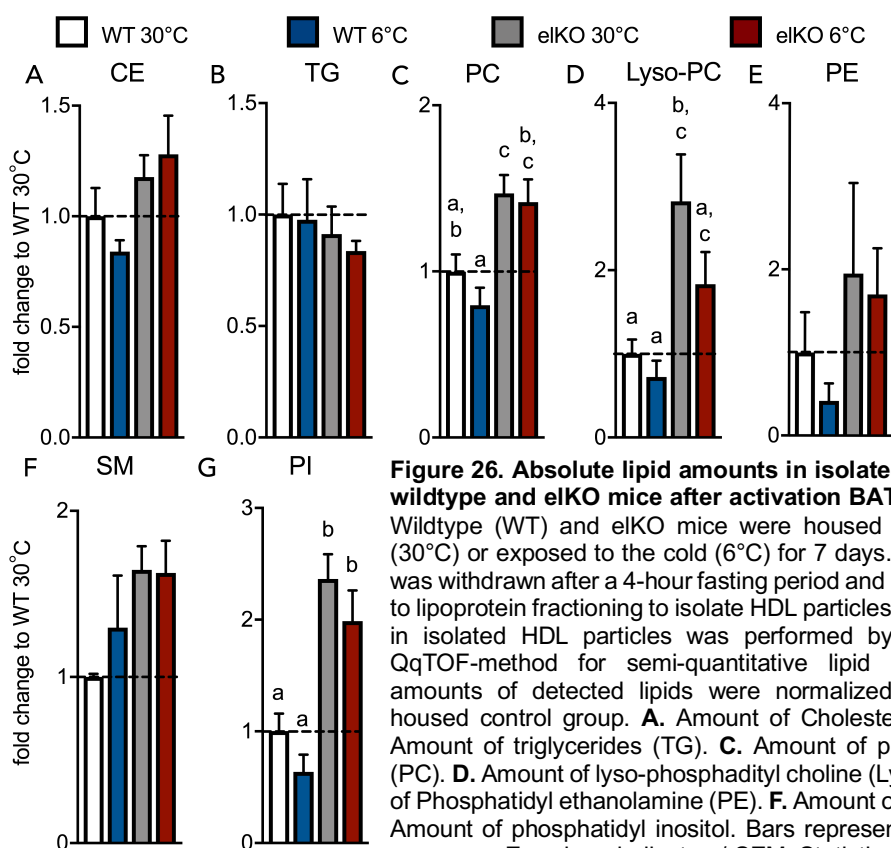


Figure 26. Absolute lipid amounts in isolated HDL particles of wildtype and eIKO mice after activation BAT by cold housing. Wildtype (WT) and eIKO mice were housed at thermoneutrality (30°C) or exposed to the cold (6°C) for 7 days. Retro-orbital blood was withdrawn after a 4-hour fasting period and plasma was applied to lipoprotein fractionation to isolate HDL particles. Lipidomic analysis in isolated HDL particles was performed by using UPLC-ESI-QqTOF-method for semi-quantitative lipid analysis. Absolute amounts of detected lipids were normalized to thermoneutral-housed control group. **A.** Amount of Cholesteryl esters (CE). **B.** Amount of triglycerides (TG). **C.** Amount of phosphatidyl choline (PC). **D.** Amount of lyso-phosphatidyl choline (Lyso-PC). **E.** Amount of Phosphatidyl ethanolamine (PE). **F.** Amount of sphingomyelin. **G.** Amount of phosphatidyl inositol. Bars represent means of 4 mice per group. Error bars indicate +/-SEM. Statistics are calculated with two-way ANOVA comparing all groups among each other.

2.3.4 Impact of EL on cold-induced acceleration of HDL turnover

In paragraph 2.3.2 and 2.3.3, it was shown that the loss of EL in mice induced alteration in HDL-C levels and lipid remodeling of HDL particles. In order to test if

observed HDL changes in eIKO mice affected HDL properties, an HDL turnover experiment was conducted in cold-housed wildtype and cold-housed eIKO mice, which allowed to follow the fate of HDL-derived cholesterol. Briefly, wildtype and eIKO were housed for 7 days in the cold and then, received an injection with double-labeled HDL particles allowing to track the protein of the particle and HDL-cholesterolether. Over the experimental duration of 5 hours, the ^3H -radioactivity labeling the HDL-cholesterolether was cleared from plasma of cold-housed wildtype and eIKO mice (Figure 27. A). Already 1 hour after particle injection, the ^3H -CEt clearance from plasma in eIKO mice was significantly attenuated and attenuation persisted over the ongoing duration of the experiment (2 hours and 5 hours) (Figure 27. A). The differences between wildtype and eIKO mice became even more obvious when calculating the selective plasma clearance (cholesterol clearance independent from whole particle clearance) over time. Figure 27. B demonstrates an accumulation of ^3H -CEt in plasma of eIKO mice which was significantly different to wildtype mice at 30 min, 1 hours, 2 hours and 5 hours after labeled HDL injection. The distribution of cholesterol within metabolically important organs is depicted in Figure 27. C: eIKO mice presented a lower amount of HDL-derived cholesterol within the liver, inguinal WAT and BAT, whereas ^3H -CEt levels in muscle and gonadal WAT were not affected. Overall, loss of EL in mice seemed to impair the cold-accelerated HDL turnover *in vivo*.

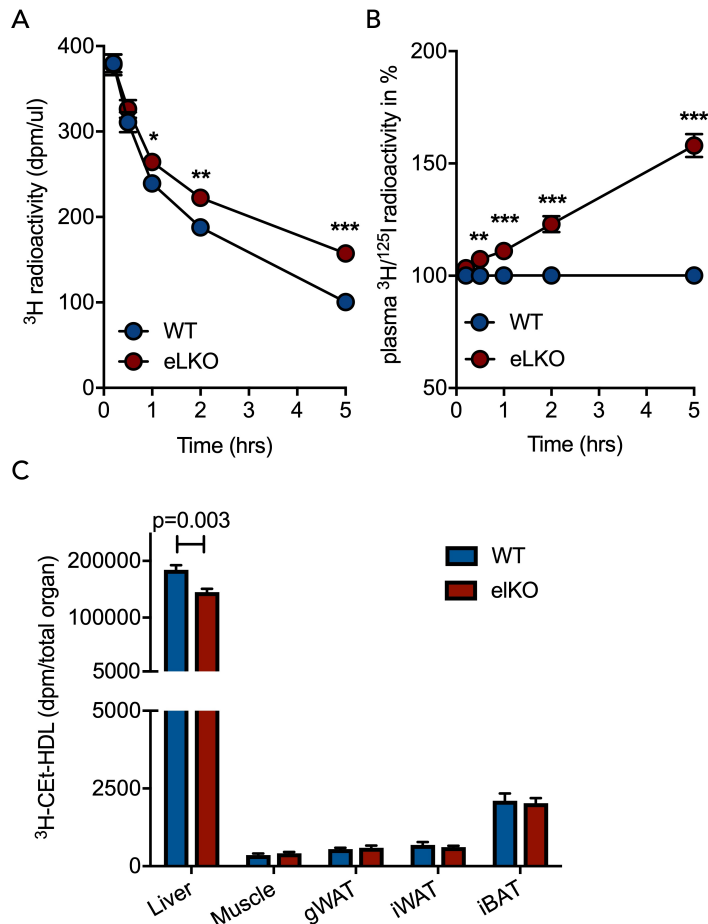


Figure 27. Impact of EL loss for HDL-C clearance. Wildtype mice (WT) or mice with genetic deletion of EL (eLKO) were housed at thermoneutrality (30°C) or exposed to the cold (6°C) for 7 days. Mice were fasted 4 hours prior to intravenous injection with double-labeled HDL particles (^{125}I in the protein compartment and ^3H in cholesteryl oleyl ether). 10, 30, 60, 120 and 300 min after injection, blood was withdrawn via the tail and radioactivity determined in extracted plasma. 300 min after injection organs were harvested and radioactivity determined. **A.** Time course of ^3H -radioactivity (cholesteryl oleyl ether) in plasma withdrawn 10, 30, 60, 120 and 300 min after double-labeled HDL particle injection. **B.** Time course of ratio of ^3H -radioactivity (cholesteryl oleyl ether) to ^{125}I -radioactivity (tyramine cellobiose) in plasma withdrawn 10, 30, 60, 120 and 300 min after double-labeled HDL injection. eLKO values were normalized to mean of WT (which was set to 100%) for each time point. **C.** ^3H -radioactivity (cholesteryl oleyl ether) depicted in dpm per total organ 300 min after double-labeled HDL particle injection. Dots/Bars in each graph represents mean of 6 mice. Error bars represent \pm SEM. Statistics were performed with Student's t-Test.

2.3.5 Distribution of EL to cold-induced enhanced reverse cholesterol transport

Next, I tested the consequences of genetic ablation of EL for reverse cholesterol metabolism. Therefore, wildtype and eLKO mice were housed at thermoneutrality or in the cold for 5 days before they were used in an *in vivo* RCT. 48 hours after the injection of ^3H -cholesterol labeled macrophages, significantly lower plasma levels of ^3H -radioactivity were found in the plasma of cold-housed eLKO mice compared to thermoneutral-housed eLKO mice. This finding mimicked the effect observed in wildtype mice. However, the ^3H -cholesterol seemed to accumulate in the plasma of

elKO mice hold under thermoneutral housing conditions as a significant elevation to the plasma levels of wildtype mice was observed (Figure 28. A).

Similarly, the ^3H -cholesterol levels in the liver of thermoneutral-housed elKO mice were significantly increased to wildtype mice at 30° C or 6° C. Cold-housed elKO mice showed a tendency to reduced ^3H -cholesterol concentrations in the liver compared to thermoneutral-housed elKO mice, however, they presented significant incorporation of ^3H -cholesterol compared to the cold wildtype control mice (Figure 28. B). The excretion of macrophage-derived cholesterol into the feces was measured 24 and 48 hours after labeled macrophage injection. After 24 hours, no significant differences between housing conditions and genotypes were observed, whereas feces collected between 24-48 hours (48 h) presented a cold-induced increase in the ^3H -recovery rate in wildtype and elKO mice. Overall, the feces defecated during the whole experimental period showed an elevated excretion of ^3H -cholesterol in wildtype mice compared to elKO mice, however, these differences did not reach statistical significance (Figure 28. C).

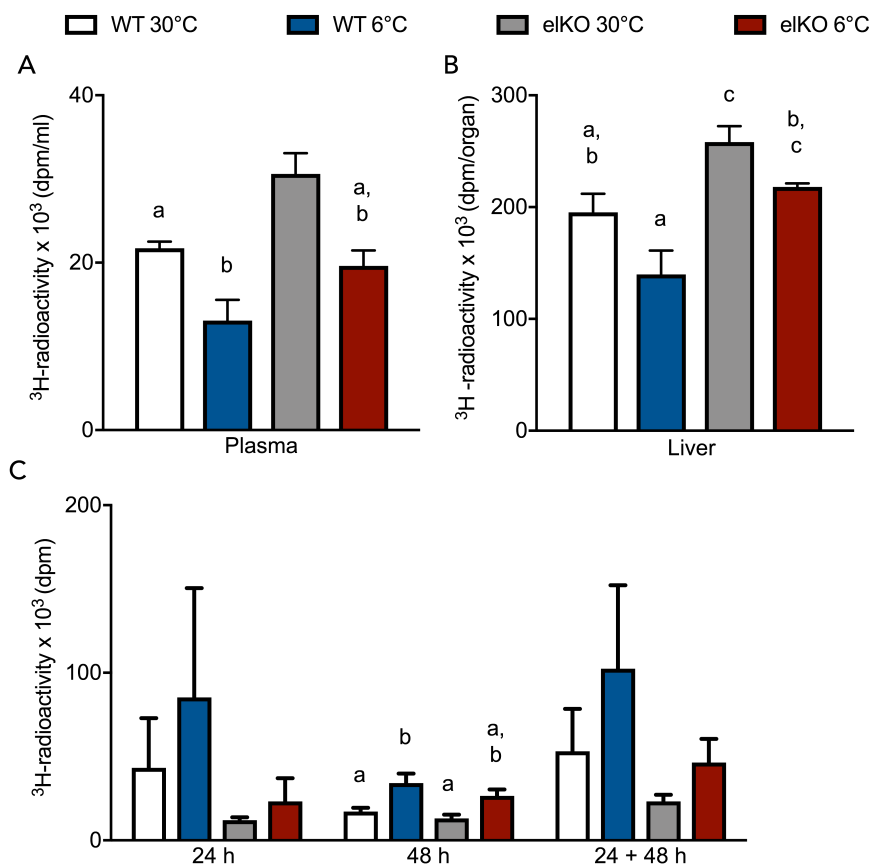


Figure 28. Impact of EL on *in vivo* RCT after BAT activation by cold housing. Wildtype mice (WT) or mice with genetic deletion of EL (elKO) were housed at thermoneutrality (30° C) or cold (6° C) for 5 days before they were intraperitoneally injected with *ex vivo* ^3H -cholesterol-labeled peritoneal macrophages. Circulation of injected macrophages was allowed for 48 hours at indicated housing temperatures prior to organ harvest after a 4-hour fasting period. **A.** ^3H -radioactivity (cholesterol) in plasma extracted from cardiac blood was determined 48 hours after labeled macrophage injection. **B.** ^3H -radioactivity (cholesterol) in the liver was determined 48 hours after labeled macrophage injection. **C.** ^3H -radioactivity (cholesterol) in feces collected 24 hours and 48 hours after macrophage injection. Bars

Part F Results

represent means of 5-7 mice. Error bars indicate \pm SEM. Statistics were performed using two-way ANOVA comparing all groups among each other.

In summary, the data observed in my PhD thesis showed cold-induced alterations in the lipid constitution and polarization of macrophages of BAT and partially in WAT. Furthermore, I could highlight the impact of LPL, SR-B1 and EL in cold-induced acceleration of HDL metabolism. The results, described in section 2.1.2 and 2.2.2, were published in Nature Communications in 2017 in a manuscript entitled "Thermogenic adipocytes promote HDL turnover and reverse cholesterol transport".

Part G Discussion

1 Immunometabolism in thermogenic adipose tissue

Lifestyle and dietary changes contribute to the high prevalence of obesity and associated secondary diseases like metabolic syndrome. The number of people affected by obesity is increasing every year and the onset of obesity is occurring at an earlier age. The most obvious intervention to tackle with this problem, i.e. to “solely” altering eating behavior and increasing energy expenditure by doing exercise, proved to be inconvertible for most patients. Therefore, there is unmet medical need to find novel treatment options that counteract increasing obesity and dyslipidemias.

Activating BAT by cold intervention led to improved metabolic parameters in humans and thus understanding BAT physiology might give rise to new therapeutic options.^{66, 67} Recently, adipose tissue macrophages were discussed as contributing to thermogenic activity. Nonetheless, the significance and underlying mechanisms need further elucidation. In my thesis, I addressed the question as to whether the elevated lipid uptake during non-shivering thermogenesis might affect the lipid composition of macrophages and influence their functionality. Therefore, thermogenesis in mice was activated for 7 days and different cell populations of BAT and inguinal WAT were analyzed by applying the MACS® separation technique. The technique allowed isolation of adipocytes, endothelial cells and macrophages with high purity as indicated by expression of signature genes in the different cell types.

Lipid analysis revealed that the adipocyte fractions from BAT and inguinal WAT were mainly constituted of TGs, as expected. Upon cold adaptation, a certain decrease in TG percentage was recognized in adipocytes isolated from BAT and WAT. This might be explained by intensified mobilization of lipid stores during adaptive thermogenesis which resulted in a reduction in cellular TG contents. Endothelial cells, as expected, presented lower amounts of TG compared to adipocytes and PLs and SM were more abundant. No remarkable differences came through when comparing endothelial cells from BAT and inguinal WAT, however, in endothelial cells isolated from BAT of cold-housed mice the TG amount decreased compared to the TN control. During cold intervention, lipolytic processes are upregulated to release FAs from TRL particles. Lipids are shuttled via the endothelial cells towards the adipocytes.^{79} By enhancing this shuttling process, it could be possible that also intracellular lipid stores of endothelial cells were targeted by high demands of thermogenic adipocytes. Since brown adipocytes have a higher energy expenditure than beige adipocytes, this might

explain why I only observed the reduction in TG content in endothelial cells from BAT and not in endothelial cells from inguinal WAT.

With the LC-MS/MS-based method, I was also able to quantify lipids in isolated macrophages from BAT and inguinal WAT. In general, distinct differences in lipid composition of macrophages from BAT and inguinal WAT were observed. This might be due to environmental differences these macrophages face, namely the different degree of thermogenic activity of the adipose tissues. In BAT, the high metabolic activity presents a higher lipid incorporation compared to the less metabolic active inguinal beiging WAT.^{46} Macrophages present high phagocytic activity and might engulf lipids from their surroundings. Recently, macrophages from adipose tissue were described to take up dying adipocytes in a non-inflammatory removal process. The uptake mediated macrophage lipid synthesis in a way that PPAR γ agonists were synthesized that supported the biogenesis of thermogenic adipocytes.^{122}

When housing mice at thermoneutrality, BAT macrophages contained large amounts of TGs, however, after housing mice at 6° C, the TG content decreased and the macrophages mainly consisted of CEs. Macrophages isolated from inguinal WAT did not present profound alterations after changing the housing temperature of the mice. In states of activated thermogenesis, whole lipoprotein particles are also incorporated into adipose tissues as shown by Bartelt et. al and one could speculate that the incorporated lipoproteins might be targeted by macrophages for uptake.^{46} As discussed in 1.2, whole HDL particles are likely to be taken up during BAT activation. They harbor large amounts of CEs within their core and might be phagocytosed by macrophages. CEs are precursors for oxysterols which activate *liver X receptor* (LXR).^{123} On the one hand, the cholesterol-induced LXR activation might regulate the cholesterol efflux from the macrophages.^{124, 125} During cold, the high amount of cholesterol accumulated in the BAT and BAT macrophages could potentially be harmful to the cells, thus feedback mechanisms are upregulated to excrete cholesterol again. On the other hand, the cholesterol increase which was observed within BAT macrophages potentially modulates the polarization of macrophages. Treatment of macrophages with LXR agonists was shown to downregulate pro-inflammatory genes, e.g. IL-6 *in vitro* and *in vivo* and to promote a polarization towards the M2 phenotype.^{126, 127} In my study, accumulation of CEs in macrophages isolated from BAT entailed a polarization towards a M2 phenotype. Namely, mRNA expression of genes used for discrimination of M1 and M2 macrophages depicted increased levels of genes associated with anti-inflammatory capacities (*Arg1* and *I110*), whereas the pro-inflammatory *I16* was downregulated compared to macrophages isolated from BAT of thermoneutral-housed mice. In macrophages

isolated from inguinal WAT of thermoneutral- and cold-housed mice, no remarkable changes were observed when analyzing the lipid composition.

However, after cold housing, gene expression might indicate a polarization of macrophages towards a more anti-inflammatory M2 phenotype as *Arg1* was upregulated and *Il6* expression decreased. Expression of *Il10* was not affected in macrophages isolated from inguinal WAT. Additionally, it was found that macrophages from BAT upregulated genes important for lipoprotein/lipid processing and lipid uptake after BAT activation. LPL and EL on the surface of macrophages might target TGs and PLs of absorbed whole HDL particles and EL was shown to promote the uptake of CEs from HDL.^{128} Thus, I speculate, that the higher expression of *Lipg* in BAT macrophages drives CE incorporation which, potentially via LXR, promotes polarization towards an anti-inflammatory M2 phenotype. This phenomenon was observed in macrophages from BAT of cold-housed mice, whereas the phenotype in macrophages from inguinal WAT of cold-housed mice was less evident. Macrophages isolated from inguinal WAT of cold-housed mice presented an increased expression of *Lipg*, however, no elevation in CE levels was observed. Based on the gene expression analysis, I hypothesize that macrophages from inguinal WAT trend towards an M2 classification after 7 days of cold housing since the M2 marker *Arg1* was upregulated and the pro-inflammatory cytokine *IL-6* was downregulated.

The various grade of metabolic activation in BAT and beige adipose tissues might explain the less pronounced alterations in macrophages from BAT and beiged inguinal WAT. Enduring the cold stress for a longer period might amplify the M2 polarization also in macrophages from inguinal WAT. In the recent years, the field of immunology has challenged the classical categorization of immune cells, regardless of looking at innate or adaptive immunity, and proposed a rather heterogenous distribution and the concept of plasticity.^{129} The discrimination of macrophages into M1 and M2 needs to be treated with caution as discrimination based on 1 or 2 markers might underestimate their heterogeneity.

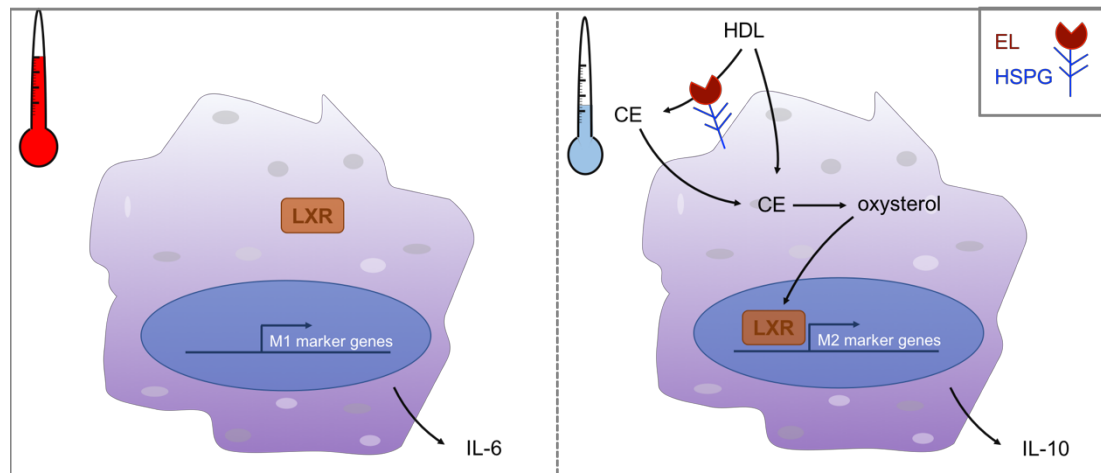


Figure 29. Macrophage polarization in BAT. During thermoneutrality LXR resides in the cytoplasm. Genes characterizing an M1 phenotype are expressed which e.g. leads to synthesis and secretion of IL-6. During cold stress, we hypothesize that CE is released from incorporated HDL particles. Furthermore, whole HDL might also be phagocytosed and thereby leading to increases in CE within the cell. CEs are converted to oxysterols which activate LXR. Upon activation, LXR translocates to the nucleus and activates genes leading to a M2 polarization of macrophages and synthesis and secretion of IL-10.

In addition to the activation of LXR, another mechanism was described to promote differentiation towards M2 macrophages within adipose tissue. Namely, Hui et. al showed a browning-induced accumulation of adiponectin in inguinal WAT which is absent in BAT, ultimately leading to a polarization of macrophages towards an M2 phenotype.^{130} My study corroborates the findings by Hui et. al, as I see high induction of adiponectin in inguinal WAT and mRNA expression of *Arg1* and *Ilf6* indicate a polarization towards an M2 phenotype (Figure 13.B). The differences in adiponectin presence between BAT and inguinal WAT might involve the β 3-adrenergic-independent production of reactive oxygen species (ROS). In inguinal WAT but not in BAT, ROS might be produced to higher abundance due to the close proximity to the cold environment and ROS induces adiponectin production.^{130}

In summary, my data and studies by others showed a cold-induced shift towards M2 macrophages in BAT and inguinal WAT. However, it remains to be elucidated whether and how M2 macrophages contribute to adaptive thermogenesis and energy expenditure. The model of catecholamine synthesis by alternatively activated macrophages which was brought up by the group of Ajaj Chawla was highly questioned by experts in the field of BAT research.^{90, 92} Another possible mechanism, how M2 macrophages contribute to the beiging process was recently proposed by Lee et. al. The authors found that M2 macrophages in fat pads undergoing browning produce *peroxisome proliferator-activated receptor γ* (PPAR γ) ligands which promote brown/beige adipogenesis.^{122} The PPAR γ ligands secreted by M2 macrophages were lipids which were synthesized due to uptake of dying adipocytes. In conclusion, evidence for the promotion of M2 macrophages during

adaptive thermogenesis exists; however, whether and how M2 contribute to energy expenditure needs further investigation.

2 Thermogenesis-induced alterations in HDL metabolism

Tissue-mediated lipoprotein processing is mandatory to support metabolically active tissues with nutrients and to store a surplus of lipids in e.g. liver or adipose tissues. The LPL family, consisting of LPL, EL and HL, yields important players in maintaining lipid homeostasis in the circulation and mutations in *LPL* locus in humans are associated with increases in plasma TGs and reduced HDL-C levels.{131} In states of activated thermogenesis, high amounts of energy are combusted by brown and beige adipocytes, thereby leading to improved plasma TG and cholesterol concentration in mice.{46, 105}

The cholesterol decrease could be mainly attributed to reduced HDL-C levels, whereas no differences were observed in HDL particle number, as ApoA1 concentration was unaltered. Activation of BAT in humans by repeated cryostimulation, however, resulted in contrary findings: in active men HDL-C were increased, and also *UCP1* expression in epicardial WAT was associated with increased HDL-C concentrations.{47,132} Interestingly, in the same line, BAT activation resulted in decreased cholesterol levels in the TRL fraction, but increased HDL-C levels in hyperlipidemic (*Apoa5*^{-/-}) or in *E3L.CETP* mice that display a humanized lipoprotein profile.{107} My data indicate that HDL particle number is unchanged after one week of cold, whereas the cholesterol content in HDL decreases. This led to the hypothesis that the removal of cholesterol from HDL particles might be accelerated in the context of BAT activation. In order to test this assumption, metabolic HDL turnover studies were performed. Notably, cold-housed mice presented an increased HDL turnover compared to their thermoneutral controls, resulting in an accelerated plasma clearance of HDL-derived cholesterol. Although no profound differences were observed in the lipoprotein profile of fasted versus refed mice, the cold-induced acceleration in HDL flux was further increased under refeeding conditions. This effect can be explained by increased insulin levels in the refeeding phase, which are known to stimulate intravascular lipolysis in adipose tissues.{79} We observed increased ³H and ¹²⁵I uptake into BAT in fasted and refed conditions that argues for increased whole HDL particle uptake. It is discussed whether internalization of ApoA1-containing lipoproteins increases energy expenditure and contributes to cholesterol efflux from adipocytes that might be important especially in states of increased cholesterol uptake occurring during adaptive thermogenesis.{133, 134}

HDL-derived cholesterol was cleared from the plasma to a similar extent in refed mice compared to fasted mice, however, increased lipolytic processes in refed mice induced higher abundance of cholesterol in the liver and in the gallbladder, which suggests an amplified reverse cholesterol metabolism. HDL-mediated RCT forms a promising target to treat cardiovascular disease, and I could show that BAT activation has the potential to increase *in vivo* RCT in mice.{135-137} These findings led me hypothesize that lipolytic processes during BAT activation drive macrophage-to-HDL-to-feces cholesterol transport, thereby appearing as a potential target to counteract cholesterol accumulation in the vasculature.{106}

Additionally, these findings highlight the importance of HDL quality rather than quantity for effective cholesterol clearance, as despite reduced HDL-C levels and unaltered ApoA1 presence after BAT activation, HDL metabolism was accelerated. These findings help to explain the uncertainties about HDL-raising drugs and validate the “HDL flux hypothesis” by Rader and Tall which highlights the importance of analyzing “*HDL-mediated cholesterol flux from macrophage foam cells or measurements of the flux of cholesterol from macrophages to the liver and feces*” rather than plasma HDL-C concentrations.{138, 139}

3 Significance of lipases in BAT-accelerated HDL metabolism

As described in 1.2., BAT-accelerated HDL metabolism could be boosted in post-prandial conditions in mice, suggesting the impact of diet-induced lipolysis on reverse cholesterol metabolism. Whereas LPL mainly targets the TG moiety within TRL particles, EL has a preference to hydrolyze PL of HDL particles.{107, 120} Here, I am the first to investigate the influence of LPL and EL on HDL metabolism in states of BAT activation. In the HDL turnover studies, wildtype mice were compared to genetically modified mice, which were both housed under conditions of cold-induced HDL metabolism and RCT.{107} LPL in adipocytes was essential to clear HDL-derived cholesterol from plasma and to incorporate HDL-C into BAT. The hydrolysis of TRL particles by LPL induces release of FAs leading to a shrinkage in particle size. A surplus of PLs occurs which encapsulates from the TRL and forms, according to the theory, a so-called surface remnant.{6, 7} By fusion with ApoA1, these surface remnants accomplish HDL functionalities and potentially contribute to RCT. Thus, BAT-induced LPL activity could enhance reverse cholesterol metabolism by generating surface remnants and increase HDL-derived cholesterol flux to the liver.

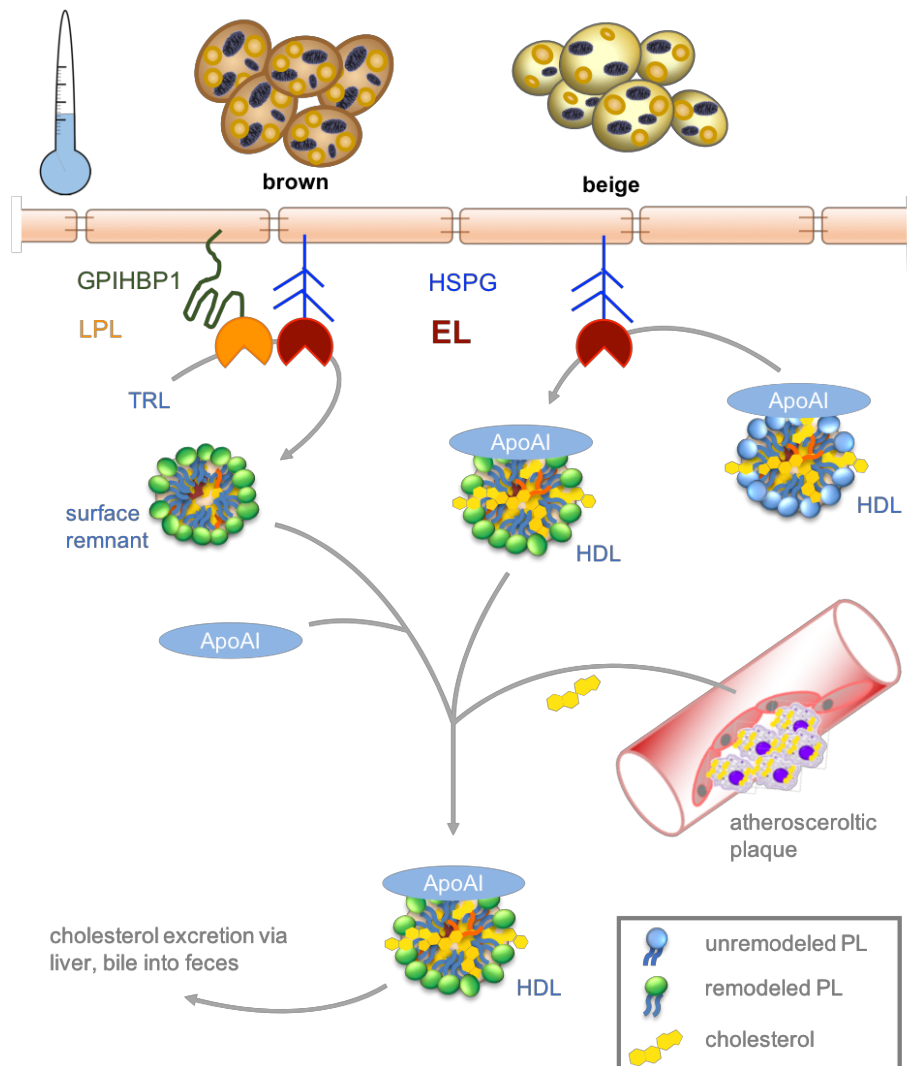


Figure 30. Working Model. In states of adaptive thermogenesis processing of triglyceride-rich lipoproteins (TRLs) is accelerated. Lipoprotein lipase (LPL) and endothelial lipase (EL) are upregulated and linked to the endothelium by *glycosylphosphatidylinositol anchored high density lipoprotein binding protein 1* (GPIHBP1) and *heparan sulfate proteoglycans* (HSPG), respectively. LPL targets the TG moiety within TRLs, thereby releasing free fatty acids for organ uptake and EL leads to a remodeling of phospholipids (PLs). During the cleavage of TRL, according to the *surface remnant theory*, a surplus of PLs detaches and forms surface remnants. These can fuse with ApoA1 and exert HDL functionalities, thereby contributing to reverse cholesterol transport. Furthermore, EL remodels PLs of HDL particles which results in accelerated reverse cholesterol transport.

At the end, this process would accelerate the excretion of cholesterol and its derivatives via the feces. During cold intervention, the liver relies mainly on the alternative pathway to metabolize cholesterol into bile acids, which was shown in an upregulation of *Cyp7b1* and is in accordance with the literature.^{140} This hypothesis was strengthened by reduced cholesterol tracer concentrations found in the gallbladder of aKO mice indicating an impairment of cholesterol excretion. However, to efficiently clear HDL-CET from plasma and facilitate excretion via feces, SR-B1 was shown to be essential in mice and humans.^{141-145} I identified SR-B1 to play a key role in the uptake of HDL-derived cholesterol also in states of high HDL turnover induced by BAT activation. Although impairment in SR-B1 functionalities result in elevated HDL-C levels, which might suggest athero-protective effects, SNPs in the

SR-B1 locus linked to tremendous HDL-C increases were associated with increased risk for CVD.^{146} Taken together, these data indicate that it is not the cholesterol content in HDL per se but rather the efflux capacity which explains the cardioprotective properties of HDL.

As well as high activity of LPL in activated BAT, increased expression of *Lipg* suggested that EL was contributing to lipoprotein remodeling. To address this question, EL-deficient mice were housed at thermoneutrality or cold. By analyzing the plasma lipoprotein profile, increased cholesterol levels in the HDL fraction in mice lacking EL was detected. This is in line with the findings that EL preferentially hydrolyzes HDL particles rather than other lipoprotein classes.^{120} It was already reported that loss of EL results in elevated HDL, whereas overexpression diminishes HDL, however, I am the first to report the relevance of EL in the physiological setting of adaptive thermogenesis.^{50, 60, 147}

The HDL lowering effects are most likely due to the catalytic activity of EL, since adenoviral overexpression of an inactive form was insufficient to reduce HDL levels in plasma. ^{148} Furthermore, *elKO* mice presented an elevation in small LDL compared to wildtype controls. Brown et. al also reported increased cholesterol concentrations in the small LDL fraction, however, only when mice were lacking both, EL and HL. In their study, single ablation of EL did not result in alterations of small LDL-C.^{55} The increase in small LDL-C might be explained by impaired processing of ApoB-containing lipoproteins in *elKO* mice, whereas in wildtype mice, effective processing of ApoB-containing lipoproteins prevents the accumulation of small LDL.^{149}

No major changes in the expression of genes involved in browning or lipoprotein processing, neither in BAT, inguinal WAT nor the liver in *elKO* mice were determined which could abet the conclusion that loss of EL does not impair cholesterol metabolism. Nevertheless, global deletion of EL reduced HDL turnover and macrophage-to-feces transport. In accordance with my findings, Takiguchi et. al found that also overexpression of EL in hepatocytes by adenoviral injection did not cause alterations on hepatic mRNA level, however, improvements in HDL-derived and macrophage-derived cholesterol excretion were observed.^{56} These data indicate that, both LPL and EL, are an important molecules in facilitating reverse cholesterol transport metabolism during the cold.

Whereas LPL mainly targets the TG moiety within TRL particles, previous studies revealed the EL preference to hydrolyze PLs within HDL particles.^{107, 120} To test lipolytic function of EL during BAT activation, the lipid composition in HDL particles which derived from wildtype and *elKO* mice housed under thermoneutral and cold

housing conditions were analyzed. As shown previously by Yang et al., the loss of EL resulted in increased levels of PLs within the HDL particles isolated from mouse plasma.^{37} The most abundant lipid class, the PC species was increased in eKO mice independently of the ambient temperature. The increased relative and absolute amounts in eKO might be explained by an increase in HDL quantity or particle size. In FPLC-separated HDL, also an elevated concentration of cholesterol was detected, arguing for increased HDL quantity or particle size in eKO compared to wildtype mice. In addition to my obtained data, determination of ApoA1 in the plasma would be necessary to discriminate between an increase in particle size or number since HDL particles are characterized by carrying one molecule of ApoA1 per each particle. Indications for an increase in particle size could be based on a study by Ma et. al, however, Ishida et. al considered the HDL-C raising effect as elevations in particle number.^{60, 147}

Yang et. al measured individual lyso-PC species from plasma of eKO mice and did not find any significant differences compared to wildtype mice.^{37} In contrast, my data showed an elevation of lyso-PCs in eKO mice housed at thermoneutrality, whereas the effect was less pronounced in HDL isolated from cold-housed eKO mice. The increase of lyso-PC was unexpected as eKO were mainly known to hydrolyze PCs, however, recent studies showed lysophospholipase activity of EL when HDL-PCs were used as substrates in order to release FAs.^{150} The findings obtained in this thesis suggest that the ambient temperature affected the levels of lyso-PCs in eKO mice, while other lipid classes did not differ between thermoneutral- and cold-housed mice. In the publication by Yang et. al, mice were housed at 22° C, a condition in which adaptive thermogenesis is already activated. It is likely that BAT activation induced a reduction in lyso-PC levels which would explain the discrepancies to our findings in the thermoneutral-housed eKO. My findings indicate that ablation of EL in mice results in an impaired remodeling of HDL particles, especially within the PLs and consequently this might increase HDL particle size and/or number. An increase in HDL particle size might explain the blunted RCT observed in our study as a recent publication by Schlicher et. al could show that the RCT promoting effect by EL is facilitated via small HDL.^{151}

In states of brown adipocyte activation, lipolytic processing of lipoproteins is induced which was evident in increased *Lpl* and *Lipg* expression within brown adipose tissue. Previous studies performed in our lab could show the importance of LPL in BAT-induced lipid remodeling of TRL particles (PhD work of Dr. rer. nat. Clara John). Measuring the HDL turnover in aKO mice highlights the importance of LPL-dependent lipoprotein remodeling for maintaining HDL-mediated cholesterol

metabolism. Furthermore, the performed HDL turnover study in eIKO mice suggests that also the lipid remodeling induced by EL during BAT activation is mandatory for efficient reverse cholesterol flux from plasma to the liver and even further to the feces as indicated in the *in vivo* RCT assay. The accumulation of injected HDL-derived ³H-CET in eIKO plasma even more pronounced compared to the plasma accumulation observed in aIKO mice. One explanation for that could be the global deletion of EL, whereas LPL was deleted specifically in adipocytes. By lack of EL in the whole vasculature the effect could not be exclusively attributed to EL loss in thermogenic adipose tissue.

In addition to the lipolytic function of EL, EL was described to modulate plasma HDL-C by a non-lipolytic bridging function which promotes lipoprotein incorporation. Namely, the high plasma accumulation of HDL-C in turnover experiments performed in mice lacking EL globally, could be explained by a reduced uptake of HDL-derived CE into the liver by the impaired bridging function.^{128} Additionally, in accordance with our findings of plasma accumulation of cholesterol-labels in eIKO mice, a murine *in vivo* study by Takiguchi et. al revealed increased clearance of HDL-derived ³H-CET and macrophage-derived cholesterol from plasma of mice overexpressing human EL specifically in hepatocytes.^{56} The effect I observed, might be more pronounced as mice were housed in 6° C which led to high activation of lipolysis in the vasculature. In summary, my experiments indicate a high lipolytic environment during BAT activation that leads to increases in HDL flux and reverse cholesterol transport. The LPL and EL are main players in lipid remodeling of lipoproteins, which is key in maintaining the increased lipoprotein processing during adaptive thermogenesis. Neither loss of LPL nor EL led to a complete loss of the cholesterol excretion capacity, so I hypothesize that they might compensate each other. Future studies with mice lacking both LPL and EL are needed to determine the relevance of intravascular remodeling for effective cholesterol flux. Evidence is based on experiments which showed that independent of EL preference for HDL-PL hydrolysis, EL presents the capacity to target TGs and furthermore is also able to target ApoB-containing (V)LDL.^{120, 149}

Another possible mechanism that might contribute to reduced HDL-CET clearance in eIKO mice might be attributed to the interplay of EL and SR-B1 for effective uptake in the liver. Remodeling processes mediated by EL are essential for adequate CET clearance by SR-B1, however, biliary secretion is independent of EL.^{152, 153} Despite my hypothesis of a negative impact in cholesterol excretion in eIKO mice due to impaired lipid remodeling, generation of anti-inflammatory HDL particles as described by others, cannot be excluded.^{154} Furthermore, I speculate that the

observed effects on HDL metabolism are mainly due to loss of lipolytic EL function, disregarding its non-lipolytic activity which contributes to a lesser extent in normolipidemic mice.{155}

Another aspect worth in considering in EL manipulation for treating atherosclerosis is its impact on cholesterol efflux from macrophages and foam cells, respectively, within atherosclerotic plaques. The EL-mediated HDL-PL remodeling might add to cholesterol efflux processes, thus reducing macrophage presence and foam cell formation.{58} In addition, pro-inflammatory cytokines, such as IL-1 β and TNF, which increase during plaque progression, induce expression of EL.{156, 157} On the one hand, EL presence within macrophages enhances binding of ApoA1 that might be a control mechanism to counteract cholesterol accumulation within the plaque.{158} On the other hand, EL induction within the plaque might intensify monocyte infiltration and thereby augment atherosclerosis progression.{159} In conclusion, the impact of EL in atherosclerosis development has been discussed in a contradictory manner so far and needs further investigation.{58, 61}

Part H References

1. Hofmann, A.F. and B. Borgstroem, *The Intraluminal Phase of Fat Digestion in Man: The Lipid Content of the Micellar and Oil Phases of Intestinal Content Obtained during Fat Digestion and Absorption*. J Clin Invest, 1964. **43**: p. 247-57.
2. Martinez-Guryn, K., et al., *Small Intestine Microbiota Regulate Host Digestive and Absorptive Adaptive Responses to Dietary Lipids*. Cell Host Microbe, 2018. **23**(4): p. 458-469 e5.
3. Beisiegel, U., et al., *The LDL-receptor-related protein, LRP, is an apolipoprotein E-binding protein*. Nature, 1989. **341**(6238): p. 162-4.
4. Brown, S.A., et al., *Apolipoprotein E-mediated binding of hypertriglyceridemic very low density lipoproteins to isolated low density lipoprotein receptors detected by ligand blotting*. Biochem Biophys Res Commun, 1986. **139**(1): p. 333-40.
5. Bittner, V.A., et al., *PCSK9 inhibitors for prevention of atherosclerotic cardiovascular disease*. J Clin Lipidol, 2018. **12**(4): p. 835-843.
6. Eisenberg, S. and T. Olivecrona, *Very low density lipoprotein. Fate of phospholipids, cholesterol, and apolipoprotein C during lipolysis in vitro*. J Lipid Res, 1979. **20**(5): p. 614-23.
7. Patsch, J.R., et al., *Formation of high density lipoprotein2-like particles during lipolysis of very low density lipoproteins in vitro*. Proc Natl Acad Sci U S A, 1978. **75**(9): p. 4519-23.
8. Brown, J.M., et al., *Targeted depletion of hepatic ACAT2-driven cholesterol esterification reveals a non-biliary route for fecal neutral sterol loss*. J Biol Chem, 2008. **283**(16): p. 10522-34.
9. Temel, R.E. and J.M. Brown, *A new framework for reverse cholesterol transport: non-biliary contributions to reverse cholesterol transport*. World J Gastroenterol, 2010. **16**(47): p. 5946-52.
10. van der Velde, A.E., et al., *Regulation of direct transintestinal cholesterol excretion in mice*. Am J Physiol Gastrointest Liver Physiol, 2008. **295**(1): p. G203-G208.
11. Lee, J.H., et al., *The transcription factor cyclic AMP-responsive element-binding protein H regulates triglyceride metabolism*. Nat Med, 2011. **17**(7): p. 812-5.
12. Goldberg, I.J., et al., *Lipoprotein ApoC-II activation of lipoprotein lipase. Modulation by apolipoprotein A-IV*. J Biol Chem, 1990. **265**(8): p. 4266-72.
13. Larsson, M., et al., *Apolipoprotein C-III inhibits triglyceride hydrolysis by GPIHBP1-bound LPL*. J Lipid Res, 2017. **58**(9): p. 1893-1902.
14. Khetarpal, S.A., et al., *A human APOC3 missense variant and monoclonal antibody accelerate apoC-III clearance and lower triglyceride-rich lipoprotein levels*. Nat Med, 2017. **23**(9): p. 1086-1094.
15. Kluger, M., J. Heeren, and M. Merkel, *Apoprotein A-V: an important regulator of triglyceride metabolism*. J Inherit Metab Dis, 2008. **31**(2): p. 281-8.
16. Merkel, M. and J. Heeren, *Give me A5 for lipoprotein hydrolysis!* J Clin Invest, 2005. **115**(10): p. 2694-6.
17. Rabacchi, C., et al., *Clinical and genetic features of 3 patients with familial chylomicronemia due to mutations in GPIHBP1 gene*. J Clin Lipidol, 2016. **10**(4): p. 915-921 e4.
18. Nilsson, S.K., et al., *Apolipoprotein A-V; a potent triglyceride reducer*. Atherosclerosis, 2011. **219**(1): p. 15-21.

19. Brown, M.S. and J.L. Goldstein, *A receptor-mediated pathway for cholesterol homeostasis*. Science, 1986. **232**(4746): p. 34-47.
20. Brown, M.S., P.T. Kovanen, and J.L. Goldstein, *Regulation of plasma cholesterol by lipoprotein receptors*. Science, 1981. **212**(4495): p. 628-35.
21. Rohlmann, A., et al., *Inducible inactivation of hepatic LRP gene by cre-mediated recombination confirms role of LRP in clearance of chylomicron remnants*. J Clin Invest, 1998. **101**(3): p. 689-95.
22. Ayyobi, A.F., et al., *Lecithin: cholesterol acyltransferase (LCAT) deficiency and risk of vascular disease: 25 year follow-up*. Atherosclerosis, 2004. **177**(2): p. 361-6.
23. Vitali, C., S.A. Khetarpal, and D.J. Rader, *HDL Cholesterol Metabolism and the Risk of CHD: New Insights from Human Genetics*. Curr Cardiol Rep, 2017. **19**(12): p. 132.
24. Morrison, A.C., et al., *Whole-genome sequence-based analysis of high-density lipoprotein cholesterol*. Nat Genet, 2013. **45**(8): p. 899-901.
25. Papp, A.C., et al., *Cholesteryl Ester Transfer Protein (CETP) polymorphisms affect mRNA splicing, HDL levels, and sex-dependent cardiovascular risk*. PLoS One, 2012. **7**(3): p. e31930.
26. Group, H.T.R.C., et al., *Effects of Anacetrapib in Patients with Atherosclerotic Vascular Disease*. N Engl J Med, 2017. **377**(13): p. 1217-1227.
27. Kuhnast, S., et al., *Anacetrapib reduces progression of atherosclerosis, mainly by reducing non-HDL-cholesterol, improves lesion stability and adds to the beneficial effects of atorvastatin*. Eur Heart J, 2015. **36**(1): p. 39-48.
28. Lie, J., et al., *Elevation of plasma phospholipid transfer protein increases the risk of atherosclerosis despite lower apolipoprotein B-containing lipoproteins*. J Lipid Res, 2004. **45**(5): p. 805-11.
29. van Haperen, R., et al., *Elevated expression of PLTP is atherogenic in apolipoprotein E deficient mice*. Atherosclerosis, 2013. **227**(1): p. 37-42.
30. Yang, X.P., et al., *Increased atherosclerotic lesions in apoE mice with plasma phospholipid transfer protein overexpression*. Arterioscler Thromb Vasc Biol, 2003. **23**(9): p. 1601-7.
31. Dugi, K.A., H.L. Dichek, and S. Santamarina-Fojo, *Human hepatic and lipoprotein lipase: the loop covering the catalytic site mediates lipase substrate specificity*. J Biol Chem, 1995. **270**(43): p. 25396-401.
32. Dugi, K.A., et al., *Human lipoprotein lipase: the loop covering the catalytic site is essential for interaction with lipid substrates*. J Biol Chem, 1992. **267**(35): p. 25086-91.
33. Griffon, N., et al., *Substrate specificity of lipoprotein lipase and endothelial lipase: studies of lid chimeras*. J Lipid Res, 2006. **47**(8): p. 1803-11.
34. Kobayashi, J., et al., *Analysis of protein structure-function in vivo. Adenovirus-mediated transfer of lipase lid mutants in hepatic lipase-deficient mice*. J Biol Chem, 1996. **271**(42): p. 26296-301.
35. Brun, L.D., et al., *Familial lipoprotein lipase-activity deficiency: study of total body fatness and subcutaneous fat tissue distribution*. Metabolism, 1989. **38**(10): p. 1005-9.
36. Kratky, D., et al., *Endothelial lipase provides an alternative pathway for FFA uptake in lipoprotein lipase-deficient mouse adipose tissue*. J Clin Invest, 2005. **115**(1): p. 161-7.

37. Yang, Y., et al., *Lipidomic analyses of female mice lacking hepatic lipase and endothelial lipase indicate selective modulation of plasma lipid species*. *Lipids*, 2014. **49**(6): p. 505-15.
38. Dewey, F.E., et al., *Inactivating Variants in ANGPTL4 and Risk of Coronary Artery Disease*. *N Engl J Med*, 2016. **374**(12): p. 1123-33.
39. Myocardial Infarction, G., et al., *Coding Variation in ANGPTL4, LPL, and SVEP1 and the Risk of Coronary Disease*. *N Engl J Med*, 2016. **374**(12): p. 1134-44.
40. Gaudet, D., et al., *ANGPTL3 Inhibition in Homozygous Familial Hypercholesterolemia*. *N Engl J Med*, 2017. **377**(3): p. 296-297.
41. Su, X. and D.Q. Peng, *New insights into ANGPTL3 in controlling lipoprotein metabolism and risk of cardiovascular diseases*. *Lipids Health Dis*, 2018. **17**(1): p. 12.
42. Korn, E.D., *Clearing factor, a heparin-activated lipoprotein lipase. I. Isolation and characterization of the enzyme from normal rat heart*. *J Biol Chem*, 1955. **215**(1): p. 1-14.
43. Wong, H., et al., *Lipoprotein lipase domain function*. *J Biol Chem*, 1994. **269**(14): p. 10319-23.
44. McIlhargey, T.L., et al., *Identification of a lipoprotein lipase cofactor-binding site by chemical cross-linking and transfer of apolipoprotein C-II-responsive lipolysis from lipoprotein lipase to hepatic lipase*. *J Biol Chem*, 2003. **278**(25): p. 23027-35.
45. Breckenridge, W.C., et al., *Hypertriglyceridemia associated with deficiency of apolipoprotein C-II*. *N Engl J Med*, 1978. **298**(23): p. 1265-73.
46. Bartelt, A., et al., *Brown adipose tissue activity controls triglyceride clearance*. *Nat Med*, 2011. **17**(2): p. 200-5.
47. Chechi, K., et al., *Brown fat like gene expression in the epicardial fat depot correlates with circulating HDL-cholesterol and triglycerides in patients with coronary artery disease*. *Int J Cardiol*, 2013. **167**(5): p. 2264-70.
48. Zhang, R., *The ANGPTL3-4-8 model, a molecular mechanism for triglyceride trafficking*. *Open Biol*, 2016. **6**(4): p. 150272.
49. Hirata, K., et al., *Cloning of a unique lipase from endothelial cells extends the lipase gene family*. *J Biol Chem*, 1999. **274**(20): p. 14170-5.
50. Jaye, M., et al., *A novel endothelial-derived lipase that modulates HDL metabolism*. *Nat Genet*, 1999. **21**(4): p. 424-8.
51. Jin, W., et al., *Hepatic proprotein convertases modulate HDL metabolism*. *Cell Metab*, 2007. **6**(2): p. 129-36.
52. Yasuda, T., T. Ishida, and D.J. Rader, *Update on the role of endothelial lipase in high-density lipoprotein metabolism, reverse cholesterol transport, and atherosclerosis*. *Circ J*, 2010. **74**(11): p. 2263-70.
53. Shimamura, M., et al., *Angiopietin-like protein3 regulates plasma HDL cholesterol through suppression of endothelial lipase*. *Arterioscler Thromb Vasc Biol*, 2007. **27**(2): p. 366-72.
54. Rosenson, R.S., et al., *HDL and atherosclerotic cardiovascular disease: genetic insights into complex biology*. *Nat Rev Cardiol*, 2018. **15**(1): p. 9-19.
55. Brown, R.J., et al., *Impact of combined deficiency of hepatic lipase and endothelial lipase on the metabolism of both high-density lipoproteins and apolipoprotein B-containing lipoproteins*. *Circ Res*, 2010. **107**(3): p. 357-64.
56. Takiguchi, S., et al., *Hepatic Overexpression of Endothelial Lipase Lowers High-Density Lipoprotein but Maintains Reverse Cholesterol*

- Transport in Mice: Role of Scavenger Receptor Class B Type I/ATP-Binding Cassette Transporter A1-Dependent Pathways*. *Arterioscler Thromb Vasc Biol*, 2018. **38**(7): p. 1454-1467.
57. Azumi, H., et al., *Immunohistochemical localization of endothelial cell-derived lipase in atherosclerotic human coronary arteries*. *Cardiovasc Res*, 2003. **58**(3): p. 647-54.
58. Ishida, T., et al., *Endothelial lipase modulates susceptibility to atherosclerosis in apolipoprotein-E-deficient mice*. *J Biol Chem*, 2004. **279**(43): p. 45085-92.
59. Edmondson, A.C., et al., *Loss-of-function variants in endothelial lipase are a cause of elevated HDL cholesterol in humans*. *J Clin Invest*, 2009. **119**(4): p. 1042-50.
60. Ishida, T., et al., *Endothelial lipase is a major determinant of HDL level*. *J Clin Invest*, 2003. **111**(3): p. 347-55.
61. Ko, K.W., et al., *Endothelial lipase modulates HDL but has no effect on atherosclerosis development in apoE^{-/-} and LDLR^{-/-} mice*. *J Lipid Res*, 2005. **46**(12): p. 2586-94.
62. Amar, M.J., et al., *Hepatic lipase facilitates the selective uptake of cholesteryl esters from remnant lipoproteins in apoE-deficient mice*. *J Lipid Res*, 1998. **39**(12): p. 2436-42.
63. Ji, Z.S., et al., *Enhanced binding and uptake of remnant lipoproteins by hepatic lipase-secreting hepatoma cells in culture*. *J Biol Chem*, 1994. **269**(18): p. 13429-36.
64. Cannon, B. and J. Nedergaard, *Brown adipose tissue: function and physiological significance*. *Physiol Rev*, 2004. **84**(1): p. 277-359.
65. Cypess, A.M., et al., *Identification and importance of brown adipose tissue in adult humans*. *N Engl J Med*, 2009. **360**(15): p. 1509-17.
66. Saito, M., et al., *High incidence of metabolically active brown adipose tissue in healthy adult humans: effects of cold exposure and adiposity*. *Diabetes*, 2009. **58**(7): p. 1526-31.
67. van Marken Lichtenbelt, W.D., et al., *Cold-activated brown adipose tissue in healthy men*. *N Engl J Med*, 2009. **360**(15): p. 1500-8.
68. Virtanen, K.A., et al., *Functional brown adipose tissue in healthy adults*. *N Engl J Med*, 2009. **360**(15): p. 1518-25.
69. Zingaretti, M.C., et al., *The presence of UCP1 demonstrates that metabolically active adipose tissue in the neck of adult humans truly represents brown adipose tissue*. *FASEB J*, 2009. **23**(9): p. 3113-20.
70. Romu, T., et al., *A randomized trial of cold-exposure on energy expenditure and supraclavicular brown adipose tissue volume in humans*. *Metabolism*, 2016. **65**(6): p. 926-34.
71. van der Lans, A.A., et al., *Cold acclimation recruits human brown fat and increases nonshivering thermogenesis*. *J Clin Invest*, 2013. **123**(8): p. 3395-403.
72. Lee, Y.H., et al., *In vivo identification of bipotential adipocyte progenitors recruited by beta3-adrenoceptor activation and high-fat feeding*. *Cell Metab*, 2012. **15**(4): p. 480-91.
73. Schulz, T.J., et al., *Identification of inducible brown adipocyte progenitors residing in skeletal muscle and white fat*. *Proc Natl Acad Sci U S A*, 2011. **108**(1): p. 143-8.
74. Wu, J., et al., *Beige adipocytes are a distinct type of thermogenic fat cell in mouse and human*. *Cell*, 2012. **150**(2): p. 366-76.
75. Gregor, M.F. and G.S. Hotamisligil, *Inflammatory mechanisms in obesity*. *Annu Rev Immunol*, 2011. **29**: p. 415-45.
76. Bartelt, A. and J. Heeren, *Adipose tissue browning and metabolic health*. *Nat Rev Endocrinol*, 2014. **10**(1): p. 24-36.

77. Cao, W., et al., *p38 mitogen-activated protein kinase is the central regulator of cyclic AMP-dependent transcription of the brown fat uncoupling protein 1 gene*. Mol Cell Biol, 2004. **24**(7): p. 3057-67.
78. Puigserver, P., et al., *A cold-inducible coactivator of nuclear receptors linked to adaptive thermogenesis*. Cell, 1998. **92**(6): p. 829-39.
79. Heine, M., et al., *Lipolysis Triggers a Systemic Insulin Response Essential for Efficient Energy Replenishment of Activated Brown Adipose Tissue in Mice*. Cell Metab, 2018.
80. Vaillancourt, E., F. Haman, and J.M. Weber, *Fuel selection in Wistar rats exposed to cold: shivering thermogenesis diverts fatty acids from re-esterification to oxidation*. J Physiol, 2009. **587**(Pt 17): p. 4349-59.
81. Van den Brandt, P.A. and P. Trayhurn, *Suppression of fatty acids synthesis in brown adipose tissue of mice fed diets rich in long chain fatty acids*. Biochim Biophys Acta, 1981. **665**(3): p. 602-7.
82. Hotamisligil, G.S., N.S. Shargill, and B.M. Spiegelman, *Adipose expression of tumor necrosis factor-alpha: direct role in obesity-linked insulin resistance*. Science, 1993. **259**(5091): p. 87-91.
83. Apovian, C.M., et al., *Adipose macrophage infiltration is associated with insulin resistance and vascular endothelial dysfunction in obese subjects*. Arterioscler Thromb Vasc Biol, 2008. **28**(9): p. 1654-9.
84. Canello, R., et al., *Increased infiltration of macrophages in omental adipose tissue is associated with marked hepatic lesions in morbid human obesity*. Diabetes, 2006. **55**(6): p. 1554-61.
85. Weisberg, S.P., et al., *Obesity is associated with macrophage accumulation in adipose tissue*. J Clin Invest, 2003. **112**(12): p. 1796-808.
86. Xu, H., et al., *Chronic inflammation in fat plays a crucial role in the development of obesity-related insulin resistance*. J Clin Invest, 2003. **112**(12): p. 1821-30.
87. Kumari, M., J. Heeren, and L. Scheja, *Regulation of immunometabolism in adipose tissue*. Semin Immunopathol, 2018. **40**(2): p. 189-202.
88. Chylikova, J., et al., *M1/M2 macrophage polarization in human obese adipose tissue*. Biomed Pap Med Fac Univ Palacky Olomouc Czech Repub, 2018. **162**(2): p. 79-82.
89. Cereijo, R., et al., *CXCL14, a Brown Adipokine that Mediates Brown-Fat-to-Macrophage Communication in Thermogenic Adaptation*. Cell Metab, 2018. **28**(5): p. 750-763 e6.
90. Nguyen, K.D., et al., *Alternatively activated macrophages produce catecholamines to sustain adaptive thermogenesis*. Nature, 2011. **480**(7375): p. 104-8.
91. Qiu, Y., et al., *Eosinophils and type 2 cytokine signaling in macrophages orchestrate development of functional beige fat*. Cell, 2014. **157**(6): p. 1292-308.
92. Fischer, K., et al., *Alternatively activated macrophages do not synthesize catecholamines or contribute to adipose tissue adaptive thermogenesis*. Nat Med, 2017. **23**(5): p. 623-630.
93. Wolf, Y., et al., *Brown-adipose-tissue macrophages control tissue innervation and homeostatic energy expenditure*. Nat Immunol, 2017. **18**(6): p. 665-674.
94. Goldstein, J.L. and M.S. Brown, *The low-density lipoprotein pathway and its relation to atherosclerosis*. Annu Rev Biochem, 1977. **46**: p. 897-930.
95. Maxfield, F.R. and I. Tabas, *Role of cholesterol and lipid organization in disease*. Nature, 2005. **438**(7068): p. 612-21.

96. Ridker, P.M., et al., *Interleukin-1beta inhibition and the prevention of recurrent cardiovascular events: rationale and design of the Canakinumab Anti-inflammatory Thrombosis Outcomes Study (CANTOS)*. Am Heart J, 2011. **162**(4): p. 597-605.
97. Benjamin, E.J., et al., *Heart Disease and Stroke Statistics-2017 Update: A Report From the American Heart Association*. Circulation, 2017. **135**(10): p. e146-e603.
98. Truett, J., J. Cornfield, and W. Kannel, *A multivariate analysis of the risk of coronary heart disease in Framingham*. J Chronic Dis, 1967. **20**(7): p. 511-24.
99. Russell, C., S. Sheth, and D. Jacoby, *A Clinical Guide to Combination Lipid-Lowering Therapy*. Curr Atheroscler Rep, 2018. **20**(4): p. 19.
100. Vavlukis, M. and A. Vavlukis, *Adding ezetimibe to statin therapy: latest evidence and clinical implications*. Drugs Context, 2018. **7**: p. 212534.
101. Investigators, A.-H., et al., *Niacin in patients with low HDL cholesterol levels receiving intensive statin therapy*. N Engl J Med, 2011. **365**(24): p. 2255-67.
102. Schwartz, G.G., et al., *Rationale and design of the dal-OUTCOMES trial: efficacy and safety of dalcetrapib in patients with recent acute coronary syndrome*. Am Heart J, 2009. **158**(6): p. 896-901 e3.
103. Khedoe, P.P., et al., *Brown adipose tissue takes up plasma triglycerides mostly after lipolysis*. J Lipid Res, 2015. **56**(1): p. 51-9.
104. Bartelt, A. and J. Heeren, *The holy grail of metabolic disease: brown adipose tissue*. Curr Opin Lipidol, 2012. **23**(3): p. 190-5.
105. Berbee, J.F., et al., *Brown fat activation reduces hypercholesterolaemia and protects from atherosclerosis development*. Nat Commun, 2015. **6**: p. 6356.
106. Dong, M., et al., *Cold exposure promotes atherosclerotic plaque growth and instability via UCP1-dependent lipolysis*. Cell Metab, 2013. **18**(1): p. 118-29.
107. Bartelt, A., et al., *Thermogenic adipocytes promote HDL turnover and reverse cholesterol transport*. Nat Commun, 2017. **8**: p. 15010.
108. Bartelt, A., et al., *Effects of adipocyte lipoprotein lipase on de novo lipogenesis and white adipose tissue browning*. Biochim Biophys Acta, 2013. **1831**(5): p. 934-42.
109. Chomczynski, P. and N. Sacchi, *Single-step method of RNA isolation by acid guanidinium thiocyanate-phenol-chloroform extraction*. Anal Biochem, 1987. **162**(1): p. 156-9.
110. Livak, K.J. and T.D. Schmittgen, *Analysis of relative gene expression data using real-time quantitative PCR and the 2(-Delta Delta C(T)) Method*. Methods, 2001. **25**(4): p. 402-8.
111. Bligh, E.G. and W.J. Dyer, *A rapid method of total lipid extraction and purification*. Can J Biochem Physiol, 1959. **37**(8): p. 911-7.
112. Havel, R.J., H.A. Eder, and J.H. Bragdon, *The distribution and chemical composition of ultracentrifugally separated lipoproteins in human serum*. J Clin Invest, 1955. **34**(9): p. 1345-53.
113. Brundert, M., et al., *Scavenger receptor class B type I mediates the selective uptake of high-density lipoprotein-associated cholesteryl ester by the liver in mice*. Arterioscler Thromb Vasc Biol, 2005. **25**(1): p. 143-8.
114. Pittman, R.C., et al., *A nonendocytotic mechanism for the selective uptake of high density lipoprotein-associated cholesterol esters*. J Biol Chem, 1987. **262**(6): p. 2443-50.

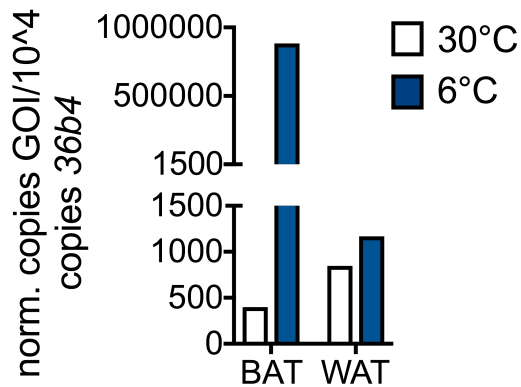
115. Morton, R.E. and D.B. Zilversmit, *Inter-relationship of lipids transferred by the lipid-transfer protein isolated from human lipoprotein-deficient plasma*. J Biol Chem, 1983. **258**(19): p. 11751-7.
116. Dole, V.P., *A relation between non-esterified fatty acids in plasma and the metabolism of glucose*. J Clin Invest, 1956. **35**(2): p. 150-4.
117. Zhang, X., R. Goncalves, and D.M. Mosser, *The isolation and characterization of murine macrophages*. Curr Protoc Immunol, 2008. **Chapter 14**: p. Unit 14 1.
118. Di Bartolo, B.A., M. Duong, and S.J. Nicholls, *Clinical trials with cholesteryl ester transfer protein inhibitors*. Curr Opin Lipidol, 2016. **27**(6): p. 545-549.
119. van der Velde, A.E. and A.K. Groen, *Shifting gears: liver SR-BI drives reverse cholesterol transport in macrophages*. J Clin Invest, 2005. **115**(10): p. 2699-701.
120. McCoy, M.G., et al., *Characterization of the lipolytic activity of endothelial lipase*. J Lipid Res, 2002. **43**(6): p. 921-9.
121. Berry, D.C., Y. Jiang, and J.M. Graff, *Mouse strains to study cold-inducible beige progenitors and beige adipocyte formation and function*. Nat Commun, 2016. **7**: p. 10184.
122. Lee, Y.H., et al., *Adipogenic role of alternatively activated macrophages in beta-adrenergic remodeling of white adipose tissue*. Am J Physiol Regul Integr Comp Physiol, 2016. **310**(1): p. R55-65.
123. Janowski, B.A., et al., *An oxysterol signalling pathway mediated by the nuclear receptor LXR alpha*. Nature, 1996. **383**(6602): p. 728-31.
124. Joseph, S.B., et al., *Synthetic LXR ligand inhibits the development of atherosclerosis in mice*. Proc Natl Acad Sci U S A, 2002. **99**(11): p. 7604-9.
125. Tangirala, R.K., et al., *Identification of macrophage liver X receptors as inhibitors of atherosclerosis*. Proc Natl Acad Sci U S A, 2002. **99**(18): p. 11896-901.
126. Han, S., et al., *Liver X Receptor Agonist Therapy Prevents Diffuse Alveolar Hemorrhage in Murine Lupus by Repolarizing Macrophages*. Front Immunol, 2018. **9**: p. 135.
127. Joseph, S.B., et al., *Reciprocal regulation of inflammation and lipid metabolism by liver X receptors*. Nat Med, 2003. **9**(2): p. 213-9.
128. Strauss, J.G., et al., *Endothelial cell-derived lipase mediates uptake and binding of high-density lipoprotein (HDL) particles and the selective uptake of HDL-associated cholesterol esters independent of its enzymic activity*. Biochem J, 2002. **368**(Pt 1): p. 69-79.
129. Gagliani, N., et al., *Th17 cells transdifferentiate into regulatory T cells during resolution of inflammation*. Nature, 2015. **523**(7559): p. 221-5.
130. Hui, X., et al., *Adiponectin Enhances Cold-Induced Browning of Subcutaneous Adipose Tissue via Promoting M2 Macrophage Proliferation*. Cell Metab, 2015. **22**(2): p. 279-90.
131. Teslovich, T.M., et al., *Biological, clinical and population relevance of 95 loci for blood lipids*. Nature, 2010. **466**(7307): p. 707-13.
132. Lubkowska, A., et al., *Changes in lipid profile in response to three different protocols of whole-body cryostimulation treatments*. Cryobiology, 2010. **61**(1): p. 22-6.
133. Ruan, X., et al., *Apolipoprotein A-I possesses an anti-obesity effect associated with increase of energy expenditure and up-regulation of UCP1 in brown fat*. J Cell Mol Med, 2011. **15**(4): p. 763-72.
134. Wang, S., D.Q. Peng, and Y. Yi, *The unsolved mystery of apoA-I recycling in adipocyte*. Lipids Health Dis, 2016. **15**: p. 35.

135. Fisher, E.A., et al., *High-density lipoprotein function, dysfunction, and reverse cholesterol transport*. *Arterioscler Thromb Vasc Biol*, 2012. **32**(12): p. 2813-20.
136. Rader, D.J., et al., *The role of reverse cholesterol transport in animals and humans and relationship to atherosclerosis*. *J Lipid Res*, 2009. **50 Suppl**: p. S189-94.
137. Rosenson, R.S., et al., *Cholesterol efflux and atheroprotection: advancing the concept of reverse cholesterol transport*. *Circulation*, 2012. **125**(15): p. 1905-19.
138. Rader, D.J. and A.R. Tall, *The not-so-simple HDL story: Is it time to revise the HDL cholesterol hypothesis?* *Nat Med*, 2012. **18**(9): p. 1344-6.
139. Khera, A.V., et al., *Cholesterol efflux capacity, high-density lipoprotein function, and atherosclerosis*. *N Engl J Med*, 2011. **364**(2): p. 127-35.
140. Worthmann, A., et al., *Cold-induced conversion of cholesterol to bile acids in mice shapes the gut microbiome and promotes adaptive thermogenesis*. *Nat Med*, 2017. **23**(7): p. 839-849.
141. West, M., et al., *Scavenger receptor class B type I protein as an independent predictor of high-density lipoprotein cholesterol levels in subjects with hyperalphalipoproteinemia*. *J Clin Endocrinol Metab*, 2009. **94**(4): p. 1451-7.
142. Acton, S., et al., *Identification of scavenger receptor SR-BI as a high density lipoprotein receptor*. *Science*, 1996. **271**(5248): p. 518-20.
143. Varban, M.L., et al., *Targeted mutation reveals a central role for SR-BI in hepatic selective uptake of high density lipoprotein cholesterol*. *Proc Natl Acad Sci U S A*, 1998. **95**(8): p. 4619-24.
144. Zhang, Y., et al., *Hepatic expression of scavenger receptor class B type I (SR-BI) is a positive regulator of macrophage reverse cholesterol transport in vivo*. *J Clin Invest*, 2005. **115**(10): p. 2870-4.
145. Vergeer, M., et al., *Genetic variant of the scavenger receptor BI in humans*. *N Engl J Med*, 2011. **364**(2): p. 136-45.
146. Zanoni, P., et al., *Rare variant in scavenger receptor BI raises HDL cholesterol and increases risk of coronary heart disease*. *Science*, 2016. **351**(6278): p. 1166-71.
147. Ma, K., et al., *Endothelial lipase is a major genetic determinant for high-density lipoprotein concentration, structure, and metabolism*. *Proc Natl Acad Sci U S A*, 2003. **100**(5): p. 2748-53.
148. Broedl, U.C., et al., *Effects of nonlipolytic ligand function of endothelial lipase on high density lipoprotein metabolism in vivo*. *J Biol Chem*, 2003. **278**(42): p. 40688-93.
149. Broedl, U.C., et al., *Endothelial lipase promotes the catabolism of ApoB-containing lipoproteins*. *Circulation Research*, 2004. **94**(12): p. 1554-1561.
150. Gauster, M., et al., *Endothelial lipase releases saturated and unsaturated fatty acids of high density lipoprotein phosphatidylcholine*. *J Lipid Res*, 2005. **46**(7): p. 1517-25.
151. Schilcher, I., et al., *Impact of Endothelial Lipase on Cholesterol Efflux Capacity of Serum and High-density Lipoprotein*. *Sci Rep*, 2017. **7**(1): p. 12485.
152. Nijstad, N., et al., *Scavenger receptor BI-mediated selective uptake is required for the remodeling of high density lipoprotein by endothelial lipase*. *J Biol Chem*, 2009. **284**(10): p. 6093-100.
153. Wiersma, H., et al., *Hepatic SR-BI, not endothelial lipase, expression determines biliary cholesterol secretion in mice*. *J Lipid Res*, 2009. **50**(8): p. 1571-80.

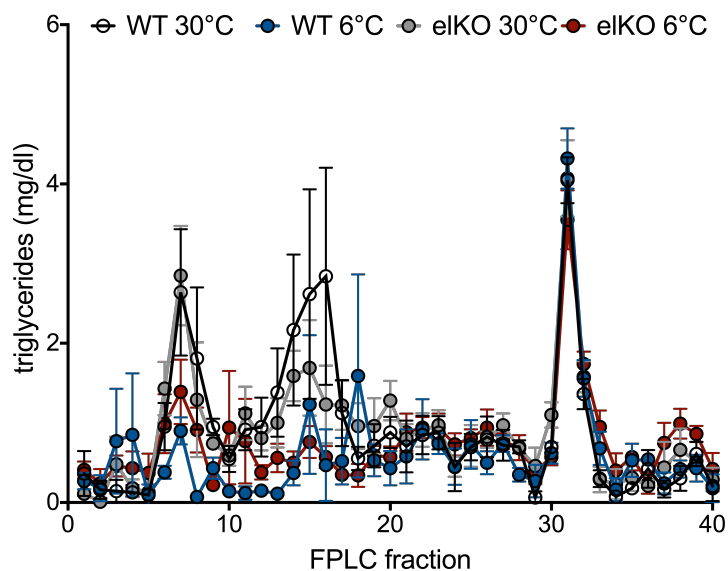
154. Hara, T., et al., *Targeted deletion of endothelial lipase increases HDL particles with anti-inflammatory properties both in vitro and in vivo*. J Lipid Res, 2011. **52**(1): p. 57-67.
155. Tanaka, H., et al., *Role of endothelial lipase in plasma HDL levels in a murine model of hypertriglyceridemia*. J Atheroscler Thromb, 2009. **16**(4): p. 327-38.
156. Hirata, K., et al., *Regulated expression of endothelial cell-derived lipase*. Biochem Biophys Res Commun, 2000. **272**(1): p. 90-3.
157. Jin, W., et al., *Endothelial cells secrete triglyceride lipase and phospholipase activities in response to cytokines as a result of endothelial lipase*. Circ Res, 2003. **92**(6): p. 644-50.
158. Qiu, G. and J.S. Hill, *Endothelial lipase promotes apolipoprotein AI-mediated cholesterol efflux in THP-1 macrophages*. Arterioscler Thromb Vasc Biol, 2009. **29**(1): p. 84-91.
159. Kojima, Y., et al., *Endothelial lipase modulates monocyte adhesion to the vessel wall. A potential role in inflammation*. J Biol Chem, 2004. **279**(52): p. 54032-8.

Part I Attachement

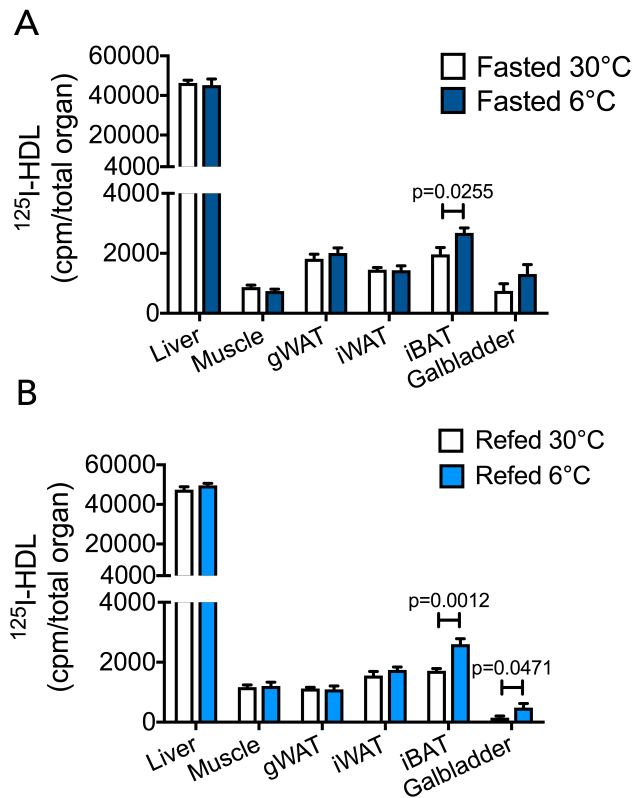
1. Supplementary figures



Supplementary Figure 1. Lipg expression in endothelial cells (CD31+) isolated from BAT or inguinal WAT via MACS® technique. Mice were housed at thermoneutrality (30°C) or exposed to the cold (6°C) for 7 days. Organs of 5 mice per group were harvested after a 4-hour fasting period. MACS®-based cell separation was performed to isolate endothelial cells (CD31⁺) and macrophages (CD11B⁺). The flow through, depleted of endothelial cells and macrophages, was considered to contain mainly adipocytes. After mRNA and cDNA preparation, gene expression analysis was conducted using TaqMan™ technique. EL (*Lipg*) mRNA expression in endothelial cells isolated from BAT and inguinal WAT of thermoneutral- or cold-housed mice. Bars represent mean of one experiment with 4 technical replicates. Expression is normalized to house keeper gene *ribosomal protein, large, P0* (*36b4*).



Supplementary Figure 2. Triglyceride concentrations in lipoprotein fractions generated via FPLC from thermoneutral and cold-housed wildtype and eIKO mice. Mice were housed at thermoneutrality (30°C) or exposed to the cold (6°C) for 7 days. Plasma lipids were determined after a 4-hour fasting period. Plasma was extracted from blood withdrawn by retro-orbital puncture. Dots represent means of 4 mice per group and error bars show ±SEM.



Supplementary Figure 3. ^{125}I -HDL organ distribution in fasted or refed mice housed at thermoneutrality or cold. Mice were housed at thermoneutrality (30°C) or exposed to the cold (6°C) for 7 days. **A.** Mice were fasted 6 hours before they were intravenously injected with double-labeled HDL particles (^{125}I in the protein compartment and ^3H in cholesteryl oleyl ether). 300 min after injection organs were harvested and radioactivity determined. **B.** Mice were fasted 6 hours before they were refed for 4 hours. Then they were intravenously injected with double-labeled HDL particles (^{125}I in the protein compartment and ^3H in cholesteryl oleyl ether). 300 min after injection organs were harvested and radioactivity determined. Dots/Bars in each graph represents mean of 6-7 mice. Error bars represent \pm SEM. Statistics are performed with Student's t-Test.

2. Materials and buffers

Table 6. Chemicals and hazards potential after GHS.

Chemical	Manufacturer	Purity	GHS-Symbol	Hazard Statement H	Precaution Statement P
		(%)			
1-heptadecanoyl-2-hydroxy-sn-glycero-3-phosphocholin, LysoPC(17:0)	avanti polar lipids, Alabaster, USA	≥ 99 %	-	-	-
1-o-pentadecanoyl-3-(9Z-octadecenoyl)-sn-glycerol	avanti polar lipids, Alabaster, USA	≥ 99 %	-	-	-
1,2-di-O-tridecyl-sn-glycero-3-phosphocholin	avanti polar lipids, Alabaster, USA	≥ 99 %	-	-	-
1,2-diheptadecanoyl-sn-glycero-3-phosphat (Natriumsalz), PA(17:0/17:0)	avanti polar lipids, Alabaster, USA	≥ 99 %	-	-	-
1,2-diheptadecanoyl-sn-glycero-3-phosphoethanolamin, PE(17:0/17:0)	avanti polar lipids, Alabaster, USA	≥ 99 %	-	-	-
1,2-dipentadecanoyl-sn-glycero-3-phosphatidylcholin, PC(15:0/15:0)	Sigma-Aldrich®, München	≥ 99 %	-	-	-
1,2-ditetradecanoyl-sn-glycero-3-phospho-L-serin (Natriumsalz), PS(14:0/14:0)	avanti polar lipids, Alabaster, USA	≥ 99 %	-	-	-
1,3(d5)-dipentadecanoyl-glycerol, 1,3(d5)DG(15:0/15:0)	avanti polar lipids, Alabaster, USA	≥ 99 %	-	-	-
¹²⁵ I-tyramine cellobiose	Perkin-Elmer, USA		na	na	na
2-propanol, LC-MS-Grade	Carl Roth	≥ 99,5 %	GHS02, GHS07	H225-H319-H336	P210-P261-P305 + P351 + P338
³ H-cholesterol	Perkin-Elmer, USA	40-60Ci (1.48-2.22TBq)/mmol, 1mCi/mL			
³ H-cholesterol ester	Perkin-Elmer, USA	40-60Ci (1.48-2.22TBq)/mmol, 1mCi/mL	GHS02, GHS07, GHS08	H225-H225-H373-H304-H315-H336	
acetic acid	Sigma-Aldrich, München	≥ 99,7 %	GHS02, GHS05	H226-H314	P280-P305 + P351 + P338-P310
acetyl chloride	Sigma-Aldrich, München	≥ 99 %	GHS02, GHS05, GHS07	H225-H302-H314	P210-P280-P305 + P351 + P338-P310
ammonium acetate, NH ₄ Ac	Sigma-Aldrich®, München	≥ 99,99 % trace metals basis	-	-	-
bovine serum albumin, BSA	Serva, Heidelberg	≥ 99 %	-	-	-
calcium chlorid, CaCl ₂	Merck, Darmstadt	≥ 99 %	GHS07	H319	P305 + P351 + P338
chloroform, Rotisolv, HPLC-Grade	Carl Roth	≥ 99,9 %	GHS06, GHS08	H302-H315-H319-H331-H336-H351-H361d-H372	P261-P281-P305 + P351 + P338-P311
CD11b micro beads	Miltenyi Biotec		-	-	-
CD31 micro beads	Miltenyi Biotec		-	-	-
cholest-5-en-3β-yl heptadecanoate CE(17:0)	avanti polar lipids	≥ 99 %	-	-	-
collagenase D	Roche		GHS06, GHS08	315-319-334-335	261-305+351+338-342+311

Part I Attachment

dispase II	Gibco		GHS07, GHS08	H315-319- 334	P305+351+338- 337+313- 332+313-261- 304+341-285
EDTA	Sigma-Aldrich®, München	≥ 99 %	GHS07	H319	P305 + P351 + P338
ethanol	Merck, Darmstadt	96%	GHS02	H225	P210
formic acid	Sigma-Aldrich, München	≥ 98 %	GHS0, GHS05	H226-H314	P280-P305 + P351 + P338- P310
glucose	Sigma-Aldrich, München	≥ 99,5 %	-	-	-
glyceryltridecanoate TG(13:0/13:0/13:0)	Sigma-Aldrich®, München	≥ 99 %	-	-	-
heparine	Braun		-	-	-
heptadecanoic aci, FA(17:0)	Sigma-Aldrich®, München	≥ 99 %	GHS07	H315- H319-H335	P261- P305+P351+P3 38
heptan	Sigma-Aldrich®, München	≥ 99 %	GHS02, GHS07, GHS08, GHS09	H225- H304- H315- H336-H410	P210-P261- P273-P301 + P310-P331- P501
Hexakis(1H, 1H, 2H- Perfluoroethoxy)phosphaz en	Apollo Scientific Ltd, Bredbury, UK	≥ 90 %	GHS05	na	na
Hexan	Sigma-Aldrich®, München	≥ 95 %	GHS02, GHS07, GHS08, GHS09	H225- H304- H315- H336- H361f- H373-H411	P201-P210- P273-P301 + P310-P308 + P313-P331
ketamine	Albrecht, Aulendorf	10 mg/ml	GHS07	H301- H315- H319-H335	261 P306+P351+P3 38
methanol, Rotisolv, Ultra LC-MS-Grade	Carl Roth	≥ 99,98 %	GHS02, GHS06, GHS08	H225-H301 + H311 + H331-H370	P210-P260- P280-P301 + P310-P311
N-heptadecanoyl-D- erythro-sphingosin, SM(17:0)	avanti polar lipids, Alabaster, USA	≥ 99 %	-	-	-
N-heptadecanoyl-D- erythro- sphingosylphosphorylcholi ne, SM(17:0)	avanti polar lipids, Alabaster, USA	≥ 99 %	-	-	-
3potassium chloride, KCl	Sigma-Aldrich, München	≥ 99 %	-	-	-
Rompun	Bayer, Leverkusen	2 %	GHS06	H301	P301+P310
sodium chloride, NaCl	Sigma-Aldrich®, München	≥ 99,5 %	-	-	-
sodium hydroxide, NaOH	Sigma-Aldrich, München	≥ 97 %	GHS05	H290-H314	P280-P303 + P361 + P353- P304 + P340 + P310-P305 + P351 + P338
sulfuric acid	Sigma-Aldrich®, München	0,5 M	GHS05	H290-H314	P280-P303 + P361 + P353- P304 + P340 + P310-P305 + P351 + P338

Part I Attachment

thioglycolate	Becton, Dickinson and Company, Franklin Lakes, USA		GHS05, GHS06	H331-H311-H301-H314	P280-P304 + 340-P302 + 352-P301 + 330 + 331-P309-P310-P305 + 351 + 338
water, LC-MS Ultra CHROMASOLV, tested for UHPLC-MS	Sigma-Aldrich®, München	≥ 99,98 %	-	-	-
na = not available					

Table 7. Kits.

Kit/Product	Manufacturer
cholesterol detection kit, Cholesterol CHOD-PAP®	Roche Diagnostics®, Mannheim
<i>High Capacity cDNA Reverse Transcription Kit</i>	Applied Biosystems
Mastermix TaqMan	Eurogentec, Deutschland
NucleoSpin RNA II	Macherey & Nagel, Düren
scintillation solution, Aquasafe 500 Plus	Zinsser Analytic, Frankfurt
triglyceride detection kit, Triglycerides GPO-PAP®	Roche Diagnostics®, Mannheim
universal PCR MasterMix	Applied Biosystems Inc., USA
ApoA1 ELISA	Cloud Clone Corp, USA

Table 8. Solutions and buffers.

Solution/Buffer	Manufacturer/Composition
10 x PBS	- 400 g NaCl
	- 10 g KCl
	- 10 g KH ₂ PO ₄ x 2H ₂ O
	ad 5 l H ₂ O dest., pH 6.9
EDTA, 0,5 M	GIBCO/BRL, Eggenstein
ESI-L, Low Concentration Tuning Mix, 100 mL	Agilent Technologies, Waldbronn
FCS	GIBCO/BRL, Eggenstein
Folch reagent	chloroform/methanol, 2/1, v/v
Folin's reagent	Merck, Darmstadt
FPLC buffer	- 100 mM Tris
	- 1.5 M NaCl
	- 100 mM EDTA
	in H ₂ O dest.
internal standard (in Folch reagent)	- 1,2-dipentadecanoyl-sn-glycero-3-phosphatidylcholine (118.85 µg/ml)
	- cholest-5-en-3β-yl heptadecanoate (593.27 µg/ml)
	- Glyceryltridecanoate (118.85 µg/ml)
	- N-heptadecanoyl-D-erythro-sphingosine (118.85 µg/ml)
	- 1-heptadecanoyl-2-hydroxy-sn-glycero-3-phosphocholine (118.85 µg/ml)
	- 1,2-diheptadecanoyl-sn-glycero-3-phosphoethanolamine (118.85 µg/ml)
	- 1-o-pentadecanyl-3-(9Z-octadecenoyl)
	- sn-glycerol (118.85 µg/ml)
	- 1,3-diheptadecanoyl glycerol (118.85 µg/ml)
	- 1,2-di-O-tridecyl-sn-glycero-3-phosphocholine (118.85 µg/ml)
	- N-heptadecanoyl-D-erythro-sphingosylphosphorylcholine (118.85 µg/ml)

	- 1,2-ditetradecanoyl-sn-glycero-3-phospho-L-serine, sodium salt (118.85 µg/ml)
	- 1,2-diheptadecanoyl-sn-glycero-3-phosphate, sodium salt (118.85 µg/ml)
	- heptadecanoic acid (237.31 µg/ml)
Ketamin, 100 mg/ml	Albrecht, Aulendorf
Lockmasse	1.082 mg Hexakis (1H, 1H, 2H-perfluoroethoxy)phosphazene/ml in 2-propanol
MeOHBHT	110 mg BHT in 200 ml methanol
NaCl, 0,9 w/v %	Braun, Melsungen
anesthesia	ketamine (100 mg/ml)/xylazine (2 %)/NaCl (0.9 %); 2.3/1.0/6.7, v/v/v; 15 µL/g bodyweight
1x PBS	GIBCO/BRL, Eggenstein
Precipath®	Roche Diagnostics, Mannheim
Thioglycolate media	Becton, Dickinson and Company, Franklin Lakes, USA
Dulbecco's Modified Eagle Medium (DMEM)	GIBCO/BRL, Eggenstein
PeqGold TriFast™	Invitrogen by life technologies®, USA
MACS buffer	- 2 mM EDTA
	- 0.5% BSA (GIBCO/BRL, Eggenstein)
	- 2 mM glucose
	in PBS dest.
adipose tissue digestion	- 1.8 U/mg dispase II
	- 0.19 U/mg collagenase D
	- 1 mM CaCl ₂
	in PBS dest.

Part J Register of figures

Figure 1. Lipoprotein Metabolism.	7
Figure 2. Morphology of white, brown and beige adipose tissues of mice.	12
Figure 3. Activation of brown adipocytes.	14
Figure 4. BAT activation elevates HDL-C and thereby attenuates atherosclerosis progression.	17
Figure 5. MACS® separation of parenchymal cells, non-parenchymal cells and macrophages from adipose tissues.	27
Figure 6. Gene expression of browning-related genes in MACS-isolated adipocytes.	28
Figure 7. Gene expression in MACS®-isolated adipocytes, endothelial cells and macrophages from BAT.	29
Figure 8. Gene expression in MACS-isolated adipocytes, endothelial cells and macrophages from inguinal WAT.	30
Figure 9. Lipid composition in adipocytes isolated from adipose tissues.	31
Figure 10. Lipid composition in endothelial cells isolated from adipose tissues.	32
Figure 11. Lipid composition in macrophages (CD11B+) isolated from adipose tissues.	33
Figure 12. Expression of genes involved in lipid processing in macrophages (CD11B+) isolated via MACS® technique.	34
Figure 13. Expression of genes regulating inflammation in macrophages (CD11B+) isolated via MACS® technique.	36
Figure 14. Plasma lipid parameters and ApoA1 concentration in thermoneutral- or cold-housed wildtype mice.	38
Figure 15. Pre- and post-prandial cholesterol concentrations in FPLC fractions from wildtype mice after cold intervention.	39
Figure 16. HDL turnover in fasted mice housed at thermoneutrality or cold.	40
Figure 17. HDL turnover in refeed mice housed at thermoneutrality or cold.	42
Figure 18. <i>In vivo</i> RCT in wildtype mice housed at thermoneutrality or cold.	43
Figure 19. HDL turnover in cold-housed aIKO mice.	44
Figure 20. HDL turnover in cold-housed Scarb1-/- mice.	46
Figure 21. Expression of browning-related genes after cold-housing in wildtype and eIKO mice.	48
Figure 22. Expression of browning-related genes in inguinal WAT after cold-housing in wildtype and eIKO mice.	49
Figure 23. Hepatic expression of genes involved in lipoprotein and cholesterol metabolism after cold-housing in wildtype and eIKO mice.	50
Figure 24. Plasma lipid parameters and lipoprotein profile in thermoneutral- or cold-housed wildtype and eIKO mice.	51
Figure 25. Lipid profiles in isolated HDL.	52
Figure 26. Absolute lipid amounts in isolated HDL particles of wildtype and eIKO mice after activation BAT by cold housing.	53
Figure 27. Impact of EL loss for HDL-C clearance.	55
Figure 28. Impact of EL on <i>in vivo</i> RCT after BAT activation by cold housing.	56
Figure 29. Macrophage polarization in BAT.	61
Figure 30. Working Model.	64

Part K Register of tables

Table 1. Lipoprotein classification.....	5
Table 2. Members of the LPL family.	10
Table 3. TaqMan™ probes used for analysis in MACS®-isolated cell fractions.....	21
Table 4. Parameters of mass spectrometer.	22
Table 5. TaqMan™ probes used for analysis in BAT, inguinal WAT and liver.....	24
Table 6. Chemicals and hazards potential after GHS.....	80
Table 7. Kits.	83
Table 8. Solutions and buffers.	83

Part L Danksagung

Mein ganz besonderer Dank gilt Jörg Heeren, der mir durch die Stelle in seinem Labor die Türen für die wissenschaftliche Forschung eröffnet hat. Danke für dein Vertrauen und deine Großzügigkeit, durch die ich viele wertvolle Erfahrungen in den letzten Jahren sammeln durfte.

Außerdem möchte ich mich sehr herzlich bei Herrn Prof. Dr. Markus Fischer bedanken, der mich während meiner Promotion unterstützt hat und als Prüfer meiner Dissertation, als auch der Disputation agiert.

I want to highlight the influence I received by Nicola Gagliani throughout my PhD work. Thank you so much for your scientific motivation and for maintaining your encouragement to teach me.

Durch die Zusammenarbeit mit Alexander Bartelt konnte ich in diesem Projekt erfolgreich teilhaben und ich möchte ihm für seine Förderung und sein Interesse danken.

Ich möchte mich beim gesamtem IBMZ für die Unterstützung und die immer wieder erheiternde gemeinsamen Erlebnisse bedanken. Die warmherzige und familiäre Arbeitsatmosphäre, die in der AG Heeren herrscht macht einen riesen Spaß!

Danke an die AG Gagliani und die AG Huber für die inspirierende Zusammenarbeit, den wissenschaftlichen Austausch und die freudige Zeit in und außerhalb des Labors.

Für unvergessliche Stunden im Labor und Privat und deine unerschöpfliche Hilfsbereitschaft möchte ich mich bei dir, Anna, bedanken! Außerdem gilt ein ganz besonderer Dank Alex, Christian und Clara für Inspiration, Wohlwollen und eine riesen Menge Spaß!

Zu guter Letzt möchte ich meinen Eltern danken, die mir durch ihren Rückhalt diesen Weg hin zur Doktorarbeit ermöglicht haben. Danke an meinen Bruder Philipp und meine Freunde, die mich durch die komplette Zeit unterstützt und ermutigt haben.

Part M Eidesstattliche Erklärung

„Hiermit versichere ich an Eides statt, die vorliegende Dissertation selbst verfasst und keine anderen als die angegebenen Hilfsmittel benutzt zu haben. Die eingereichte schriftliche Fassung entspricht der auf dem elektronischen Speichermedium. Ich versichere, dass diese Dissertation nicht in einem früheren Promotionsverfahren eingereicht wurde.“

Datum, Unterschrift